The Dissertation Committee for Russell James Borduin Certifies that this is the approved version of the following dissertation:

Development of a PES-Zeolite Fuel Cell Humidification Membrane and Humidification Membrane Analysis System

Committee:

Wei Li, Supervisor

Dongmei Chen

Jonathan Chen

Rich Crawford

Carolyn Seepersad

Development of a PES-Zeolite Fuel Cell Humidification Membrane and Humidification Membrane Analysis System

by

Russell James Borduin

Dissertation

Presented to the Faculty of the Graduate School of

The University of Texas at Austin

in Partial Fulfillment

of the Requirements

for the Degree of

Doctor of Philosophy

The University of Texas at Austin

August 2017

Dedication

To my family

Acknowledgements

I would like to thank Dr. Wei Li, my advisor and committee chair, for his continuous advice and support during my time at The University of Texas at Austin. He has been a great mentor, both patient as well as motivating.

I would also like to thank the members of my doctoral committee: Dr. Dongmei Chen, Dr. Jonathan Chen, Dr. Rich Crawford and Dr. Carolyn Seepersad. Their support and feedback have been invaluable.

I would like to thank my current and former colleagues from the lab: Dr. Sriharsha Sundarram, Dr. Yongha Kim, Dr. Wei Jiang, Dr. Hao Xin, Dr. Jingyu Ock, Xiaoran Li, and Daniel Justiss. I will always appreciate their friendship and advice.

Development of a PES-Zeolite Fuel Cell Humidification Membrane and Humidification Membrane Analysis System

Russell James Borduin, Ph.D.

The University of Texas at Austin, 2017

Supervisor: Wei Li

The purpose of this study is to develop PES-zeolite mixed matrix membranes for use in fuel cell humidification and to study their water permeability as well as physical and thermal properties. A solvent casting process was used to develop the initial PES-zeolite mixed matrix membranes (MMM), followed by solid state foaming to alter their morphology and create a porous microstructure. The effects of zeolite weight loading and solid state foaming duration on membrane water permeability were investigated. The best performing films achieved water permeation measurements close to that of Nafion. Next, an extrusion and hot pressing process was developed to replace solvent casting and create PES-zeolite MMM with improved zeolite dispersion. The extruded films were then solid state foamed. The effects of zeolite weight loading and foaming on water permeability, mechanical properties and thermal properties were investigated. Improved zeolite dispersion allowed the extruded films to achieve excellent permeation performance with improved tensile strength. Dynamic mechanical analysis revealed the PES-zeolite membranes have a higher glass transition temperature and storage modulus than Nafion, making them more suited to for use in high temperature fuel cell operation. Finally, a rapid membrane measurement system was developed and modeled to aid in evaluation of small size (<2 cm^2) membrane materials.

Table of Contents

List of Tables

List of Figures

Chapter 1: Introduction

1.1 Fuel Cell Background

Polymer electrolyte membrane (PEM) fuel cells have the potential to replace fossil fuel sources in both automotive and stationary power generation applications. Increased implementation of fuel cells would decrease dependence on oil and reduce greenhouse gas emissions. One major obstacle preventing widespread adoption of fuel cells is cost. The Department of Energy (DOE) has set a target cost of $30/kW for automotive fuel cells by the year 2015. This is the estimated value fuel cells must reach to be competitive with competing technologies in the projected automotive market. The latest cost analysis report commissioned by the DOE prices systems at $55/kW for a production rate of 500,000 systems per year, nearly twice the target value [1]. Major improvements must be made rapidly to meet the DOE's goal, a difficult task considering estimated cost remained the same from 2012 to 2013.

PEM fuel cells convert hydrogen into electric energy, producing water and heat that exit the system as waste products. The reaction can be expressed as

$$2H_2 + O_2 \leftrightarrow 2H_2O \tag{1.1}$$

Error! Reference source not found. illustrates the operation of a PEM fuel. ressurized hydrogen gas is supplied to the anode side of the fuel cell, which has channels to direct the gas evenly to a platinum catalyst. The catalyst speeds up the separation of hydrogen gas into H+ ions and electrons. The H+ ions pass through the electrolyte membrane to the cathode. The electrons cannot pass through the electrolyte membrane and are directed through a circuit as usable electricity. The electrons and H+ ions meet with incoming air in the cathode, which supplies oxygen to form water in the presence of another platinum catalyst layer.

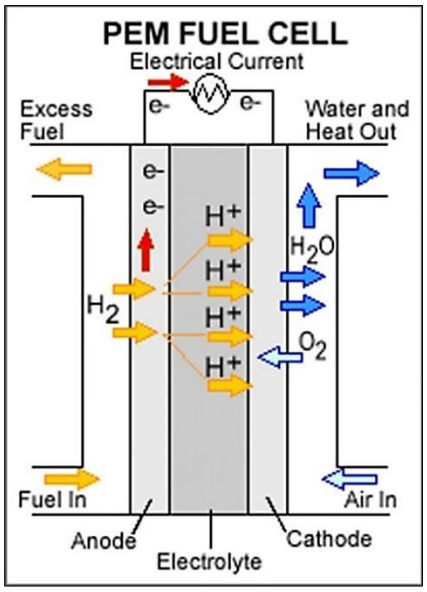

Figure 1-1. Schematic of PEM fuel cell [2]

1.2 Humidity Control

The two largest contributors to fuel cell costs are platinum catalyst loading and fuel cell power density [1]. Market fluctuations in platinum prices have held estimated fuel cell prices constant over the past few years despite improvements in fuel cell systems and materials. There is a major research focus on developing new catalysts to reduce cost by creating composite catalysts with reduced platinum loading or nanostructured catalysts with no platinum at all [3-5]. These new catalysts may decouple fuel cell prices from platinum fluctuations. The general strategy for increasing power density and decreasing costly catalyst loading remains unchanged regardless of the catalyst used, i.e., to run the fuel cell at higher temperatures and pressures. Present-day automotive fuel cells typically operate over a temperature range of 50-90°C and pressures up to 3 atm. Temperature and pressure are somewhat coupled due to cathode stoichiometry. The Nernst Equation

demonstrates cell voltage has a linear dependence on temperature and a logarithmic dependence on pressure, assuming the concentration ratio of reactants is held constant:

$$\Delta V = \frac{RT}{2F} \ln \frac{\alpha \beta^{1/2}}{\delta} P^{1/2} \tag{1.2}$$

where R is the universal gas constant, T is temperature, F is Faraday constant, P is system pressure and α, β, and δ are constants that represent the concentration of H_2, O_2 and H_2O [6].

Increasing temperature and pressure allows for reduced catalyst loading and higher voltage output from the fuel cell. These harsher operating conditions require new thermal and water management solutions. Currently, fuel cell humidification costs generally make up less than 15% of total system cost [1, 7]. However, a fuel cell system analysis recently conducted by Argonne National Labs estimated a ten-fold increase in membrane humidifier surface area is needed when the exit temperature at the cathode was raised from 85°C to 95°C [5]. Humidification costs may further increase as the DOE has targeted temperature values of 120°C for automotive applications and 150°C for stationary applications [1, 8].

Careful control of relative humidity levels within the electrolyte membrane is required for both efficiency and reliability. Currently available electrolyte membranes require humid conditions to function; if humidity levels are too low, membrane conductivity and power output are reduced. Higher than optimal humidity levels cause excess water to flood the PEM, blocking gas flow and reducing output [9]. There are a variety of options for fuel cell humidification, but membrane humidifiers are currently the most promising solution. They are the only system that can recycle waste heat and humidity passively with no moving parts. A semi-permeable membrane is used to selectively transfer water vapor from the humid waste stream to the dry air inlet stream while preventing gas crossover between streams.

1.3 Membrane Materials

There are a variety of humidification membrane materials under investigation, but none have satisfied the requirements outlined by the DOE. Nafion was the material of choice until recently due to its excellent water and ion transport characteristics. However, its ion transport properties are not necessary for humidification and its high price (~\$1000/m^2) drives up the cost. Nafion also experiences chemical degradation due to anhydride formation and mechanical degradation due to humidity cycling. Materials currently in development include Gore M311, Tetramer "PFCB" and various sulfonated hydrocarbons [8, 10-14]. The Gore M311 membrane is a thin selective ionomer layer sandwiched between two porous PTFE support layers. Although it offers high water permeability, it suffers from anhydride formation at temperatures above 80°C, making it currently less viable than Nafion [15, 16]. The Tetramer "PFCB" membrane is a multiblock polymer that combines blocks for mechanical strength, water transport and stability [8]. Although it offers high water permeability and no anhydride formation, it suffers from rupture due to mechanical stress induced by swelling, limiting it to operating temperatures below 100°C [8]. The sulfonated hydrocarbon materials are more environmentally friendly than Nafion, but generally have higher swelling, lower chemical resistance and lower water flux than Nafion [13]. Developing a less expensive humidification membrane capable of operating at the new conditions outlined by the DOE is necessary to increasing fuel cell efficiency and lower humidification costs.

1.4 Membrane Evaluation

Humidification membrane development must be guided by performance. Membrane performance can be measured in a permeation system, which research groups and companies often design and construct to compare membrane samples based on their specific needs. It can be difficult to compare two membranes without testing them in the same system under the same conditions; there are no DOE standards for water permeation and values can vary by orders of magnitude for the same material due to differences in the experimental setup and procedure. Systems described in literature are generally steady state, and function by flowing humid gas or liquid water over one side of a membrane and dry gas over the other side. These systems usually require long measurement time and a large membrane area to achieve sufficient humidity in the dry gas stream. These conditions are not conducive to membrane development, where it may only be possible to produce small samples and short measurement time is desired. Furthermore, these systems may not accurately predict membrane performance under the transient conditions present in a fuel cell. There is a need for the development of a new, transient measurement system capable of measuring small membrane samples.

Water permeability is of primary importance in humidification membranes, but other secondary requirements must be met for use in commercial fuel cells. Gas permeability, mechanical strength, and chemical resistance must all be characterized to determine material suitability. Gas permeation measurement for thin films is a well-established topic in literature and helpful for material development and characterization. However, detailed gas permeability results are not required by the DOE. Mechanical strength and gas crossover are measured in the same DOE standard, where stress is induced in the membrane via humidity cycling and then pressurized gas is applied periodically to test for gas crossover. The membrane fails the test when it exceeds the

maximum allowable gas crossover level. Chemical resistance is also important, but the guidelines set forth by the DOE are ambiguous and acknowledge the need to tailor chemical resistance tests to each individual material.

1.5 Research Objectives

The goal of the proposed research is to develop a composite membrane and permeability measurement system for automotive PEM fuel cell applications. The new composite membrane material will be capable of high temperature (>100°C) operation and resistant to relative humidity cycling. The permeation system will be used to characterize the humidification property of the material. Mechanical properties of the developed membrane material will also be characterized. The specific objectives are:

- To develop a permeability measurement system for rapid material development
- To study the effects of processing parameters, such as zeolite loading, solid-state foaming, on the membrane water permeability.
- To study the effects of processing parameters on membrane mechanical properties.

1.6 Organization of This Dissertation

This dissertation is divided into six chapters. Chapter 1 is an introduction to the research topics and objectives. Chapter 2 is a literature review focused on polymer electrolyte membrane (PEM) fuel cells, fuel cell humidification, humidification materials and analysis of these materials. Next, Chapter 3 covers development of a solvent cast PES-zeolite material designed for fuel cell humidification. Chapter 4 details the development of an extruded, hot pressed PES-zeolite material designed for fuel cell humidification, with analysis of physical properties, dynamic mechanical analysis and

water vapor permeability. In Chapter 5, a measurement system and resistance model are developed to analyze humidification material performance. Chapter 6 summarizes research contributions and future work.

Chapter 2: Literature Review

2.1 Introduction

Chapter 2 begins with a discussion of present day fuel cell operating parameters as well as future performance targets defined by DOE and industry sources. The requirements are followed by a summary of various humidification technologies with a focus on their suitability for use in automotive applications. Establishing these requirements is important to help guide the development of new materials. Next, various material development strategies are explained and their strengths and weaknesses evaluated with respect to satisfying the aforementioned fuel cell performance requirements. Finally, existing humidification membrane materials are discussed along with new materials currently in development. The properties, advantages and disadvantages of each material are evaluated for membrane humidification applications. Existing gas and water permeation systems as well as modeling approaches are also reviewed to understand current measurement standards and determine areas for improvement. The review of measurement methods will aid in the development of a new rapid measurement system more suited to development of new humidification materials.

2.2 Requirements for PEM Fuel Cells

A clear understanding of fuel cell operating conditions is required in order to evaluate the suitability of existing humidification systems and materials and to develop new candidates. Table 2-1 was compiled from multiple DOE commissioned reports and commercially available products in an effort to consolidate relevant operating conditions. The 2017 data represents targets set by the DOE with the goal of reaching $30/kW at a fixed 80 kW power output. The 2012 cost and configuration data is based on a Design for

Manufacturing and Assembly analysis (DMFA) conducted each fiscal year to estimate the current cost per kW generated for various fuel cell configurations based on the latest research [17]. A range of possible production values are explored, with the final values reported for cars at a rate of 500,000 units per year. The analysis focuses on fixing some operational parameters and simplifying the system as much as possible. Current membrane properties are based on Nafion. DOE projects in progress have reported superior values to some of the 2012 auto technology numbers, but all of the membranes have significant deficiencies as well and are not yet commercially available. These improvements and shortcomings will be discussed in detail under each individual material section.

Table 2-1. Summary of relevant parameters for auto and bus technology [8, 16-20]

Module Properties	2012 Auto Tech.	2017 DOE Target
Cost ($/kWh)	55	30
Net Power (kW_{net})	80	80
Operating Press. (atm)	2.5	-
Peak Stack Temp (°C)	87	≤120
Air Humidification	Tubular Membrane	Flat Plate
H_2 Humidification	None	None
Volume (L)	5-10	5
Weight (kg)	-	5
Cost @500k/yr. ($)	<100	100
Flow Cross Over (%)	1-3	<.5
Membrane Properties		
H_2O Flux ($g*sec^{-1}m^{-2)}$	.14-2.5	5
Lifetime (hrs)	2500	5000
Cost @500k sys/yr. ($/m^2)	-	$10/m^2
Max ΔP (kPa)	70	75
Membrane Temp (°C)	80-83	>95

Further increases in peak stack temperature and operating pressure could improve fuel cell efficiency, but would require materials capable of operating under such conditions [5]. Temperatures of anywhere from 80°C up to 120°C have been suggested

for automotive applications [1, 8]. The DOE has targeted an even higher value of 150°C for stationary fuel cell applications. Size and weight are primary concerns for automotive applications, but stationary fuel cells can have heavier components and larger dedicated cooling systems.

2.3 Humidification Systems

There are a multitude of air humidification methods currently used in industrial and consumer applications, but most are not suitable for automotive fuel cell systems where size, weight and energy consumption are at a premium. Solutions that recycle heat and humidity exiting the system are more promising than those that require a liquid water source for operation due to efficiency and maintenance. Adding a separate consumable water source for humidification would increase system weight, complexity and create an extra task for vehicle owners. For these reasons, the DOE has only considered recycling type humidifiers in fuel cell system cost analyses each year. Designing a system capable of providing adequate humidification from the cathode exhaust stream while meeting DOE target values for temperature, weight and operational lifetime remains a challenge. Potential solutions can be categorized into active and passive control systems, which will be evaluated below. Typical waste stream recycling humidifier placement in a fuel cell system can be seen in Figure 2-1.

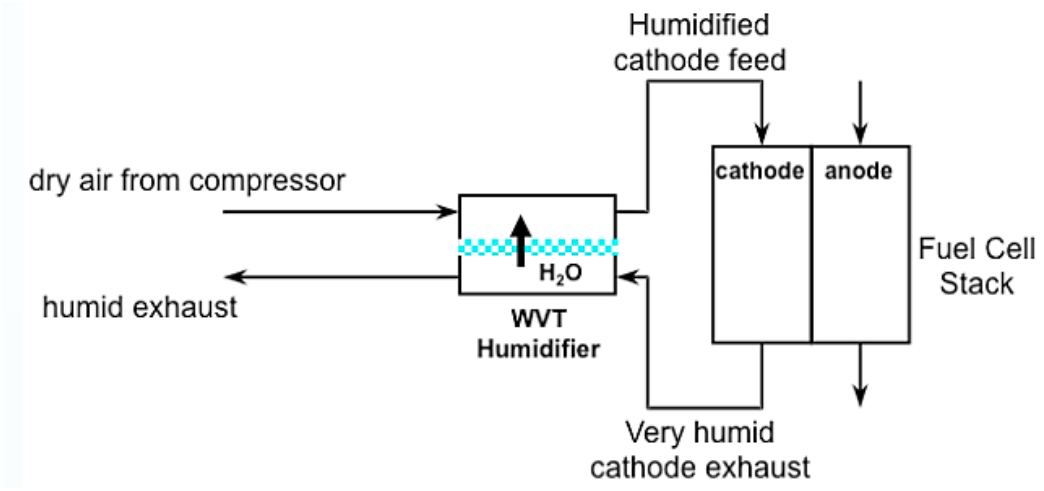

Figure 2-1. Diagram of humidifier in fuel cell system [8]

2.3.1 Powered Humidifiers

Active humidity control offers greater regulation of fuel cell humidity conditions than passive options at the cost of complexity and parasitic power loss. Although there are a variety of devices capable of actively controlling fuel cell humidity levels including bubblers and steam injection, the only active humidity control device to be considered by the DOE is an enthalpy wheel manufactured by Emprise, seen in Figure 2-2. Enthalpy wheels occupy the same system location as a membrane humidifier and are the only active control option capable of recycling waste stream heat and humidity. This is achieved by transferring heat and water vapor from the humid exhaust airstream to the dry incoming airstream with a rotating wheel. The wheel contains a ceramic honeycomb structure comprised of hexagonal tubes coated with desiccant. As the wheel rotates, humid exhaust air transfers water to the desiccant and heat to the honeycomb structure. Once these tubes reach the dry air stream, heat and water vapor are transferred to the cool, dry incoming air. Humidity control is achieved by adjusting the speed of rotation;

faster speeds increase vapor transfer up to a maximum of ~50 rpm [21]. The enthalpy wheel was tested for humidification performance alongside a Perma-Pure hollow membrane humidifier and a dPoint flat plate humidifier [18]. The enthalpy wheel outperformed the passive humidifiers and was the only design to reach the target humidification levels [18].

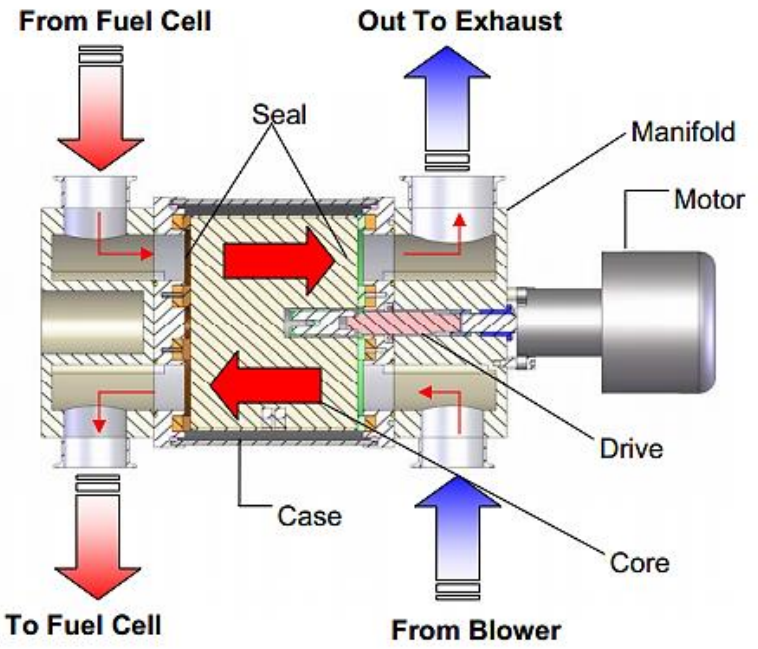

Figure 2-2. Enthalpy wheel from Emprise [21]

There are significant limitations associated with the use of enthalpy wheels, however. Enthalpy wheels are normally operated at ambient pressure and require modification with Teflon seals to reduce air leakage in fuel cell applications. Emprise reports a 1-2% rate of crossover contamination, but one group measured crossover air leaks up to 18% when using this device [18, 21]. Estimated manufacturing cost is also quite high at ~$160, three times as expensive as the estimated cost of passive options [22]. The device is also quite heavy (17 kg for the model tested by Honeywell), uses

~100 W of power and adds complexity by introducing moving parts to the humidification system [18]. Although it is the only device to meet or exceed humidification demands thus far, it will likely not be implemented due to cost and complexity [18].

2.3.2 Passive Humidifiers

There has been a trend towards overall system simplification to reduce costs and improve reliability [17]. Membrane humidifiers maximize efficiency by recycling waste heat and water leaving the cathode, transferring it through a semi permeable membrane to the incoming air stream. They also operate passively which improves reliability over systems that contain moving parts. Two types of membrane humidifiers will be discussed: hollow fiber and flat plate humidifiers.

2.3.2.1 Hollow Fiber Humidifiers/Dryers

Hollow fiber membrane humidifiers/dryers offer the benefit of passive operation with minimal maintenance and are both widely used to condition the humidity levels of air in medical and industrial applications [23]. Both hollow fiber humidifiers and dryers share the same principle of operation: air passes through a bundle of hollow cylindrical fibers that selectively transport water from a humid airstream to a dry airstream, as seen in Figure 2-3. Dryers and humidifiers can be used interchangeably: running a humidifier in reverse makes it a dryer and vice versa. The fibers are bonded together at each end of the bundle with epoxy, which is then sliced to expose the open ends of the fibers. The bundles are contained in an enclosure that directs the airstream to be dried or humidified through the hollow fibers and channels the waste stream around the fibers, depending on configuration.

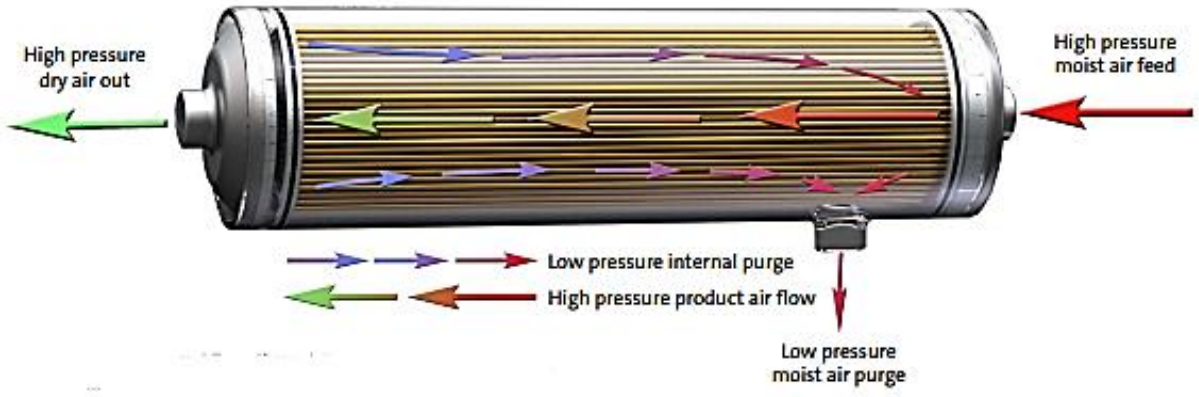

Figure 2-3. Airflow diagram of Cactus PC membrane dryer from Air Products [24]

Despite their interchangeability, humidifiers and dryers tend to have design features that separate them depending on their intended application. Dryers use either a sulfonated polymer membrane, such as Nafion, or a molecular filtration membrane [25]. Dryers with a molecular filtration membrane are classified as permeation dryers and generally use microporous membranes to preferentially permeate water molecules based on their small size. These dryers are typically used to dry pressurized gas, as they require a large pressure difference between the moist incoming air and dry purge air to function optimally [24]. In a fuel cell the inlet and outlet airstreams have a very small pressure difference (75 kPa/10 psi max), as mentioned earlier. The Cactus dryer from Air Products, for instance, is designed to operate with an air inlet pressure of 100 psi, making it unsuitable for use in a fuel cell environment [24].

Hollow fiber membrane dryers and humidifiers featuring sulfonated polymer membranes are more suited to fuel cell applications. Although their overall construction is similar, they do not require a pressure difference to function at the maximum capacity. The devices can handle two gas streams of equal pressure because water concentration, not pressure difference, is the driving force of water transfer. Perma-Pure is currently the

only supplier of Nafion hollow fiber humidifiers due to their exclusive license from Dupont [25]. A Perma-Pure Nafion humidifier, seen in Figure 2-4, shares a similar design to the Cactus dryer but contains an extra port to allow for humid exhaust recycling instead of internal purging. The largest model available is the FC600 which contains 7000 .045" OD Nafion tubes, has a volume of 5L and is capable of humidifying a 50 kW fuel cell [18, 25].

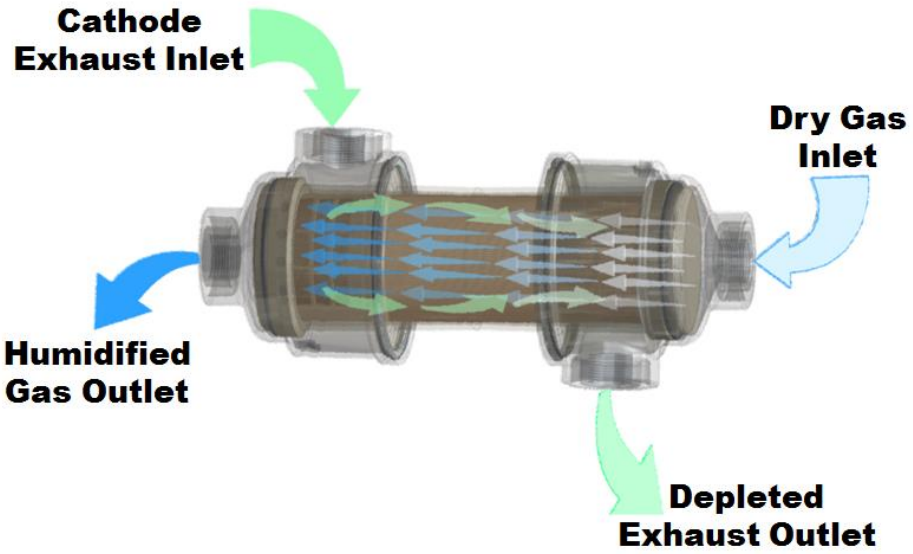

Figure 2-4. Perma-Pure hollow fiber humidifier [25]

Past DOE technology reviews focused on implementing the Perma-Pure humidifier in fuel cell performance and cost analysis, but the high cost and 90°C maximum operating temperature have opened the door for alternatives. The devices also show reduced performance over time due to anhydride formation, though that is a feature of the material used and not the humidifier design.

2.3.2.2 Flat Plate Humidifiers

Some of the humidification membranes currently in development are very thin and require mechanical support from another structure (generally polymer or ceramic) for stability. These composite membranes cannot be extruded into hollow fibers. A new flat plate humidifier geometry, seen in Figure 2-5, was developed by dPoint to accommodate these composites. A pleated design was considered during early development for increased surface area but dPoint appear to have abandoned that design in favor of a flat plate configuration.

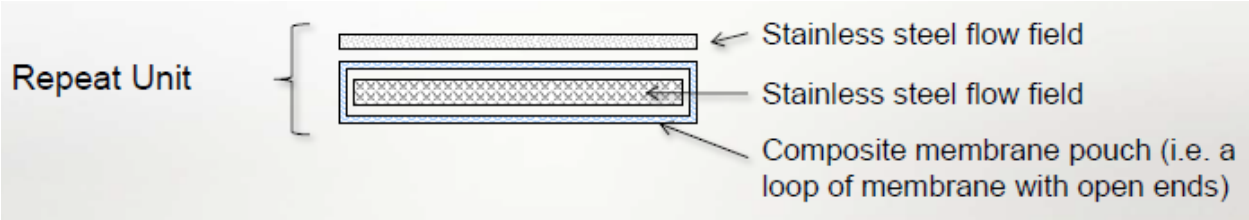

Figure 2-5. Flat plate humidifier with pouch geometry [14]

The new flat plate humidifier geometry was developed and optimized using fluid mechanics software. In essence it functions the same as a tube humidifier, but the cross section geometry has been changed from tubes into large rectangular pouches that are heat laminated together rather than extruded. Stainless steel structure provides support for the membranes and directs the flowing air. Dry incoming air flows outside of the pouch, while humidified air exiting the system flows inside. In a test conducted by Honeywell, the humidifier achieved similar performance to the Perma-Pure tube humidifier, although it takes up twice the volume at ~10 L [18].

2.4 Humidification Membrane Materials

2.4.1 Material Development Strategies

The primary performance metric for a new humidification membrane is water permeation rate, but maximizing operational temperature and minimizing cost are also important. Materials must also have a low air permeation rate, high oxidative resistance and sufficient mechanical strength to withstand pressure differences and RH/temperature cycling [26]. Membranes can generally be classified as homogenous, composite, asymmetric, ion exchange, microporous, or some combination of these, as seen in Figure 2-6 [27]. Some of the key benefits and disadvantages of these structures will be evaluated. Table 2-2 summarizes the various strategies employed to achieve these structures.

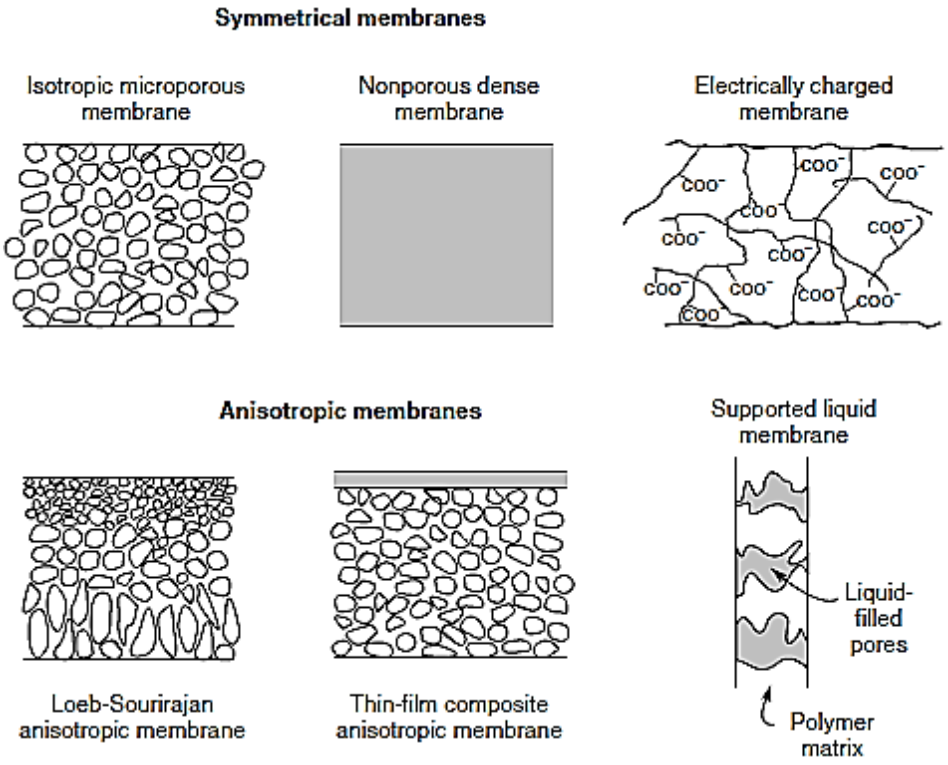

Figure 2-6. Diagram of membrane types [28]

Table 2-2. Summary of membrane development approaches

Strategy	Pros	Cons
Reduce thickness	- Increased permeability	- Reduction in tensile strength
Anisotropic composite	- Retains permeability of thin active layer - Increased strength from support layer	- CTE mismatch can induce stress and cause delamination - Swelling can induce stress and cause delamination
Mixed matrix membrane	- Higher strength - Simple fabrication - Filler can increase permeability and selectivity - Can be melt processed	- Lower permeability than thin film anisotropic - Difficult to achieve uniform dispersion - Polymer-filler interaction can be difficult to achieve
Multiblock polymers	- Potentially improved properties	- Unpredictable properties - Time consuming to develop
Sulfonation	- High water permeability - Highly selective	- Limited operating temperature - Anhydride formation concerns - Increased swelling can cause stress and rupture

One of the most common strategies used to increase water permeation rate through materials is reducing cross sectional thickness. According to Darcy's law liquid mass flow rate, Q, through a membrane is governed by

$$Q = \frac{-kA(p_b - p_a)}{\mu L} \tag{2.1}$$

where k is intrinsic permeability, A is cross sectional area, Δp is pressure drop, μ is viscosity of the fluid, and L is thickness. The simplest way to increase Q is to make the membrane as thin as possible. This approach is applicable to all membrane types, however reducing thickness comes at the cost of decreased mechanical stability [17].

One approach to improving thin membrane strength is to create a thin-film composite anisotropic membrane by fixing a thin selective membrane to a porous support structure. The support structure provides mechanical strength and the thin membrane

remains highly permeable [28]. This approach requires careful design to avoid delamination. Membrane separation could occur as a result of stresses induced by thermal cycling due to a coefficient of thermal expansion (CTE) mismatch between the active membrane and support structure. Relative humidity cycling also causes delamination due to induced mechanical stress from membrane swelling [26]. The support structure can be polymer or inorganic, with inorganic ceramic supports often employed in desalination. One method of making these composites is dip coating the porous support structure in a polymer-solvent solution. Depending on the wetting characteristics of the support structure and solution, the polymer and solvent may penetrate too far into the support structure. This can be mitigated by pre-wetting the support with water [29].

Composite materials can also be created by adding particles to a polymer to create a mixed matrix membrane (MMM) [28, 30]. Researchers have attempted to enhance membrane properties with many inorganic additives including silica, zeolite, titania and carbon nanotubes [13]. These particles interact with the surrounding polymer and have been shown to enhance separation factor, polymer free volume, and ion transport characteristics. In order to be effective, the fillers must be well distributed within the polymer; often additives will prefer to aggregate rather than bond to the polymer and require surface functionalization to disperse [13]. Amphiphilic surfactants can be useful in this regard, as they have both hydrophilic and hydrophobic properties that allow them to bond to the base polymer and additive [13].

Another strategy to meet both water permeation and strength requirements is to blend hydrophobic and hydrophilic polymers. Hydrophobic polymers generally have high crystallinity and therefore superior mechanical properties compared to hydrophilic polymers at increased temperature [26]. Hydrophilic polymers have superior water transport characteristics. Combining the two can result in a permeable polymer capable of

operating at higher temperatures. Schult et al. blended hydrophobic polysulfone (PSF) with hydrophilic water-soluble poly (vinyl pyrrolidone) (PVP) to enhance water sorption and permeability [31]. Weight loading had to be limited to 40% PVP as greater loadings caused phase separation and loss of PVP by liquid water. Similar results were achieved by mixing polyethersulfone (PES) with up to 20% polyethyloxazoline (PEOX) [32].

Another approach to increasing water permeation rate and selectivity is adding sulfonic, carboxylic, or phosphoric acid sites to make a polymer more hydrophilic [12, 13]. The most common process is sulfonation, which replaces a hydrogen atom on an arene with a sulfonic acid group, as seen in **Error! Reference source not found.**. This an be accomplished either through copolymerization of a sulfonated and non-sulfonated polymer or through polymer sulfonation. Copolymerization offers better control of sulfonation and can create ordered water channels between hydrophobic and hydrophilic domains [13]. The placement of sulfonic acid sites during sulfonation is dependent on the method used as well as the polymer structure [13]. The degree of sulfonation can be controlled by the agent concentration, exposure time and reaction temperature [13]. In addition to water transport enhancement, sulfonation also gives a polymer desirable ion transport characteristics, as it allows protons to move between ion groups across the membrane without conducting electrons.

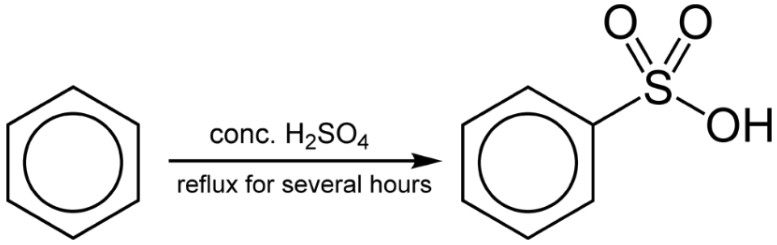

Figure 2-7. Illustration of a sulfonation reaction **[33]**

However, sulfonated materials often suffer mechanical failure due to mechanical stress induced during relative humidity cycling. This stress may be induced by material swelling due to movement of sulfonated ion groups during water transport. Swelling can be reduced by increasing polymer free volume or crosslinking, but crosslinking increases brittleness [13]. Some polymers do not respond well to sulfonation, and lose mechanical strength or become water soluble [12]. The possibility of desulfonation also limits operational temperature. Increasing polymer free volume also tends to increase water permeation rate [31].

2.4.2 Established Materials

2.4.2.1 Nafion

Nafion was developed by DuPont in the 1960's to process chlorine and caustic soda [34]. It has excellent water and ion transport characteristics that have made it the most commonly used material in fuel cells [35]. Nafion is classified as sulfonated tetrafluoroethylene, consisting of a hydrophobic PTFE structure supporting sulfonated ion side chains [36]. This combination of hydrophobic backbone and hydrophilic side chains results in highly ordered water transport channels that reduce swelling and increase water transport [13]. It is initially hydrophobic when dry but becomes hydrophilic as water contact draws sulfonic acid domains to the material surface, as seen in Figure 2-8 [36]. Sulfonic acid domains provide the means of water transport through Nafion, and as they move to take on water Nafion swells. As a result there is no convective water flow across the membrane [35].

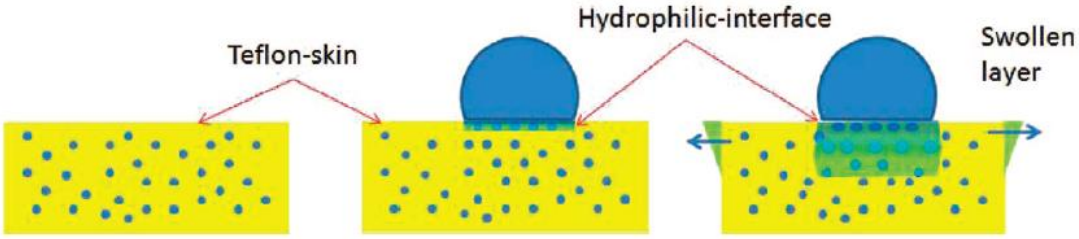

Figure 2-8. Nafion swelling in response to water exposure [36]

The exact structure of Nafion is a topic of debate because it is very difficult to image. Part of the difficulty in imaging Nafion arises from the fact that its structures span multiple size domains; Small-angle X-ray scattering (SAXS) has shown a distance of ~5 nm between hydrophilic domains, while the crystalline Teflon backbone is much larger [35]. Further complicating matters are the conformational changes the structures undergo when exposed to water as Nafion swells. One of the proposed Nafion structural models, the cluster network model, can be seen in Figure 2-9. Despite the presence of well-ordered water channels, there is still a large shift in domain size and subsequent swelling when Nafion is exposed to water. Alternating hydrated and dehydrated states result in significant mechanical stress from relative humidity cycling during fuel cell operation. A standard DOE mechanical stress test demonstrated Nafion failure after ~3500 humidity cycles [37].

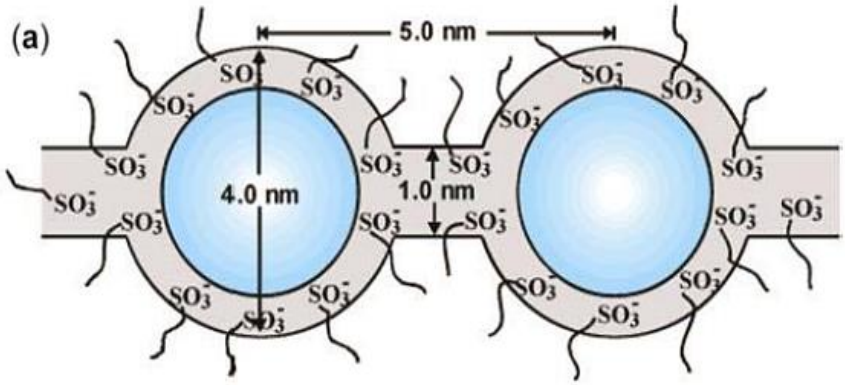

Figure 2-9. Nafion cluster network model [38]

Nafion has a maximum operating temperature of ~100°C, after which it becomes difficult to maintain membrane moisture content [39]. Even if moisture content is maintained, the material begins to decompose at 110°C due to the glass transition temperature of its PTFE support structure [39]. Furthermore, anhydride formation occurs due to oxidation under normal fuel cell operating conditions an can result in performance decreases of up to 70% [8]. Researchers have developed a variety of inorganic Nafion composites to increase maximum operation temperature [38]. These Nafion composites show improved performance in some areas but generally have reduced water transport characteristics and proton conductivity because the composites contain fewer sulfonated groups [39]. A new material is required to improve maximum fuel cell operational temperature and overall reliability.

2.4.3 Materials in Development

2.1.1.1 Gore M311

W. L. Gore & Associates is developing a high water flux membrane to be used in fuel cell humidification applications. They have combined an unspecified 5 micron thick PFSA ionomer membrane with ePTFE backing layers for support. The material is very thin to increase water flux rates, but needs to be supported due to lack of mechanical strength, making this a thin-film composite anisotropic membrane. According to James et al., the steps most likely used to create the thin ionomer membrane structure are to unroll ePTFE layer on Mylar® backer, die-slot coat layer of ionomer onto ePTFE, unroll second ePTFE layer onto ionomer, pass through continuous curing oven, laminate with PET layer, and wind onto roll [14].

Initially, Gore tried coating the ionomer on ePTFE then Mylar. Eventually they settled on a sandwich structure, seen in Figure 2-10. A diagram of the final structure can be seen below in Figure 2-11.

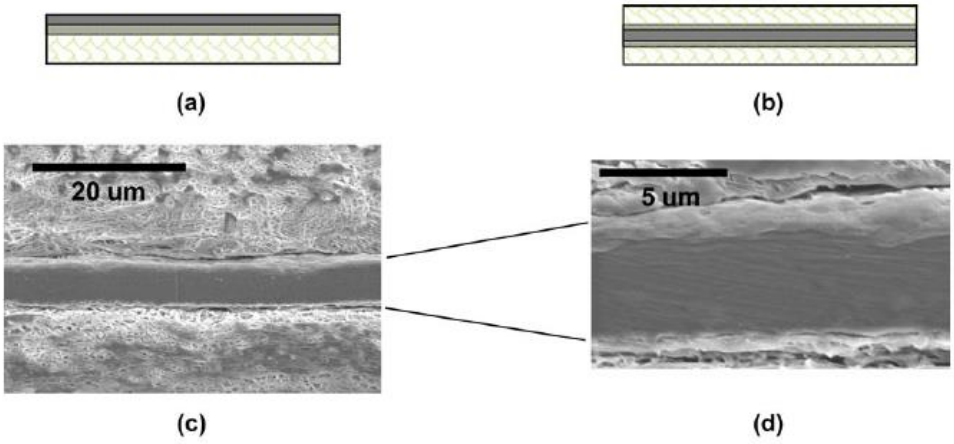

Figure 2-10. Ionomer on microporous substrates, seen in (a) and sandwich form seen in (b). The 5 micron ionomer layer is more clearly seen in (c) and (d) [40]

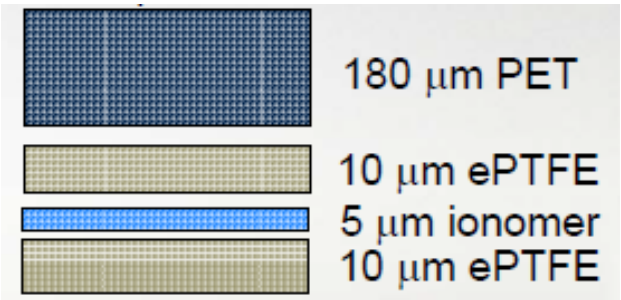

Figure 2-11. Diagram of composite membrane [14]

Gore has been able to achieve high flow rates with M311, but available information is limited because the material is proprietary and currently in development. Objective Initial testing shows the material suffers from degradation at temperatures above 80°C due to ionic species contamination and formation of sulfonic anhydride [15]. A lower operating temperature than Nafion is undesirable when fuel cells will need increased operating temperatures to increase efficiency.

2.4.3.1 "PFCB" Material

Tetramer is working in conjunction with the DOE to develop new humidification membrane materials. Their approach is to use something they call "PFCB polymer technology" to combine different functional groups and synthesize new polymers capable of meeting the demands placed on humidification membranes. They categorized these demands into four groups: water permeability, mechanical strength, stability and processing. Their approach to meeting each of these needs can be seen in Figure 2-12.

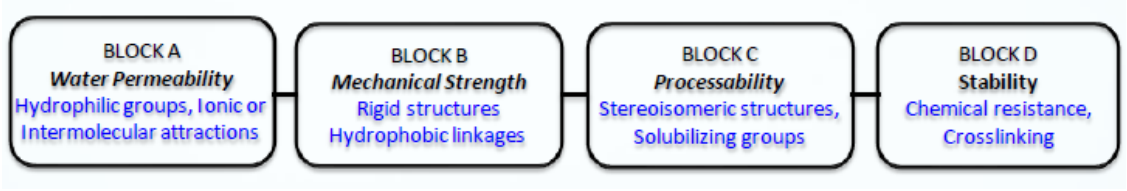

Figure 2-12. Tetramer approach to synthesizing new humidification membranes [8]

As a result they have synthesized 15 new monomers and 26 new polymers with the goal of providing multiple water transport pathways and reduced degradation [8]. The best result achieved is testing for 240 hours at 80°C, 95°C and 4 hours at 140°C with no anhydride formation detected. Water permeation testing produced a value of 2.58g/m^2*s, although little information was given about testing conditions. However, like the Gore membrane the Tetramer membrane cannot operate above 100°C over extended periods of time. Like Nafion, mechanical stress cycling due to relative humidity changes generated leaks and the material no longer functioned as a barrier to gas. Their initial analysis indicates the residual solvent (dimethlyacetamide) is to blame and are exploring other solvent options.

2.4.3.2 Wicking Materials

A stainless steel passive wicking humidifier was proposed for use in fuel cell applications by TeGrotenhuis et al [41]. The design uses Pall Supramesh, a material made from stainless steel powder sintered to stainless steel woven wire mesh, as a humidification membrane. The main water transport mechanism is capillary action, which drives water from the humid cathode exhaust to evaporate in the dry inlet air stream. The use of stainless steel in a thin film for humidification is counter-intuitive, but it can withstand high temperatures and is resistant to thermal and humidity cycling. Tensile test samples showed no significant change in strength after freeze/thaw cycling at 95% RH for 28 days (MIL-STD-331C) [41].

Wicking humidifiers rely on bubble point pressure to prevent air crossover between the dry and humid air streams. When porous structures and meshes are fully wetted the capillary forces between the structure and water oppose gas flow, which can be quantified as a bubble point pressure. Capillary performance in wicks is dependent on

both the effective pore radius and contact angle within the wick [42]. The effective pore radius of a mesh can be calculated by a bubble point test, where pressure difference across a wetted sample is increased until a continuous stream of bubbles forms on the other side. Effective pore radius r_c is given by

$$r_c = \frac{2\sigma \cos\theta}{\Delta P_c} \tag{2.2}$$

where σ is surface tension in N/m, θ is contact angle, and ΔP_c is capillary pressure difference in Pa. Contact angle between the mesh and fluid is measured with an optical microscope [42].

Although the Supramesh material showed promise, alternatives were sought to reduce cost and increase performance. Direct powder rolling of 430 stainless steel was explored as an alternative. Initial testing showed powder rolling could produce a material with twice the bubble point pressure of Supramesh and similar water permeability. The microstructure of the powder rolled 430 SS can be seen in Figure 2-13, produced with a thickness of .03 to .05 inches [41].

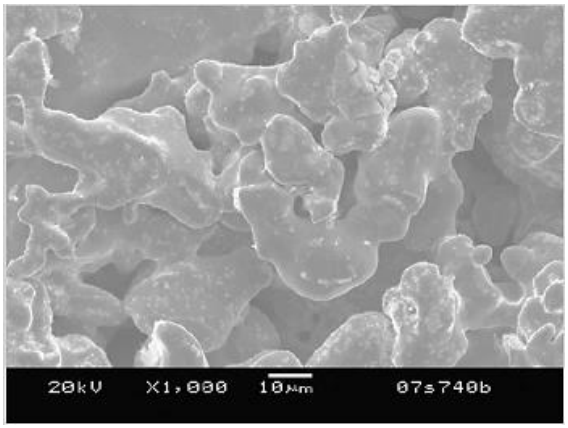

Figure 2-13. 430 SS wick structure [41]

The stainless steel wicking material was bonded together with low temperature epoxy sheets to form the channels for a flat plate humidifier. The CAD concept and

completed prototype of a 1 kW scaled model can be seen in Figure 2-14. The 3D model on the left shows a cutaway of the humidifier geometry. The grey slices are the stainless steel wicks that separate flow channels and transfer water vapor across channels. The red and blue materials are polymer spacers that bind the wicks together and define channel geometry. The colored arrows on the prototype image show the flow of heat and humidity for a counter-flow configuration. The red arrow represents warm, humid air leaving the cathode and the dark blue arrow represents cool, dry ambient air. The ambient air becomes heated and humidified before entering the cathode and the exiting cathode air loses heat and humidity before rejection to the atmosphere.

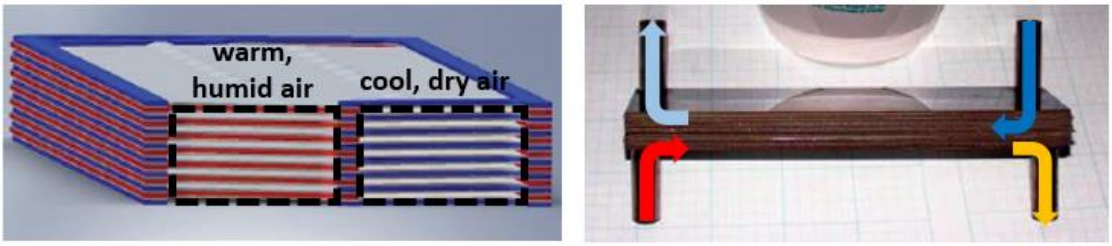

Figure 2-14. 3D Model of 1kW humidifier and image of the assembled prototype [43]

One of the main downsides to this material is the high cost of stainless steel. Material prices were estimated at $110 per device alone, driving the total humidifier cost to nearly $170. The other main drawback is that, like Nafion, the device must be wet to function as a barrier. This means significant start up time (30 minutes during testing) before optimal operation can be achieved. The startup time could be somewhat mitigated if humidifier is not allowed to dry out, however. The 80 kW mesh humidifier was projected to weigh less than 9 kg, which is less than an enthalpy wheel but above the DOE target of 5 kg [43]. While the design was not feasible, the concept of using bubble point may be applicable to future materials.

2.4.3.3 Polyamides

Polyamides are dense, nonporous membranes usually used for gas separation up to temperatures of ~70°C [27]. They are susceptible to oxidation and surface fouling which make them unsuitable for use as a fuel cell humidification membrane [27]. They are commonly used for water desalination, where the highest water flux polyamides available can achieve flow rates of ~10 g/m^2*s but require a pressure differences of 250 psi [44]. The operational temperature range is also quite low for polyamide reverse osmosis membranes. FILMTEC-30, available from Dow chemical, is a thin aromatic polyamide membrane supported by a porous polysulfone layer with a maximum operating temperature of 45°C [45].

2.4.3.4 Polyimides

UBE Industries offers a polyimide membrane designed for dehydration of solvent-water mixtures with an operating temperature of up to 120°C, but it requires a vacuum on the permeate side [46]. There is no mention of water transfer rate. Sulfonated polyimide has been investigated for use in direct methanol fuel cells (DMFC).

2.4.3.5 PDMS

Silicone is a gas permeable dense polymeric membrane with high water permeability, despite its hydrophobicity [29]. As a result, PDMS composites are often used for separation of ethanol/water mixtures in pervaporation. Permselect offers fuel cell humidifiers with hollow silicone fibers, similar in principle to the Perma-Pure Nafion humidifier. However, the system requires an external water supply and is not available for gas-gas humidification, indicating its water vapor transfer rate is too low.

2.4.3.6 Sulfonated Hydrocarbons

Various non-fluorinated sulfonated polymers have been developed as an environmentally friendly replacement for Nafion in PEM fuel cells. These polymers tend to have more swelling when hydrated and lower chemical resistance than Nafion [13].

Sulfonated poly(ether ether ketone) (sPEEK) has a higher water content, lower gas crossover and more hydrophilic domains than Nafion, yet has only demonstrated water flux rates about ~50% of those recorded in Nafion for similar material thickness [11]. Water flux for Nafion and sPEEK can be seen in Figure 2-15. The difference in water flux between the two materials demonstrates that organization of sulfonated domains is an important consideration, not just the total level of sulfonation. Furthermore, sPEEK tends to swell and dissolve under high temperature and relative humidity [11]. For these reasons, sPEEK tends to be used in direct methanol fuel cells.

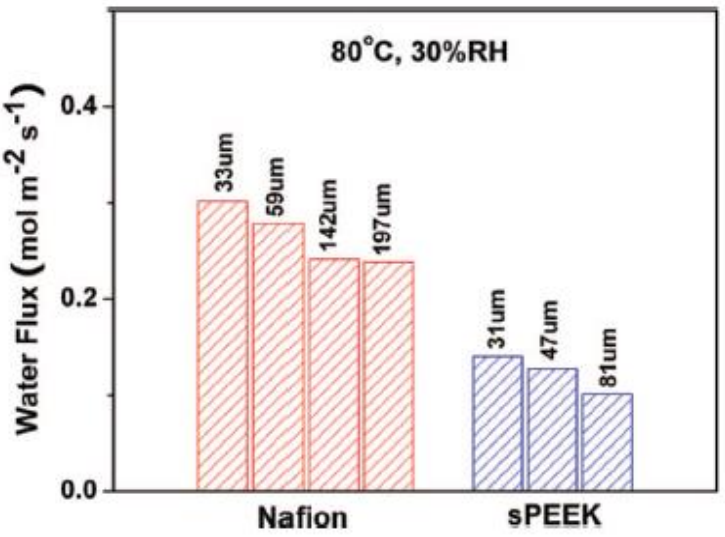

Figure 2-15. Liquid-vapor permeation of Nafion and sPEEK membranes [11]

Nexar is a sulfonated pentablock styrene based copolymer membrane from Kraton [10, 12]. There is limited information available but it appears to be a promising desalination membrane. However, water permeation rate data is only available up to

55°C, with a maximum rate of ~.8 g/m^{2}s for the MD9150 variant and ~1.1 8g/m^{2}s for the MD9200 variant [10]. These flux rates are less than half those achieved in Nafion, although the maximum operating temperature is unclear. Lower water permeability could be acceptable if it comes with higher maximum operating temperatures.

2.4.3.7 Zeolite Composites

Zeolite composites are a promising humidification membrane material, currently being researched primarily for desalination applications [47-59]. Zeolite is a naturally occurring, microporous aluminasilicate material, generally available in particulate form. Figure 2-16 shows a scanning electron microscope (SEM) image of zeolite particles, uniform in morphology and size. Zeolite is both highly permeable and selectively permeable; it has uniformly sized pores that do not allow larger sized molecules to pass through, separating them from smaller molecules [30, 47]. Zeolite pore size varies with species, making it an ideal material for use in gas/gas or liquid/gas separation [59]. NaA zeolite is a popular variant due to its hydrophilic nature, high water flux and separation factor [29].

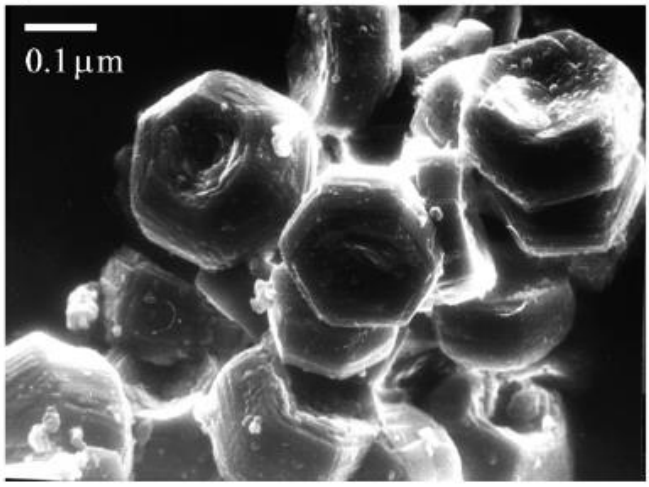

Figure 2-16. SEM image of zeolite particles [ZEO3]

Zeolites are also mechanically and thermally stable above 500°C, which makes them suited to a fuel cell operational environment [29, 30, 48]. Since zeolite is quite brittle, it is generally deposited on a support structure to create a composite membrane or used as an additive in melt processing to create a symmetric membrane [29, 47]. Composite membranes usually achieve higher fluxes than symmetric membranes in pervaporation [29]. However, the composite membranes are usually zeolite deposited onto a hollow ceramic support [29]. These composites are generally developed for desalination and water purification in order to lower the pressure difference and energy required to separate water from a given contaminant [51]. Zeolite has been combined with a variety of polymers including PDMS, EPDM, and PVA.

Zeolite can also be added to polymers to create a MMM. Gongping et al. combined zeolite with PDMS for pervaporation applications [29]. Zeolite deposited into a hydrophobic material may aggregate instead of interacting with the polymer. Gongping et al. grafted zeolite with n-octyl chains using ocyltriethoxysilane to increase polymer-filler interaction. Zeolite has also been added to a porous polysulfone support structure for

desalination [50]. The addition of zeolite into polymers can enhance gas separation properties and improve membrane water retention [27, 28].

Direct comparison between Nafion and zeolite water flux rates is difficult due to the large number of Nafion and zeolite varieties as well as the differences in experimental setups and test conditions. Zhou et al. reported a flux rate of up to 3.37 kg/m^2h of pure water through a thin zeolite membrane deposited on a support layer [48, 58]. Data from Shao et al. shows flux rates between 9 and 11 kg/m^2h for zeolite membranes, although this was for an ethanol solution at 75°C [55]. Data from Adachi et al. reported flow rates between 3 and 9 kg/m^2h for Nafion NRE211 at 70°C (after unit conversion, data estimated from figure) making the zeolite membranes competitive [60]. The flow rate of zeolite composites is often limited by the support structure, not the zeolite. A highly porous support structure could meet or exceed Nafion permeability [55].

2.5 Review of Permeability Measurement Systems

2.5.1 Gas permeation

Although detailed gas permeation characterization is not required for fuel cell humidification membrane development, it is worth examining gas permeation system construction to understand the principles of operation. There are a variety of transport mechanisms for gas transport in polymer membranes including Poiseuille flow, Knudsen diffusion, molecular sieving and solution-diffusion, as seen in Figure 2-17 [27]. Convective flow through porous membranes is described by Poiseille flow, while Knudsen diffusion occurs when the mean free path of gas is larger than the average pore radius of the material [27, 28]. Molecular sieving occurs in zeolite and other materials with very small pore sizes (5-20 Å) and is a combination of both gas diffusion and

surface diffusion in the pores. Most materials used for gas separation, however, are dense polymer membranes that transport gas through solution diffusion. Gas separation through these membranes depends on differences in solubility and diffusivity. Generally the more selective a membrane, the slower its permeation rate. Systems designed to measure gas separation membranes must be very sensitive.

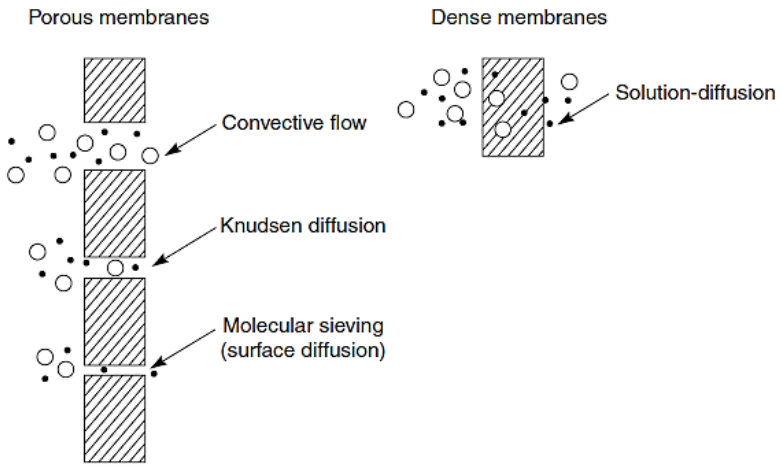

Figure 2-17. Gas permeation mechanisms through various membranes [28]

Gas flux through membranes is often measured with a permeation cell using one of two configurations: constant-volume variable-pressure or constant-pressure variable-volume [61]. Constant-volume variable-pressure systems are very sensitive and therefore more suited to measuring low flow gas barrier materials. This type of system provides upstream pressure to the membrane via a gas cylinder, and downstream pressure in a fixed container is monitored with a pressure sensor, as seen in Figure 2-18 [62]. A vacuum pump is used to evacuate the entire system before experiments, at which point the leak rate is measured [61, 62]. Pressure downstream must be kept low to maintain a constant pressure difference across the membrane, which means choosing the correct downstream container volume [61]. Koros et al. fitted their permeation system with a

ball-bearing pressure relief valve to prevent pressure transducer damage in case of membrane rupture [62]. The entire system is either temperature controlled in a chamber or submerged in water and regulated with a microcontroller connected to a heater. The constant-pressure variable-volume method is better suited to higher flow membranes, and involves pressurizing the upstream side of the membrane while using a bubble flow meter to measure flow on the downstream side.

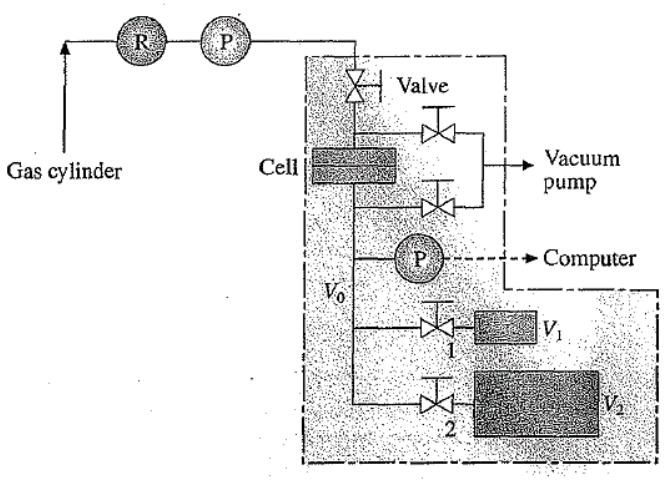

Figure 2-18. Constant-volume variable-pressure gas permeation setup [61]

As a result of the low permeability measured, gas separation membranes are very sensitive to pinhole and other defects [28]; convective flow through pores in the membrane occurs far faster than solution diffusion and prevents accurate measurement of polymer properties [61]. Thus, membranes with pinhole defects are often coated with a thin layer of PDMS to block convective flow and obtain a more accurate measurement of membrane properties [27, 28].

2.5.2 Water Permeation Measurement

There are a variety of membrane water permeability measurement systems discussed in literature; this review will focus on those that most closely mimic fuel cell operating conditions. Pervaporation systems, for instance, require a large membrane pressure differential and a vacuum applied to the permeate side. While these are indispensable for evaluating desalination membranes, they do not reflect the conditions seen during normal fuel cell humidifier operation. As discussed in the fuel cell requirements section, PEM fuel cells operate with a small pressure differential between the cathode inlet and outlet. Water transfer between the humidified waste stream and dry incoming stream is driven by water concentration difference and not pressure. Systems designed to measure the properties of Nafion have similar operating conditions to fuel cell humidifiers since water permeation in Nafion is mostly independent of pressure [35]. The driving force in these systems is water concentration difference across the membrane.

Water permeation measurement systems can generally be classified as gravimetric, isostatic or accumulation systems [61]. Gravimetric systems determine water permeation rate through a membrane by either mass loss or mass gain from a fixed container sealed by the membrane. Mass gain systems measure the mass increase of a desiccant that absorbs water transported through the membrane from the surrounding humid atmosphere. Mass loss systems operate in reverse; the fixed container holds liquid water which evaporates through the membrane into the humidity controlled atmosphere. ASTM standard E96-00 describes such systems in detail [63]. Measurement time depends on mass measurement sensitivity and membrane permeation rate, but it is typically very slow and can be on the order of days for a single test. Slow measurement time makes

these systems unsuited for rapid development of materials. A gravimetric mass loss system designed to measure Nafion can be seen in Figure 2-19.

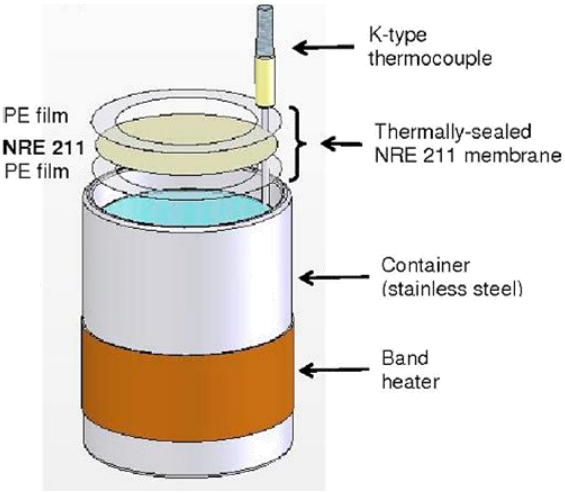

Figure 2-19. Adachi et al. steady state permeation cell [60]

Isostatic systems comprise the bulk of systems seen in literature and industry, and are generally a flow through design. Most water permeability measurement systems in literature are designed to measure steady state, one-dimensional water permeation through membranes. Liquid water or humid air is supplied upstream to the membrane and dry gas flows past the membrane downstream [64]. Such a system from Majsztrik et al. can be seen in Figure 2-20. Here, mass flow controllers modulate the upstream relative humidity by adjusting the ratio of humid to dry gas. The water permeation rate is determined based on the relative humidity increase of the downstream air and mass flow rate.

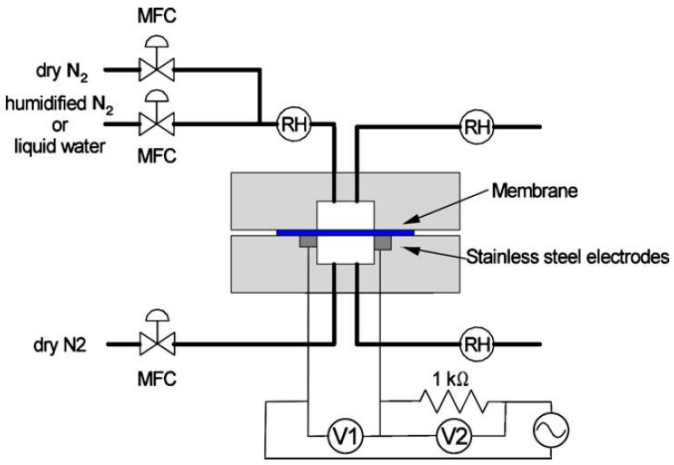

Figure 2-20. Steady state permeation cell from Majsztrik et al. [64]

Similar systems were constructed by Hussaini et al. to measure both through-plane and in-plane permeation in Nafion [65]. Since water permeation rates are low compared to the volume of air streams in most systems, it can take many hours for systems to stabilize for each measurement. Either a large membrane area or very slow air flow rate is required to obtain significant relative humidity in the downstream air. Moutopally et al. use a membrane surface area of 50 cm^2 [66]. Obtaining repeat trials and measuring different relative humidity conditions is very time consuming. Commercial isostatic systems are available from Mocon and Illinois-Instruments, but are mostly used for measuring barrier materials and packaging [67, 68]. The highest permeability that can be measured on any of the systems is 10,000 g/m^2/day by Illinois-Instruments Model L80-5000, which is far too low to measure Nafion [68]. ASTM Standards regarding isostatic systems are F1249-01 for continuous flow with an IR sensor and F1770-97 for continuous flow with water concentration sensor [69, 70].

Accumulation systems operate on a similar principle to gravimetric systems in that they rely on water passing through a membrane and entering a fixed volume. There are a few critical differences between the systems, however. Water permeation rate is

measured at a much higher frequency with a relative humidity sensor, instead of measuring mass with a scale. Relative humidity sensors are much more sensitive and therefore allow for shorter tests to be conducted. In an accumulation system there is no desiccant in the receiving volume and relative humidity in the chamber changes over time. Thus, the chemical potential driving force changes over time making the measurement transient. Although this makes measurement of direct properties more complicated, it is also closer to real world fuel cell operating conditions [71]. ASTM Standard E398 describes permeation measurement with an accumulation system and relative humidity sensor [72].

The materials of chamber construction are very important, and a variety of issues can arise during system design. Some strategies to combat error include measuring baseline leak rate and ensuring it is well below expected permeation rate. Downstream pressure is also kept far below upstream. Schult et al. designed a system to measure water vapor permeation through polymer films [73]. They outlined difficulties with designing such a system, one key being that water has "a tendency to adsorb on high energy surfaces such as glass or metal" [73]. HDPE reduces adsorption and may be a good chamber material. Schult et al. wrapped HDPE with metal tape to minimize adsorption of water while preventing air permeation [73]. Prewetting has been attempted, but does not completely eliminate measurement error. One solution for dealing with this is blank or baseline subtraction of mass. High heat of vaporization of water can also change temperature in the membrane, although a liquid feed may help negate this effect.

2.5.3 Modeling Water Transport

In addition to careful measurement system design, modeling is required to obtain membrane properties. The modeling approach selected depends on the specific system and material to be measured. The mechanisms of water transport are very different in sulfonated materials versus microporous materials. Porous media is usually modeled using Darcy's Law, as described earlier [65]. In porous media viscous forces are small compared to capillary forces making pore size and tortuosity important factors [65]. Darcy's law may be invalid at very small flow rates, so this must be taken into consideration for barrier-type materials where diffusion driven transport dominates [74].

A system designed to measure sulfonated polymer permeability often takes swelling, sorption, desorption and self-diffusion data into account [66, 75]. Many researchers also attempt to account for polymer specific interactions that depend on surface chemistry. Some polymers, including Nafion, experience a discontinuity in water uptake values for liquid water versus saturated water vapor [34]. This phenomenon is known as Schroeder's Paradox and varies for each membrane material. Water uptake is defined as the number of water molecules available per surface sulfonation site. Water uptake for Nafion exposed to humid air can be expressed by

$$\lambda_1 = (0.043 + 17.81a_1 - 39.85a_1^2 + 36.0a_1^3 \qquad (2.3)$$

where a is relative humidity. Saturated water vapor follows the relation above with a water uptake value of ~14, while liquid water is ~22.

Some models treat the surrounding interface of films as in equilibrium with the adjacent channels [66]. Each material has different surface chemistry and sorption rates that determine interfacial resistance and boundary layer characteristics. Modeling these characteristics closely is time consuming and not conducive to the development of new

materials. A visualization of water concentration in a system fitted with a Nafion membrane can be seen in Figure 2-21 [64].

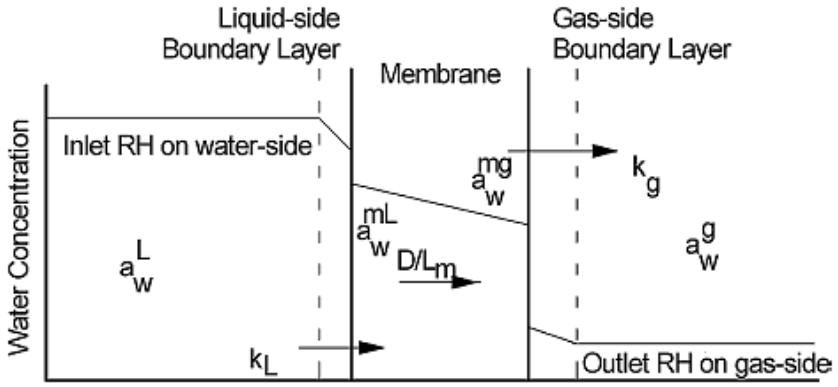

Figure 2-21. Water concentration profile in permeation system [64]

While the above equations are appropriate for modeling specific materials, a more general approach is required for a system designed to measure a wide range of membranes. Here are some guiding equations for modeling flow through an unspecified membrane in an accumulation system. Schult et al. determined a correction factor, n, that should be minimized in order to ensure the system measures membrane properties accurately. The correction factor is given by

$$n = \frac{SRTAl}{22{,}414V} \tag{2.4}$$

where S is solubility, R is the universal gas constant, A is membrane surface area, l is membrane thickness, and V is container volume [73]. Container volume can be adjusted to make n as small as possible based on the size of membrane to be measured. Permeability can be determined from the slope of the natural logarithm of left side of the following equation versus time:

$$\frac{p_2 - p_1(t)}{p_2 - p_1(0)} = e^{-Kt} \tag{2.5}$$

where p_2 is the partial pressure upstream, $p_1$is the partial pressure downstream, and K is defined by

$$K = \frac{PRTA}{Vl} \tag{2.6}$$

These equations were adapted from a slightly different type of measurement system and testing is required to find out if they are suitable for modeling a new type of accumulation system.

2.6 Conclusions

Current and target system specifications were reviewed from industry and DOE sources to clearly establish requirements for new humidification solutions. High temperature stability and ability to withstand repeated changes in relative humidity were determined to be the most important membrane properties. Review of existing humidification systems established that passive humidity recycling systems are the most likely to be employed for future use due to simplicity, low cost and efficiency. A variety of established materials and materials in development were examined. The strengths and weaknesses of each were studied with particular attention to their suitability for high-temperature operation. The approaches used to create these materials and various material structures were also examined. Each of the existing materials and methods has strengths and weaknesses. Overall, none of them can satisfy automotive humidifier requirements. For the current research, thin cross section and mixed matrix membranes were determined to be the most promising approaches as they offer increased water flux and selectivity while avoiding swelling and temperature limits imposed by thin film composites and sulfonated materials.

Both gas and water permeation systems were studied and analyzed for their suitability in new membrane development. Measurement speed and relative humidity range were emphasized over accuracy, as these help to quickly identify new potential membranes. An accumulation type system was selected as the most promising approach for this reason.

Chapter 3: Fabrication of Foamed Solvent Cast PES-Zeolite Mixed Matrix Membranes[1]

3.1 Introduction

One of the key factors impacting fuel cell cost is power density [1]. Power density can be increased by operating fuel cells at a higher temperature and pressure. Most automotive fuel cells currently on the market operate over a temperature range of 50-90°C and reach pressures up to 3 atm. Currently fuel cell humidification only accounts for <15% of total fuel cell system costs [1, 7]. However, an analysis conducted by Argonne National Labs estimated a ten-fold increase in membrane humidifier surface area is required when the exit temperature at the cathode was raised from 85°C to 95°C [5]. Although Nafion permeability increases with higher temperatures, a low glass transition temperature (T_g) of 110°C means Nafion experiences degradation of mechanical properties and becomes unusable above 90°C. Humidification costs may further increase as the DOE has targeted temperature values of 120°C for automotive applications and 150°C for stationary applications [1, 8].

Rising humidification costs and increased exhaust temperatures require the development of a new humidification membrane. Humidification membranes often consist of a thin selective layer of material bonded to a porous support structure [27]. The support structure provides mechanical support for the thin selective layer without restricting permeation. However, bonding two different polymers together can result in delamination with repeated humidity and temperature cycling due to coefficient of thermal expansion mismatch and stress induced by swelling. An alternative approach is to develop a mixed matrix membrane (MMM). The MMM approach involves combining a

[1] This chapter has been adapted from: Borduin, R., Li, W., "Fabrication of Foamed Polyethersulfone-Zeolite Mixed Matrix Membranes for Polymer Electrolyte Membrane Fuel Cell Humidification," *Journal of Manufacturing Science and Engineering*, 2017. **139**(2): p. 02100-1-7. Dr. Wei Li supervised the project.

polymer membrane with an inorganic filler material or matrix to improve selectivity and permeability. This approach has the advantage of embedding the active selection layer within the polymer to protect it from delamination. The main drawback to MMM is generally reduced permeability when compared to sulfonated materials.

Polyethersulfone (PES) was selected as the base polymer for membrane fabrication due to its excellent thermal and mechanical properties. However, like many polymers with high mechanical strength and temperature resistivity PES is hydrophobic. A common solution to this problem is chemical modification of base hydrophobic polymers through sulfonation. The sulfonation process adds highly hydrophilic sulfonated ion groups to a polymer to make it water permeable. This approach has been applied to a variety of polymers including Nafion, which has a hydrophobic PTFE backbone. The process has drawbacks, however. In addition to its low maximum operating temperature Nafion suffers from a short operational lifetime. Nafion swells when exposed to high humidity as hydrophilic sulfonated ion groups shift to the material surface [36]. Repeated humidity cycling causes the material to rupture due to stress induced by cyclical shrinking and swelling. A DOE stress test revealed Nafion fails after ~3500 dry/humid cycles [37].

We developed a MMM using inorganic fillers to improve membrane transport properties followed by solid state foaming to create a porous microstructure. The foaming process effectively embeds the porous support structure within the membrane to increase water permeability. Zeolite, a porous aluminasilicate material, was chosen for its ability to enhance permeability and selectivity in polymers [27, 28]. Humidification membranes must selectively transport water vapor from the humid fuel cell exhaust stream to the dry inlet stream while blocking crossover airflow. Zeolite has a highly uniform pore structure that inhibits transport of larger air molecules while readily adsorbing smaller water vapor

molecules [30, 47]. Zeolite is also well suited to fuel cell environmental conditions since it retains thermal and mechanical stability at temperatures exceeding 500°C.

In this study PES-zeolite membranes were solvent cast at 0%, 30% and 50% weight loadings. The membranes were then solid state foamed at two different time lengths to create a porous microstructure within the material. The membranes were imaged via SEM to examine their morphology. The effect of both foaming duration and zeolite weight loading on membrane water permeability was investigated by measuring the membranes in an accumulation type water permeability apparatus and comparing their performance to Nafion and virgin PES. The membranes were then measured for Nitrogen gas crossover to determine whether they met DOE standards for fuel cell humidification membranes.

3.2 Materials and Methods

3.2.1 Film Casting

A film-making protocol was devised to cast PES-zeolite membranes. Dimethylformamide (DMF) was chosen as the casting solvent since it is compatible with PES and commonly used for making PES films [32]. Veradel PESU A-301 pellets obtained from Solvay were vacuum-dried at 80°C for 24 hours to remove excess water. The pellets were weighed and added to DMF at 2.5% by mass then dissolved while stirred for 24 hours. Dissolving more than ~10% PES in DMF by mass resulted in a viscous solution unsuitable for casting or sonication. Type 13X zeolite powder from Sigma-Aldrich was vacuum-dried at 80°C for 24 hours and added to the PES-DMF solution at 30% and 50% by mass (relative to the PES). Relevant thermal and mechanical properties of PES and zeolite are shown in Tables Table **3-1** and Table 3-2. An upper

limit of 50% zeolite was selected because Ciobanu et al. found polyurethane zeolite nanocomposites with >50% zeolite became brittle and mechanically unstable [49]. The solution was then agitated for 30 minutes with a magnetic stir bar followed by 1 hour of sonication in a water bath to break up and disperse zeolite clumps evenly throughout the solution. Vacuum was applied to the solution after sonication to remove trapped air. The solution was cast into a PTFE dish and left to dry into films at 60°C. Lower temperatures resulted in opaque, gelatinous films due to solvent water absorption. Higher temperatures resulted in faster drying times but more visible membrane defects such as cracks and through holes. Test samples were cut from the centers of cast films and closely inspected for visible defects under a bright light.

Table 3-1. Thermal and mechanical properties of PES

Density	1.37 g/cm^3
Melting Temp.	345 °C
Glass Transition Temp.	220 °C
Tensile Strength	88.9 MPa
Young's Modulus	2.69 GPa

Table 3-2. Physical properties of zeolite

Bulk Density	0.48 g/cm^3
Density	2 g/cm^3
Avg. Particle Size	2 µm
Avg. Pore Diameter	10 Å

3.2.2 Polymer Foaming

Polymer foaming, specifically the temperature increase method, was selected to create a porous structure in the PES-zeolite membranes. Temperature increase foaming involves saturating a polymer with high-pressure gas in a pressure vessel until the desired gas saturation level is achieved, followed by depressurization and heating the polymer above its glass transition temperature for a set time [76, 77]. As the polymer is heated, saturated gas expands and desorbs from the material and forms a porous structure. Pore size and density vary with gas saturation level, foaming temperature, foaming time and desorption time. Producing foams with interconnected pores and a controlled pore size requires optimizing these parameters.

PES-CO_2 saturation was plotted versus saturation pressure in order to choose a suitable saturation pressure, as seen in Figure 3-1. Data from literature suggests pressures higher than 6 MPa provide only a marginal increase in CO_2 saturation. Our experiments (the final two data points) returned higher saturation values than predicted. Measurements were obtained by measuring the mass of thin PES films before and immediately after 72 hours of CO_2 saturation in a pressure vessel at the prescribed pressure. The discrepancy could be due to differences in sample dimensions or a shorter desorption time before sample measurement. A 9 MPa saturation pressure was selected for saturation as it was the largest feasible pressure possible with the available equipment; Krause et al. demonstrated that average cell diameter decreases and cell density increases with increasing CO_2 saturation [77].

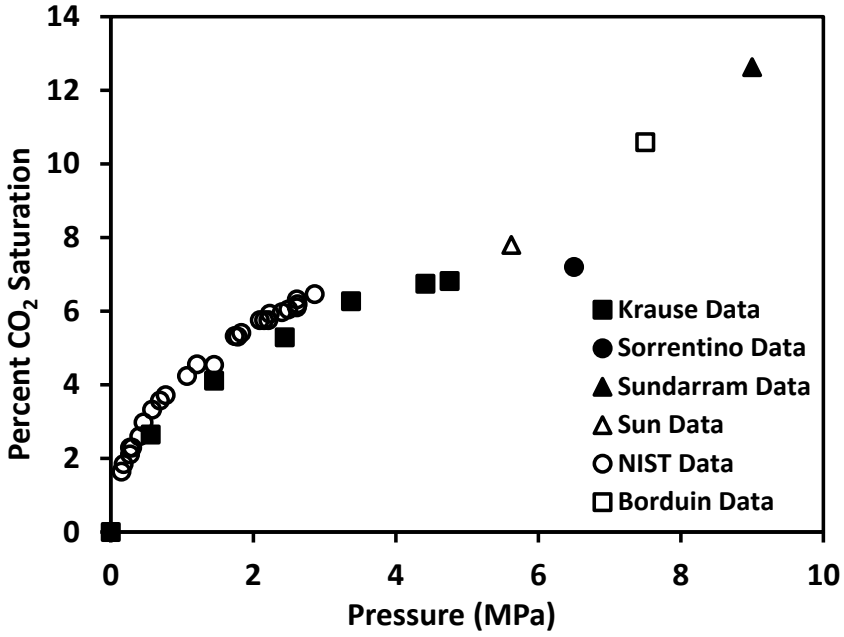

Figure 3-1. Percent CO_2 saturation versus saturation pressure for PES [78-80]

PES-zeolite films were saturated with CO_2 in a pressure vessel at 9 MPa for 72 hours. Films were foamed immediately after depressurization to minimize desorption time. Longer desorption times increase the thickness of an impermeable skin layer that forms at the exposed membrane surfaces during foaming [77]. The films were then foamed by submersion in a temperature-regulated glycerol bath at 185°C for either 1 or 3 seconds. Foams were immediately quenched in room temperature water after removal from the bath. The temperature and two foaming duration levels were selected based on both our experience with thin film foaming and preliminary experiments where foam structure was examined via SEM. Figure 3-2 illustrates the foaming process. Experimental conditions for the various samples are shown in Table 3-3.

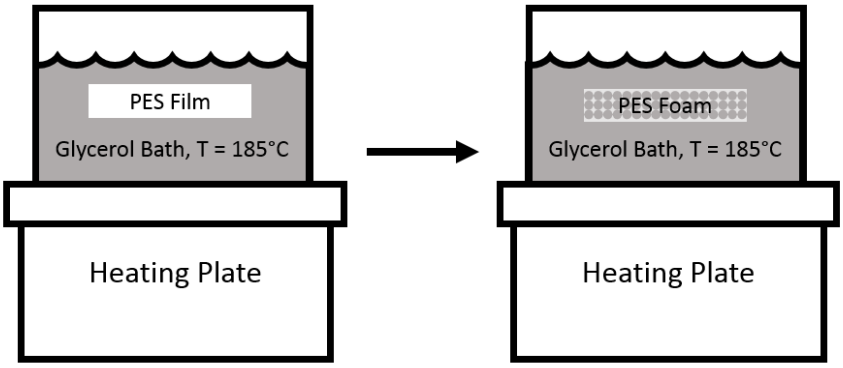

Figure 3-2. Solid state foaming process for PES films

Table 3-3. Casting and foaming conditions of samples

Sample	Zeolite Loading (% Wt.)	Casting Temp. (°C)	Foaming Temp. (°C)	Foaming Time (s)	Vacuum Applied
A	30	60	185	0,1,3	Y
B	30	60	185	0,1,3	Y
C	50	60	185	1,3	N
D	30	60	185	1,3	N

3.2.3 Membrane Water Permeability Measurement

Membrane water permeability was evaluated with an accumulation type system, as detailed in ASTM E398-13 [72]. The humidification membrane measurement, along with a labeled diagram can be seen in Figure 3-3 and Figure 3-4. Prior to conducting each experiment, dry air was circulated through the container with an impermeable membrane mounted in the system. This ensured consistent, low relative humidity conditions for each experiment by purging water vapor from the system. Next, the test membrane was secured in the system.

Figure 3-3. Image of experimental setup inside environmental control chamber connected to immersion circulator

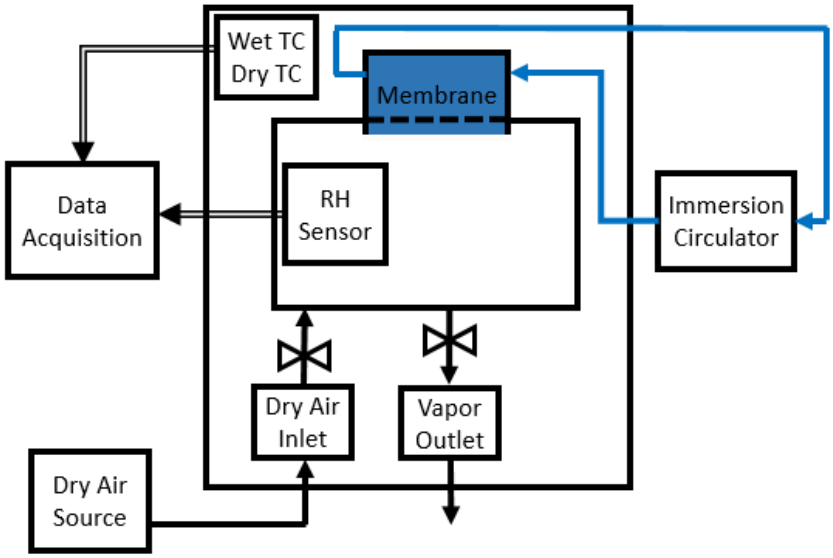

Figure 3-4. System diagram of accumulation permeability measurement system

Baseline runs to characterize systems leaks were carried out with an impermeable membrane, while calibration runs were conducted with Nafion membranes. Both the ESPEC SH-240 environmental control chamber and the Thermo Scientific Haake SC100 immersion circulator were set to the desired temperature and the environmental chamber was set at the desired relative humidity. The system was then left running for a minimum of 1 hour so the measurement system could reach the desired temperature. The quick disconnect tubes were removed next, sealing the system. The water circulation pump was switched on to provide a steady supply of water to the membrane. Data from the Omega RH-USB relative humidity/temperature sensor as well as the wet and dry bulb thermocouples in the environmental control chamber was recorded with software from Omega. Next, the system was left to run for 6 hours to continuously record data at a sample frequency of 0.2 Hz as the relative humidity in the container increased. The dry air supply was then reconnected and hooked into the water supply tubes in series to flush the system of water for the next experiment.

3.2.4 Membrane Gas Permeability Measurement

Membrane gas permeability was measured to ensure the membranes met the minimum DOE standards for gas crossover. Samples were measured in a fixed-volume variable-pressure gas permeation system as described in the Springer Handbook of Materials Measurements and Methods [61]. The test samples, shown in Figure 3-5, were mounted to brass shims with epoxy and allowed to cure. The sample was then fixed in the permeation measurement system and lowered into a temperature controlled water bath. A vacuum was drawn on both sides of the membrane for 24 hours to remove moisture and gas from the system and membrane. The system was then closed off from vacuum and the system pressure was monitored to establish a baseline leak rate. Once the leak rate

was confirmed to be on the order of 10^{-7} Torr, the upstream pressure was set to the first desired value and downstream pressure was monitored for ~1 hour. Downstream pressure was plotted against time and once it showed linearity the time constant was calculated and the experiment was allowed to run for 6 times the time constant calculated. Pressure was then increased for the next setting until all three desired upstream pressures of 5, 15 and 30 psi were tested. The procedure was then repeated for the next two samples to determine gas permeability for all test membranes.

Figure 3-5. Samples prepared for gas permeation testing

3.3 Results and Discussion

3.3.1 Morphological Results

Virgin PES films were cast and foamed as a control. The films appear free of large defects after visual inspection under a bright light and uniform both on the surface and through the cross section. A SEM image of the virgin PES film can be seen in Figure 3-6.

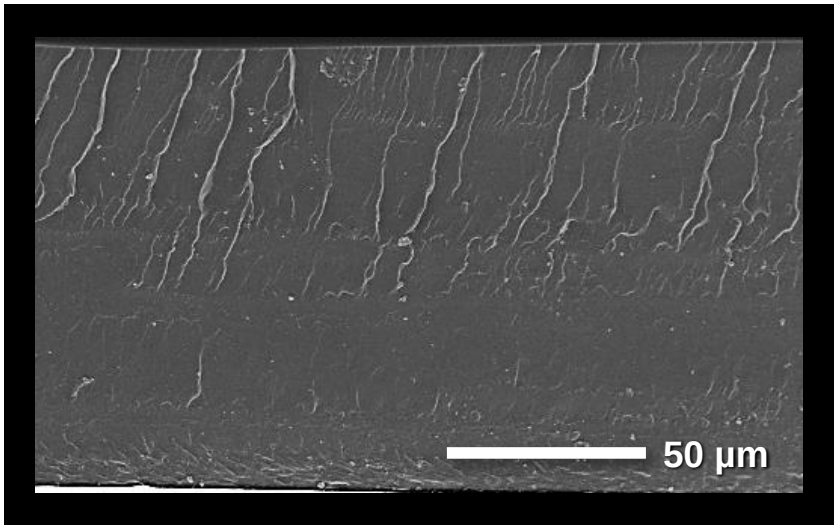

Figure 3-6. SEM of PES membrane cross section at 600X magnification with no added zeolite

Both Krause and Siripurapu reported skin layer formation during temperature increase polymer foaming [77, 81]. An impermeable skin layer forms when CO_2 desorbs from the surface of the membrane to the atmosphere after removal from the pressure vessel and during the foaming process. The skin layer formed in the virgin PES foams was ~40 µm thick, as seen in Figure 3-7. Attempts were made to reduce the skin layer formation through various means: in vessel foaming, surface area restriction, mechanical removal and solvent removal. None of these methods were successful at reducing skin layer thickness.

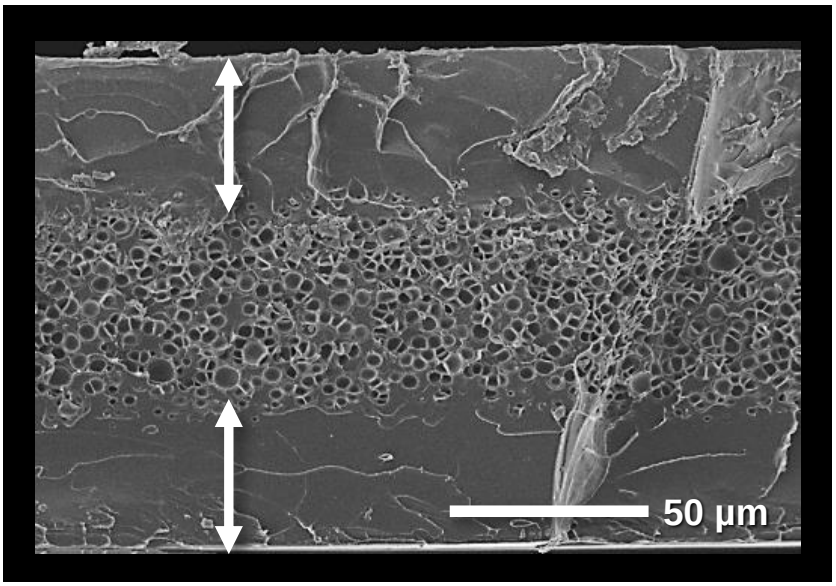

Figure 3-7. SEM of foamed PES film cross section at 600X magnification showing porous region and surrounding skin layer

Zeolite particles were relatively evenly dispersed across the x-y plane of the 30% and 50% zeolite films. The z-direction in both 30% and 50% cases shows aggregation on the bottom side of the films, as seen in all films in Figure 3-8 and Figure 3-9. Zeolite is about twice as dense as the PES-DMF solution (~2g/cm^3 versus ~1 g/cm^3) and settles to the bottom of the films during casting. A lesser number of zeolite particles are distributed throughout the upper half of the unfoamed film, visible as light gray dots. Increasing the solution viscosity and rapidly evaporating the DMF before the zeolite has time to settle could improve dispersion by slowing the rate at which particles sink. However, increasing viscosity makes casting a thin film more difficult and also reduces the effectiveness of sonication to disperse the zeolite particles in the solution.

The unfoamed 30% and 50% zeolite film morphology is shown in Figures Figure **3-8**a and Figure **3-9**a, respectively. Zeolite dispersion in the x-y plane appeared more uniform with increased weight loading because the densely clumped zeolite section

occupies more volume. However, the films became increasingly brittle with higher weight loading. The 50% zeolite film is fairly strong under routine handling, but repeated bending quickly causes the film to split and crack apart. The 30% film is more durable under routine handling.

Foaming the films greatly altered their morphology, as seen in Figure 3-8 and Figure 3-9. The sections of film with a high zeolite loading appear largely unchanged, but the less densely populated upper sections of all foamed films became highly porous. The zeolite appears to act as a nucleation agent for pore formation since some of the visible pores contain zeolite particles. The impermeable skin layer also appears much thinner in the PES-zeolite foams. The films now appear to be permeable, whereas before foaming there were large material sections with low zeolite loading and no pores to create a path for water transport. The best balance of permeability and mechanical strength likely lies at a lower zeolite weight loading with even dispersion throughout. Unfortunately there is still no method for achieving even zeolite dispersion at anything less than a high weight loading.

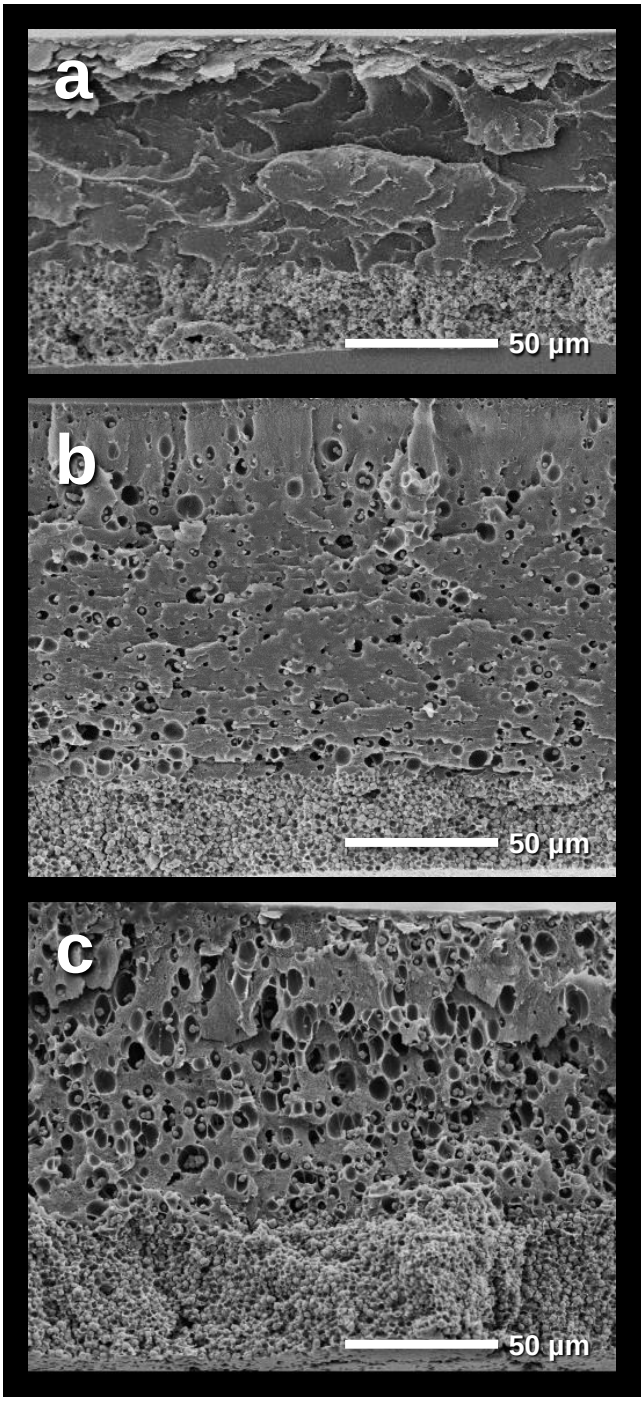

Figure 3-8. SEM of 30% zeolite film cross sections at 600X magnification for unfoamed (A), 1 second foamed (B) and 3 second foamed (C) conditions

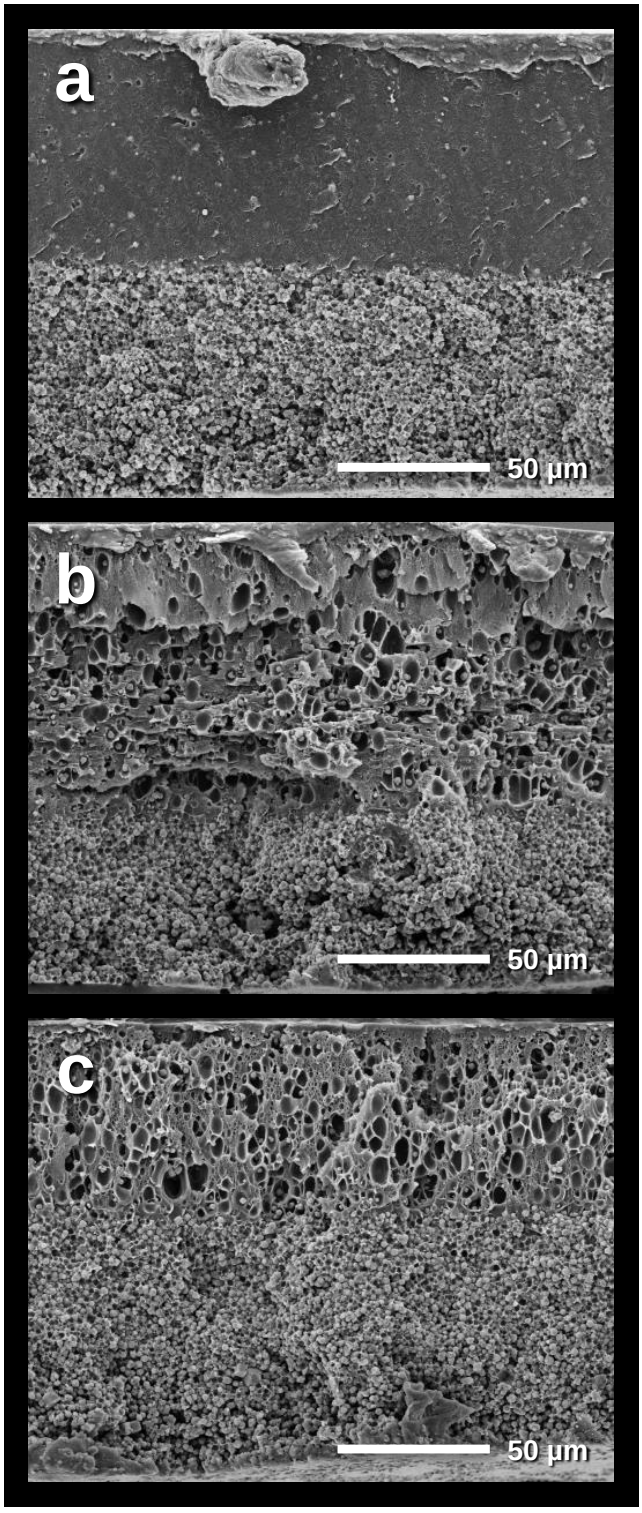

Figure 3-9. SEM of 50% zeolite film cross sections at 600X magnification for unfoamed (A), 1 second foamed (B) and 3 second foamed (C) conditions

Figure 3-8 and Figure 3-9 confirm film thickness was consistent between the 30% and 50% zeolite samples with the exception of the 30% control case in Figure 3-8a. The samples used in testing had less of a thickness discrepancy, which may be due in part to local variation inherent to the solvent casting process. However, the 30% zeolite films also expand more during foaming due to the larger porous region. The thick zeolite layer does not form any of the large pores characteristic of the low zeolite region.

Pore size and density were similar for the 1 second and 3 second foaming conditions in the 50% zeolite samples in Figure 3-9a and Figure 3-9b. The difference in foaming time was insufficient to see any large changes in morphology in this case. Visual inspection during the foaming process indicated otherwise. The 3 second foaming cases continued to rapidly release gas for the duration of their foaming, and were more deformed than the 1 second duration foams upon foaming completion. Figure 3-8b and Figure 3-8c show visibly different morphologies for the 30% zeolite 1 and 3 second foaming durations. The longer foaming time produced pores of a larger diameter and an overall higher porosity. The densely packed zeolite region is thinner in the cross section shown in Figure 3-8b. The short foaming duration may not have been sufficient to reach a high enough internal temperature for complete foaming.

3.3.2 Water Permeability Results

The effect of solid state foaming on membrane water permeability was explored by testing foamed and unfoamed samples cut from the same solvent-cast films. Each sample was measured in the system twice and then plotted as the average of the two curves. Performance comparisons can be made by comparing the relative position of each curve. The curve for a given sample shows relative humidity increase inside the measurement chamber as a result of water vapor passing through the sample; Samples with higher

permeability have a higher final relative humidity value than less permeable samples over the same time period.

The effect of foaming on permeability is demonstrated in Figure 3-10. Unfoamed samples A and B, were tested for permeability along with samples cut from the same films foamed for short (1s) and long (3s) durations. All samples in Figure 3-10 contain 30% zeolite by weight, allowing the effects of foaming on permeability to be examined independent of zeolite weight loading. Foamed sample B (3s) was damaged during gas permeability testing and could not be measured for water permeability. The performance curves strongly indicate that foaming enhances permeation performance compared to unfoamed samples. The three foamed samples lie close to one another on the plot just under Nafion. The Foamed A (1s) sample was the highest performer of all 30% zeolite membranes and achieved ~95% of the final humidity value obtained by Nafion.

The only difference between the two Foamed A samples was foaming duration. Gas foaming has two competing processes occurring at the same time: bubble growth and gas escape from the polymer sample. Initially, majority of the gas is contributing to bubble growth, leading to increased porosity. As the process continues, longer foaming times could allow more gas to escape the polymer, resulting in bubble collapse and thus lower porosity. With lower porosity, slightly lower permeability was expected. However, the proximity of the two lines indicates foaming duration effects are far less pronounced than the effects of foaming in general. Unfoamed samples A and B achieved much lower permeation rates than the foamed films and are grouped near the virgin PES film, which represents the baseline measurement value for an impermeable membrane. Unfoamed sample B lies below this line, which may be due to measurement error or a defect within the PES film.

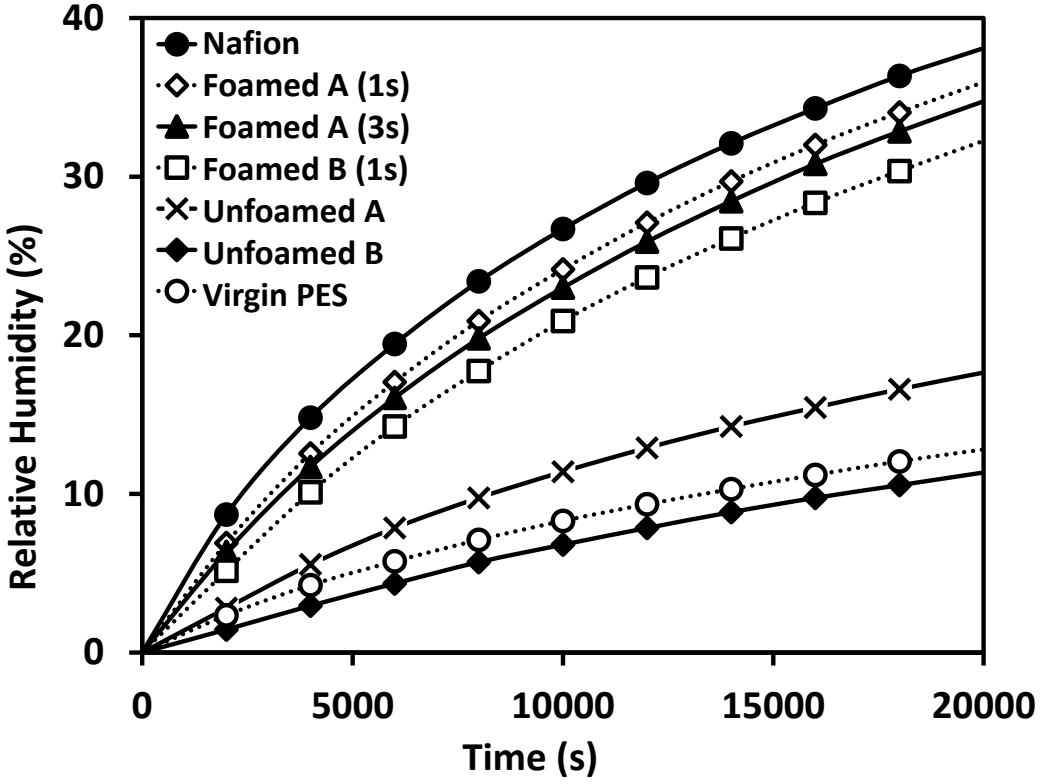

Figure 3-10. Effect of solid state foaming on membrane water vapor permeation rate

The effect of zeolite weight loading on foamed membrane permeation performance was examined by comparing foamed samples from membrane C (50% zeolite loading) to foamed samples from membrane D (30% zeolite loading). These membranes were prepared identically with the exception of their zeolite loading. Figure 3-11 shows the results of the permeation rate tests for these materials. The plot indicates that increased zeolite loading enhances water transport on the same order of magnitude as foaming. The 50% zeolite samples achieved a system relative humidity nearly double that of the 30% zeolite samples, with the Foamed C (1s) sample overlapping Nafion in performance near the end of the test. Again, the close proximity of samples foamed under the same conditions for different durations indicates foaming duration has little effect on permeability compared to the zeolite loading.

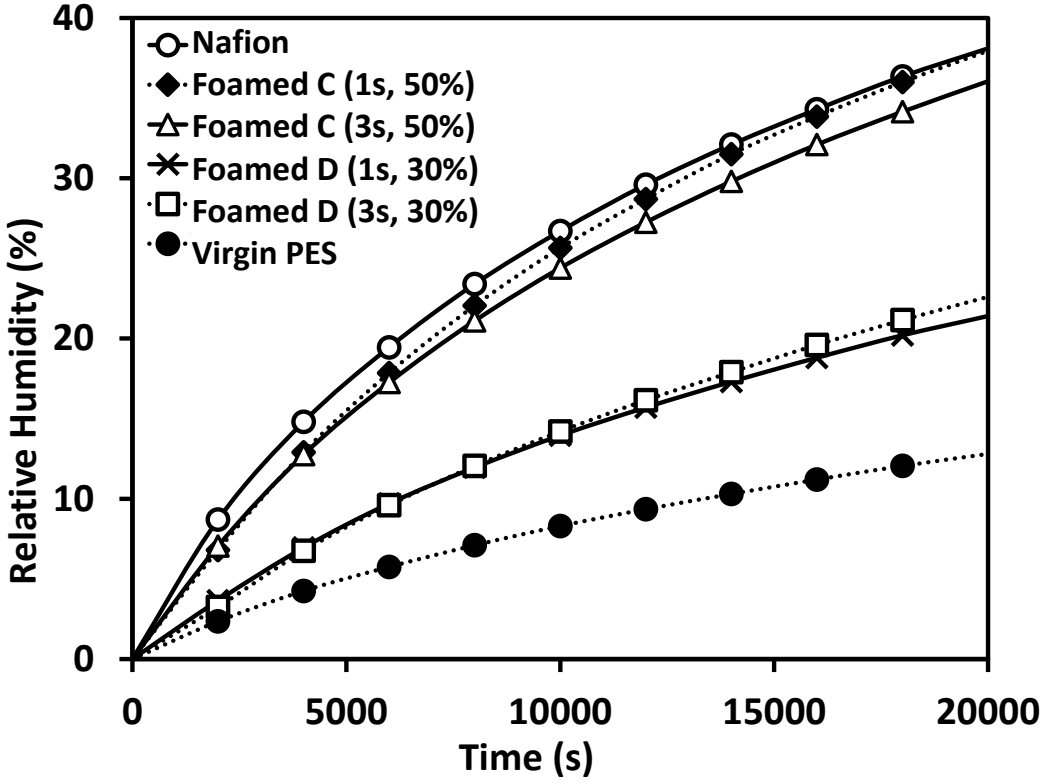

Figure 3-11. Effect of zeolite weight percent on membrane water vapor permeation rate

Measurement repeatability was quantified by a ratio between the range and expected measurement values at each time step. This ratio is represented as % *Error* and defined as

$$\%\, Error = 100 \cdot \frac{2 \cdot (Meas.\ 1 - Meas.\ 2)}{(Meas.\ 1 + Meas.\ 2)} \tag{3.1}$$

where *Meas. 1* and *Meas. 2* were the two trials taken in permeability measurements. This percent error was then averaged for all data points to calculate an average percent error for each sample. It should be noted that this percent error is not measurement error, but a measure to indicate the repeatability of permeability measurements. In our experiments, each sample was measured twice with an average error <10% across all cases except the Unfoamed B sample, which had an average error of 29.74%. This large error is due to the low permeability measurement value of the sample. While the absolute error was

comparable to those of other samples, the relative error as defined in Eq. (1) is much higher. All calculated error values can be seen in Table 3-4.

Table 3-4. Average percent measurement error across two trials for each foamed sample

Sample	Avg. *% Error*
Nafion	1.01
Foamed A (1s)	3.35
Foamed A (3s)	8.50
Foamed B (1s)	5.31
Unfoamed A	7.94
Unfoamed B	29.74
Foamed C (1s, 50%)	8.72
Foamed C (3s, 50%)	6.24
Foamed D (1s, 30%)	7.92
Foamed D (3s, 30%)	9.01
Virgin PES	7.08

3.3.3 Gas Permeability Results

The Nitrogen gas crossover rate was obtained for three foamed samples as seen in Table 3-5. Not all samples could be tested due to time and equipment usage constraints so a representative selection was measured. Samples 1 and 2 share identical foaming conditions but contain different zeolite weight loadings. Increasing zeolite loading from 30% to 50% in these samples did not affect N_2 crossover, indicating that no discernable difference on gas permeability has been caused by different zeolite loadings. Sample 3 permeability was an order of magnitude higher than the other samples suggesting longer foaming time greatly increases gas crossover. However, there is little evidence to suggest longer foaming time led to a large enough morphological change to increase gas crossover by an order of magnitude. No such difference was detected in the water

permeation experiments or seen in the SEM images. It is possible that a small leak in the epoxy seal or membrane pinhole defects caused the high readings.

Table 3-5. Foamed PES-zeolite N_2 flow rate versus upstream pressure

	N_2 Flow Rate (SCCM)		
Sample	5 psi	15 psi	30 psi
1 (50% zeolite, 1s foam)	0.04	0.13	0.31
2 (30% zeolite, 1s foam)	0.04	0.13	0.29
3 (30% zeolite, 3s foam)	0.698	1.94	4.08

The test conditions used were standard for measuring the permeability of gas barrier membranes, but the DOE standard for humidification membranes is more suited to evaluating this material. Fick's First Law was used to calculate the gas crossover rate from measured membrane permeability for comparison to the DOE standard [28].

$$Q = \frac{P(\Delta p)A}{L} \tag{3.2}$$

where Q is gas crossover rate in cm^3/s (STP), P is membrane permeability in Barrers ($l0^{-10}$ $cm^3(STP)\cdot cm^{-1}\cdot s^{-1}\cdot cmHg^{-1}$), Δp is the pressure gradient across the membrane in cmHg, A is membrane cross sectional area in cm^2 and L is membrane thickness in cm. The DOE criteria establishes 10 SCCM as the maximum allowable gas crossover for humidification membrane materials tested at a pressure differential of 5 psi [37]. Samples 1 and 2 were well below the failure criteria at all tested pressures. Even sample 3 was an order of magnitude below the failure criteria for the prescribed 5 psi test condition despite an abnormally high measurement. These results indicate the material passes the minimum initial gas crossover criteria, but more rigorous humidity and temperature cycle testing is required to characterize material operational lifetime. The DOE Membrane Mechanical Cycle and Metrics Table prescribes cycling the test membrane between 0% RH and the

90°C dew point every two minutes until gas crossover exceeds 10 SCCM or 20,000 cycles are complete [37].

3.4 Conclusions

A method was devised to cast mechanically stable, water vapor permeable PES-zeolite membranes. PES-zeolite films alone had very low water permeability, but when combined with solid state foaming, were able to achieve water permeability near that of Nafion. SEM images reveal that foamed PES-zeolite films had much thinner, if any, skin layers formed during foaming suggesting the MMM and foaming approach have a synergistic effect. The exact mechanism is unclear, but the zeolite particles are likely working as a nucleation agent to aid in pore formation during foaming. Testing in the accumulation membrane measurement system showed foaming enhanced water transport through the membranes in all cases, while the shorter foaming duration time had a minor positive effect on water permeability compared to the longer duration. Similarly, increased zeolite loading resulted in increased water permeability on the same order of magnitude as foaming.

The materials meet the gas permeability requirements set by the DOE, but likely contain small pinhole defects indicating the casting process could be further refined. High temperature membrane performance as well as humidity cycling durability still require testing to DOE standards. The materials performed well to routine handling, but become noticeably more brittle at higher than 50% weight loadings. However, it is likely that the permeability of the 50% zeolite foams can be reached by a much lower weight loading if through-thickness dispersion is improved.

Chapter 4: Fabrication of Foamed Extruded PES Zeolite Mixed Matrix Membranes

4.1 Introduction

We have previously fabricated solvent cast, solid state foamed PES zeolite mixed matrix membranes. The materials were permeable to water vapor, showing increased permeability with increasing zeolite loading up to 50% by weight. Here we have prepared PES zeolite MMM with an entirely new process, using extrusion and film pressing followed by solid state foaming.

The extrusion and film pressing processes were selected to improve on results obtained with solvent casting. Solvent film casting typically requires a large volume of solvent to ensure the base polymer is fully dissolved. Previously we used 10% PES polymer pellets in dimethyformamide, resulting in a low viscosity solution. Zeolite dispersion in solution was achieved with sonication, but the dense zeolite particles settled during solvent evaporation resulting in poor particle distribution. A number of researchers have used melt mixing without particle surface modification to achieve even dispersion of inorganic fillers in a polymer matrix [82-84].

Melt mixing was used to evenly disperse zeolite in PES at four different weight loadings ranging from 0-30%, with dispersion confirmed by SEM images of material cross sections. Solid state foaming was then used to generate a porous microstructure and make the films permeable to water vapor. The foaming process and zeolite loading showed a combined effect for water vapor permeation. Mechanical testing was performed to study the effects of zeolite loading and foaming on mechanical properties and to determine whether the films are stable enough for use in a membrane humidifier application. Finally, dynamic mechanical analysis was performed to study the effects of

zeolite loading and foaming on dynamic mechanical performance as well as estimation of high temperature stability.

4.2 Experimental Methods

Zeolite weight loadings of 0-30% in increments of 10 were selected for film preparation based on experience from preparing solvent cast PES-zeolite membranes as well as preliminary extrusion experiments. The upper limit of 30% was selected because solvent cast films beyond this loading were weak and brittle, cracking under routine handling. Furthermore, weight loadings beyond 30% pose difficulties for both extrusion and pressing due to high viscosity.

4.2.1 Melt Mixing

Veradel 3500 PES powder and Sigma Aldrich zeolite powder were pre-dried under vacuum at 135°C for 24 hours [85]. After drying, the PES and zeolite powder were weighed to correct proportions and pre mixed in 5g batches. Initially, zeolite powder was combined with PES pellets rather than PES powder, but obtaining an even mixture was difficult. Powder tended to separate from the larger PES pellets and the mixture could not be evenly loaded into the extruder. The use of PES powder greatly improved pre mixing and therefore the repeatability of the compounding process.

A Thermo Scientific Haake Minilab II, shown in Figure 4-1, was used for melt mixing. Prior to mixing, the compounder was cycled with ASACLEAN PF grade high temperature purge compound to remove residual polymer from the mixing screws. The purge compound was cycled through the compounder until the feed and extrudate material showed minimal color difference. A barrel temperature of 320°C was selected to

keep shear forces high to achieve even zeolite dispersion. Keeping the temperature at 320°C also prevented the extrudate from stretching out and changing diameter upon extrusion, as well as limiting thermal damage. Screw RPM was set as high as possible without exceeding the maximum screw torque of 5 Nm to maximize shear. Each 5g shot of material was recirculated for 2 minutes to ensure proper mixing. The compounder was then purged with the next PES-zeolite mixture to reduce possible contamination from using the purging compound. Running two full cycles of the new weight loading through ensured the first samples of each new mixture were at the proper weight loading rather than the average value of the previous and new weight loading. After compounding, the samples were immediately quenched in room temperature water.

Figure 4-1. Thermo Scientific HAAKE Minilab II micro compounder

4.2.2 Film Pressing

As extruded PES-zeolite samples were vacuum dried for 24 hours at 135°C before cutting into small pellets for hot pressing. Initial experiments were conducted to determine suitable clamping temperature, pressure and time. The extruded mixture was heated at 295°C for 2 minutes, and then pressed for 2 minutes with 5 tons of force on a

Specac Manual Hydraulic Press with electrically heated platens. The press was modified with polished stainless steel plates to protect the aluminum platens and provide a smooth surface for film pressing, as seen in Figure 4-2. These settings were held constant for different weight loadings of zeolite. The films were immediately quenched in room temperature water after pressing.

Figure 4-2. Hydraulic press and heated platens setup for film pressing

In order to prevent the film samples from bonding to the hot press plates, 1100 series .005" thick aluminum foil was used a release agent. The film was carefully peeled from the polymer films at a steep angle to prevent bending or fracturing the films. Teflon film is commonly used when pressing polymer samples, but the high pressing temperature quickly degraded the Teflon. Consumer grade aluminum foil was unsuitable since it was too fragile to peel from the polymer films without tearing.

4.2.3 Solid State Foaming

The temperature increase polymer foaming process described in Chapter 3 was used to generate a porous structure in the extruded PES-zeolite films. Temperature increase foaming involves saturating a polymer with high-pressure gas in a pressure vessel until the desired gas saturation level is achieved, followed by depressurization and heating the polymer above its glass transition temperature for a set time [76, 77]. As the polymer is heated, saturated gas expands and desorbs from the material and forms a porous structure. Pore size and density vary with gas saturation level, foaming temperature, foaming time and desorption time. The foaming process is illustrated in **Figure 4-3**.

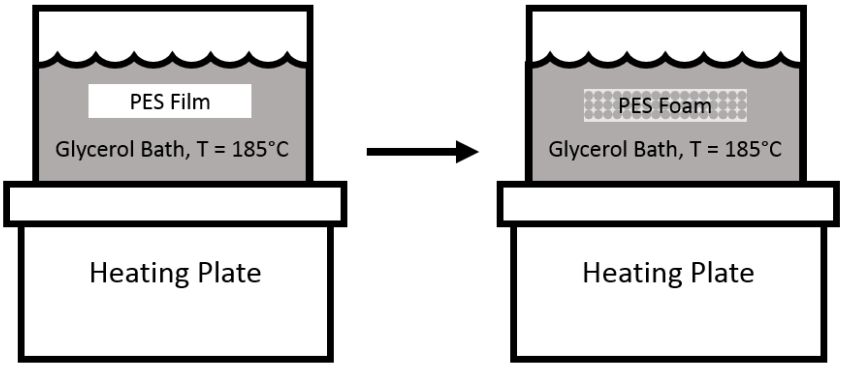

Figure 4-3. Solid state foaming process for PES films

Since the goal was to compare solvent casting to extrusion and hot pressing, the foaming parameters were held constant. Prior findings indicated little to no difference between foaming durations of 1 and 3 seconds; the longer time of 3 seconds was selected to ensure films were fully foamed. PES-zeolite films were saturated with CO_2 in a pressure vessel at 9 MPa for 72 hours. Films were foamed immediately after depressurization to minimize desorption time. Longer desorption times increase the thickness of an impermeable skin layer that forms at the exposed membrane surfaces

during foaming [77]. The films were then foamed by submersion in a temperature-regulated glycerol bath at 185°C for 3 seconds. Foams were immediately quenched in room temperature water after removal from the bath. Experimental conditions for the various samples are shown in Table 4-1.

Table 4-1. Casting and foaming conditions of samples

Sample	Zeolite Loading (% Wt.)	Foaming Temp. (°C)	Foaming Time (s)
1	0	N/A	N/A
2	10	N/A	N/A
3	20	N/A	N/A
4	30	N/A	N/A
5	0	185	3
6	10	185	3
7	20	185	3
8	30	185	3

4.2.4 Water Permeation Measurement

Membrane water permeability was evaluated with an accumulation type system similar to the one described ASTM E398-13 [72]. The humidification membrane measurement system along with a labeled diagram can be seen in Figure 4-4 and Figure 4-5. The system was constructed from Schedule 40 PVC pipe bonded with PVC cement. Threaded connections were sealed with liquid PTFE pipe sealant. Dry air was circulated through the container with an impermeable membrane mounted in the system to remove moisture before experiments and create consistent test conditions.

Figure 4-4. Permeation measurement system for film analysis

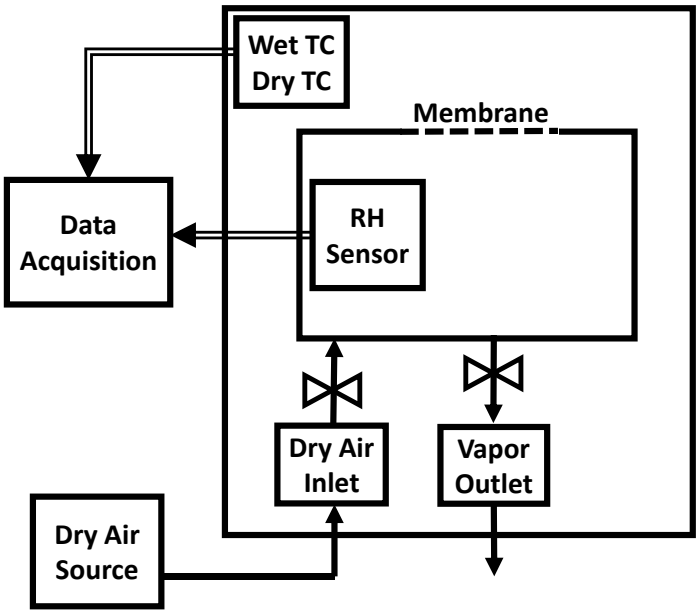

Figure 4-5. System diagram of accumulation permeability measurement system

After dry air circulation, the impermeable membrane was replaced with the desired test membrane. The ESPEC SH-240 environmental control chamber was set to 30°C and 95% RH prior to each test. The system was then left running for a minimum of 1 hour to reach the desired steady state temperature. The quick disconnect tubes were removed next, sealing the system. Data from the Omega RH-USB relative humidity/temperature sensor as well as the wet and dry bulb thermocouples in the environmental control chamber was recorded with software from Omega. Next, the system was left to run for 20 hours to continuously record data at a sample frequency of 0.2 Hz as the relative humidity in the container increased. The dry air supply was then reconnected and hooked into the water supply tubes in series to flush the system of water for the next experiment.

4.2.5 Mechanical Testing

Tensile strength was measured on an Instron 3300 series machine using the ASTM D638-08 standard [86]. The films were cut into evenly sized rectangular samples, with a test area measuring 2.54 cm long by 0.7 cm wide. The films were conditioned for 48 hours at 60% RH and 25°C. An extension rate of 5 mm/min was used. Clamping pressure was set at 50 psi after initial experimentation, as higher pressures caused film damage and premature failure at the clamp surface. Film thickness was measured in multiple locations using a micrometer and then the measurement nearest the failure location was used for stress calculations. Five repetitions were performed for each of the 8 test conditions.

4.2.6 Thermal Testing

Dynamic mechanical analysis was carried out to determine relevant thermal properties of the PES-zeolite films. A TA Instruments DMA Q800 was used for testing of glass transition temperature, storage loss and storage modulus. Test samples were cut into strips of 8 mm width with a free unclamped length of 8 mm. Samples were mounted in a film tension clamp with 5 in-lb torque, enough to prevent slipping but low enough to avoid damaging the samples. Test frequency was held at a constant 1 Hz, with 8 μm amplitude and .01 N preload force. Testing started at room temperature and ramped up to 260℃ at a rate of 3℃/min.

4.3 Results and Discussion

4.3.1 Film Morphology

Figure 4-6 and Figure 4-7 are images of the film samples as tested in the permeation measurement system. As zeolite loading increases in the unfoamed films, they become increasingly opaque. The foamed films are completely opaque and white/grey in appearance, due to the large number of pores formed during foaming.

Figure 4-6. Unfoamed PES with zeolite loadings of 0%, 10%, 20% and 30%, respectively

Figure 4-7. Foamed PES with zeolite loadings of 0%, 10%, 20% and 30%, respectively

Figure 4-8 and Figure 4-9 show the difference in dispersion between solvent cast and extruded films. In Figure 4-8, the SEM cross section shows zeolite is heavily concentrated on the bottom half of the film. The higher density of zeolite relative to the polymer solution causes it to sink to the bottom of the dish during solvent casting. Figure 4-9 shows a cross section of a PES-zeolite film containing the same 30% weight loading of zeolite. However, no large clumps or thick layers of zeolite are visible. The extrusion

and pressing process maintain a high enough viscosity to prevent zeolite from settling to the bottom of the films.

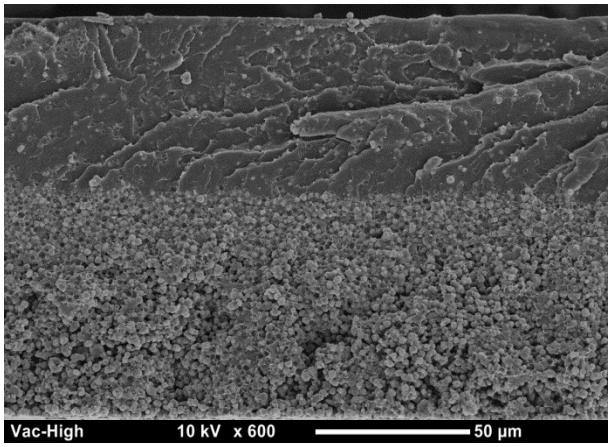

Figure 4-8. Solvent cast unfoamed PES film with 30% zeolite loading

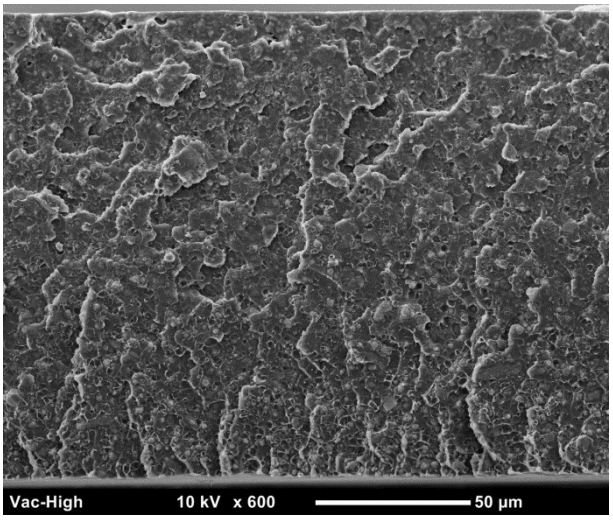

Figure 4-9. Extruded unfoamed PES film with 30% zeolite loading

Figure 4-10 shows the cross sections of unfoamed PES zeolite films from 0-30% weight loading. Each film shows even particulate dispersion. Zeolite concentration visibly increases with increasing weight loading, as expected.

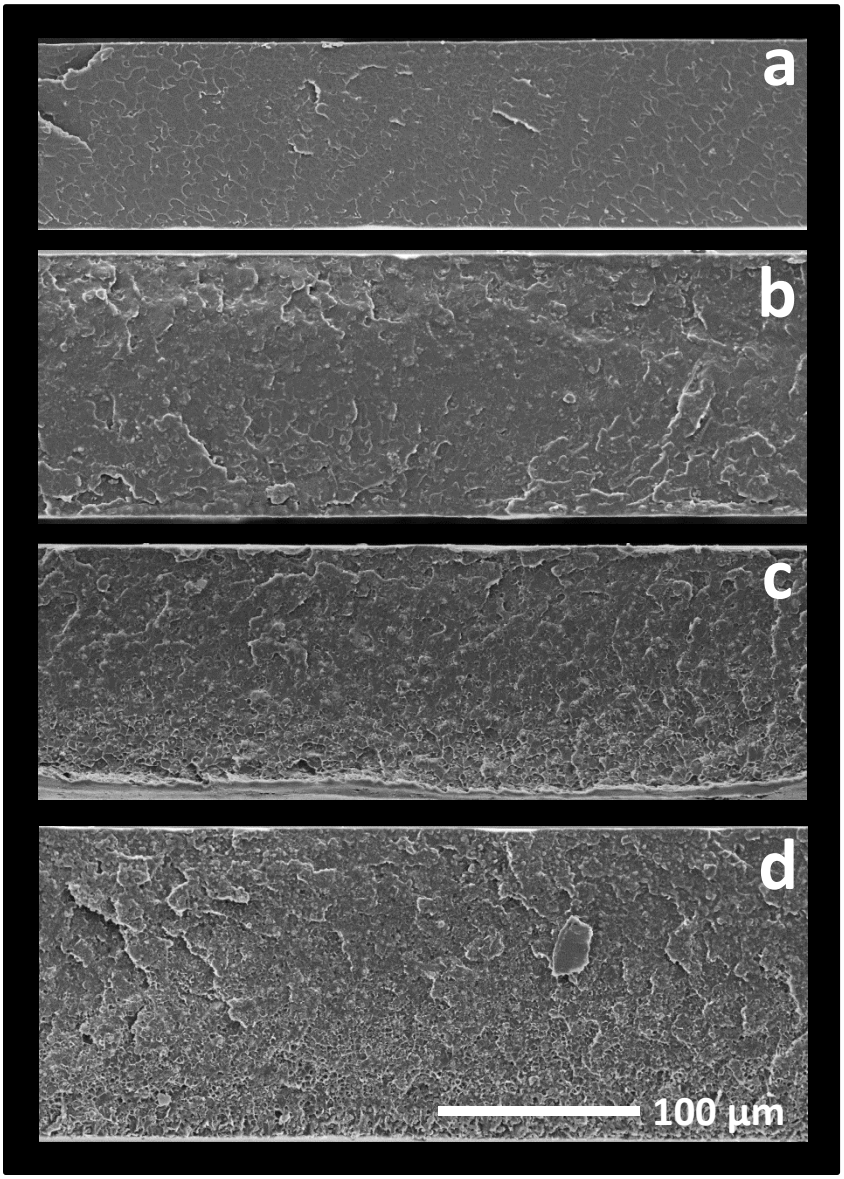

Figure 4-10. SEM cross section of unfoamed PES with zeolite loadings of 0% (a), 10% (b), 20% (c) and 30%, respectively

Figure 4-11 shows the cross sections of foamed PES-zeolite films from 0-30% zeolite weight loading. Although difficult to see, the 0% zeolite foamed film shown in Figure 4-11a has an unfoamed skin layer ~10 µm thick. This skin layer was also present in the solvent cast foamed films with no zeolite loading, due to CO_2 diffusion from the

surface of the film before and during foaming. Pore size in the 0% zeolite film is also fairly uniform and quite a bit smaller than the other films at around ~ 1 μm in diameter. Both porosity and the appearance of large pores increase with weight loading in the 10-30% films. Pore size in these films is less uniform than the 0% film. Each of the foamed films with zeolite also has a reduced or nonexistent skin layer in contrast to the 0% film. Zeolite particles are visible poking through both sides of the film and the 10 μm region near the surface of the films contains pores. Here, zeolite may serve the dual purpose of acting as a nucleating agent for the formation of pores as well as providing a path for water vapor diffusion through nonporous regions.

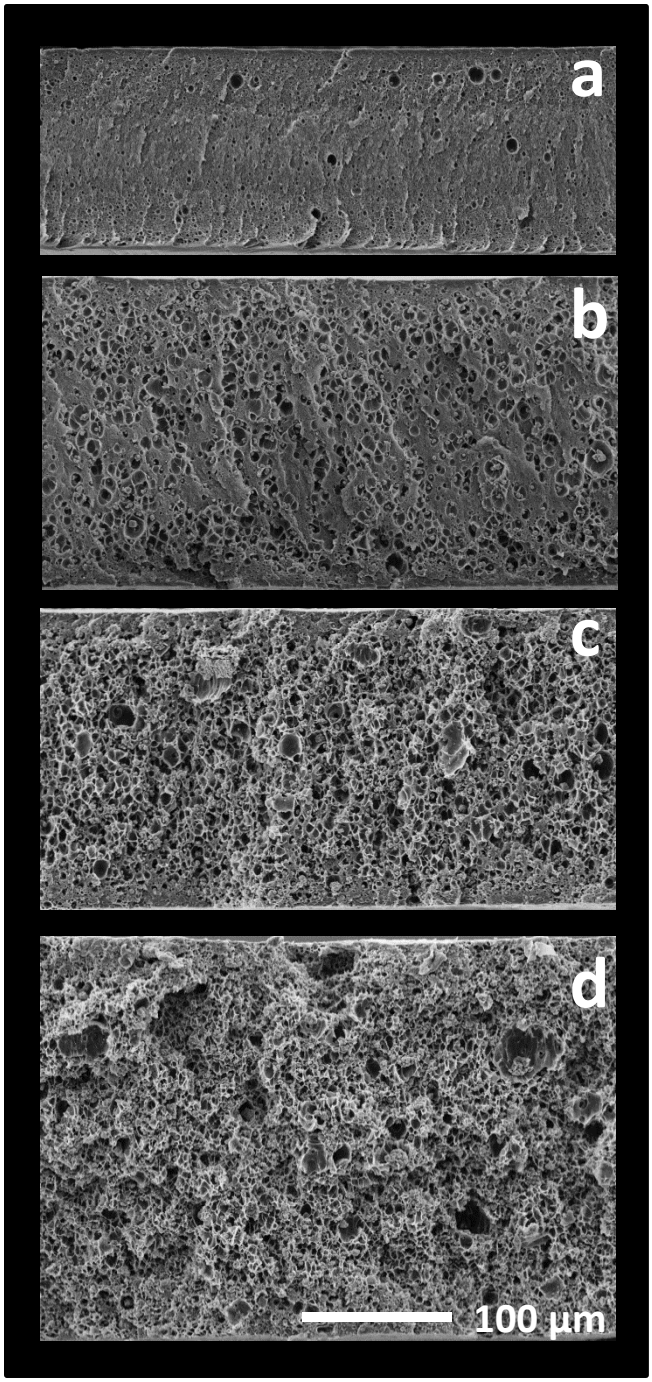

Figure 4-11. SEM cross section of foamed PES with zeolite loadings of 0% (a), 10% (b), 20% (c) and 30% (d), respectively

Sample thickness was measured at five different locations on each film with a micrometer and the average values were plotted in Figure 4-12. The micrometer applied even pressure for each measurement, which was critical for getting repeatable thickness measurements on the compressible foamed films. Thickness generally increased for both foamed and unfoamed films as zeolite weight loading increased. Increased zeolite filler raised material viscosity, resulting in films with higher weight loading being thicker for identical pressing conditions. Foaming further increased film thickness by an average of 43.6% when compared to unfoamed films, caused by expansion due to the formation of pores.

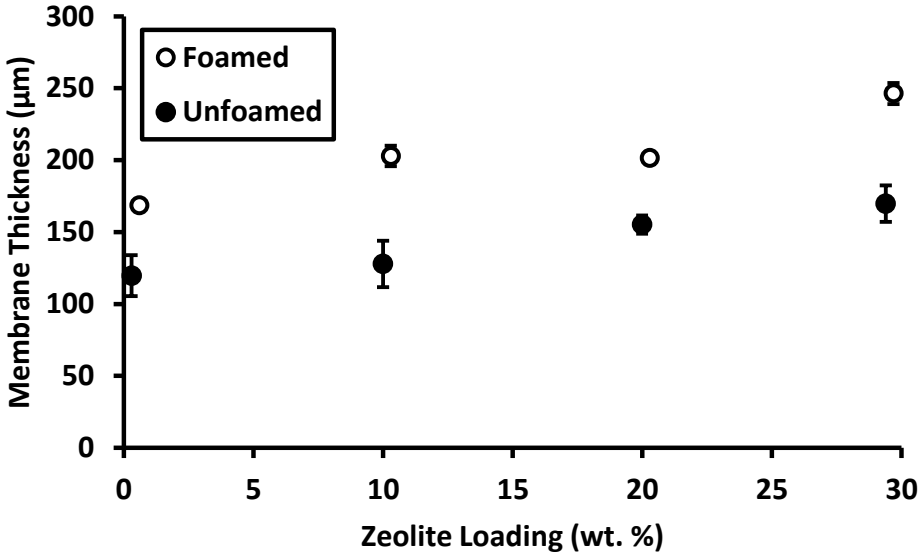

Figure 4-12. Zeolite loading versus membrane thickness, n=2

Film mass was measured before and after saturation to determine CO_2 concentration. After correcting for the average zeolite mass present in the films, there was only a slight difference in concentration between the various weight loadings. Both corrected and uncorrected CO_2 concentration are plotted in Figure 4-13. There is a slight

decrease in average corrected CO_2 concentration as zeolite loading increases. The decrease could be due to the order of sample measurement or variation in zeolite weight loading. However, nearly all the samples have overlapping error bars and the measurement differences lie within the uncertainty.

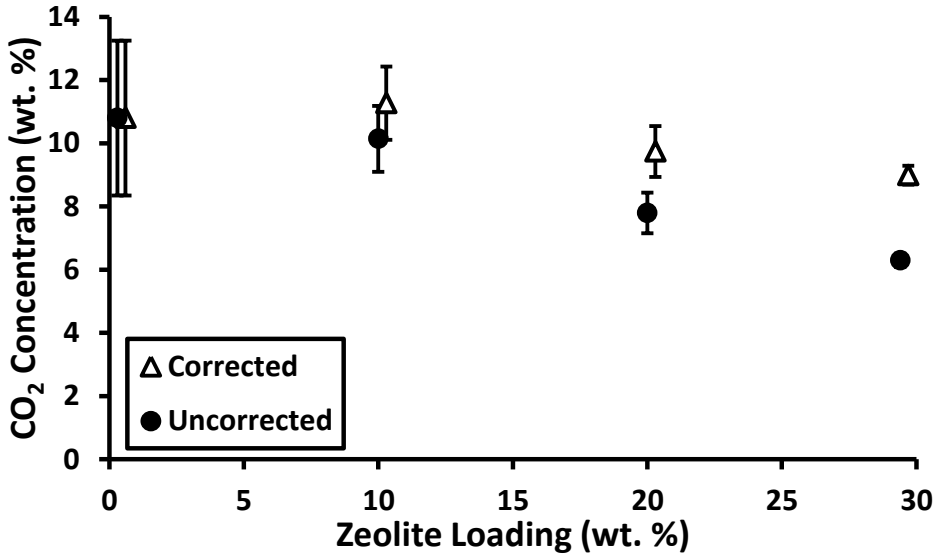

Figure 4-13. CO_2 concentration of PES zeolite films after removal from pressure vessel, corrected for zeolite loading, n=2

4.3.2 Mechanical Testing Results

The tensile strength of unfoamed samples decreases with increasing zeolite weight loading, as seen in Figure 4-14. Tensile strength drops by, 12.7%, 16.1% and 54.5% as zeolite loading increases from 0-10%, 10-20% and 20-30%, respectively. Ceramics possess a poor ratio of tensile to compressive strength, which could partially account for the decrease. Furthermore, any zeolite particles with a weak interfacial connection to the surrounding polymer would contribute to the observed trend. The first two strength

decreases align fairly well with the increase in zeolite loading, but the decrease in strength from 20-30% loading is significantly higher. The large decrease in strength suggests 30% is at or near the feasible maximum weight loading for producing usable films.

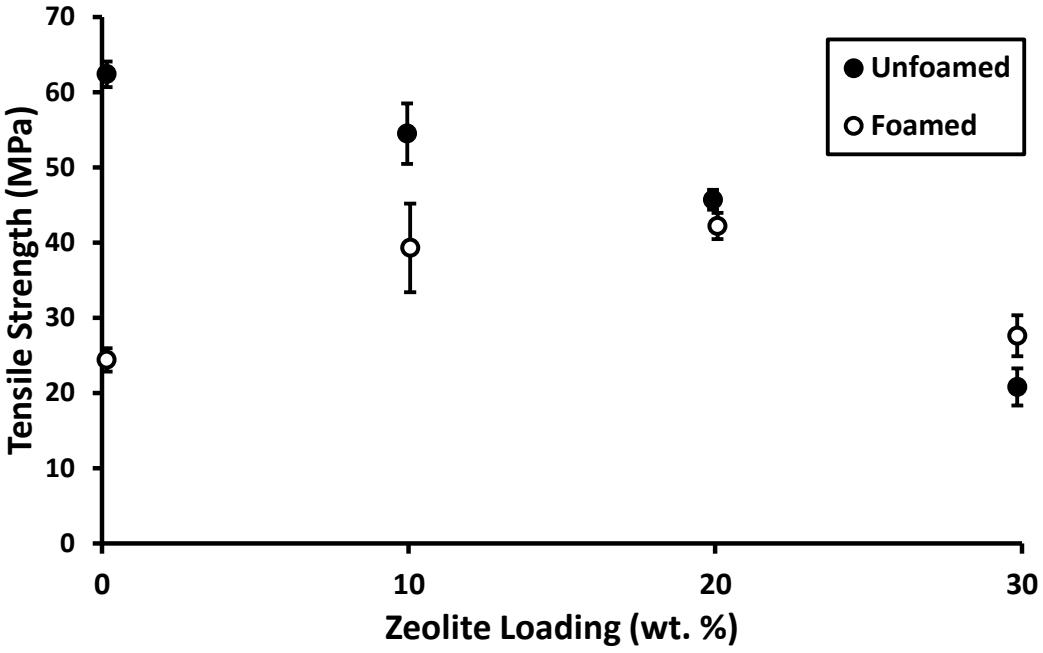

Figure 4-14. Tensile strength of PES-zeolite film samples, n=5

The foamed samples exhibit very similar strength to the unfoamed samples at the highest weight loadings of 20% and 30%. The foamed samples ranged in tensile strength from 24.4-42.4 MPa, which is very close to the 23-45 MPa listed for various types of Nafion [87]. The 0% foamed average is only 39.1% as strong as the 0% unfoamed average with a low level of uncertainty. However, this data point is deceiving. Since the virgin films were quite thin, they deformed the most during the solid state foaming process. The wrinkles formed during foaming meant it was very difficult to obtain a completely flat sample, which led to a far greater deformation with little resistance as the

wrinkles were pulled flat under tension. This trend is visible in Figure 4-15, where the 0% foamed samples have more than twice the extension at break over the 0% unfoamed samples. The large error bars indicate the wrinkling reduced the repeatability of the 0% foamed measurements.

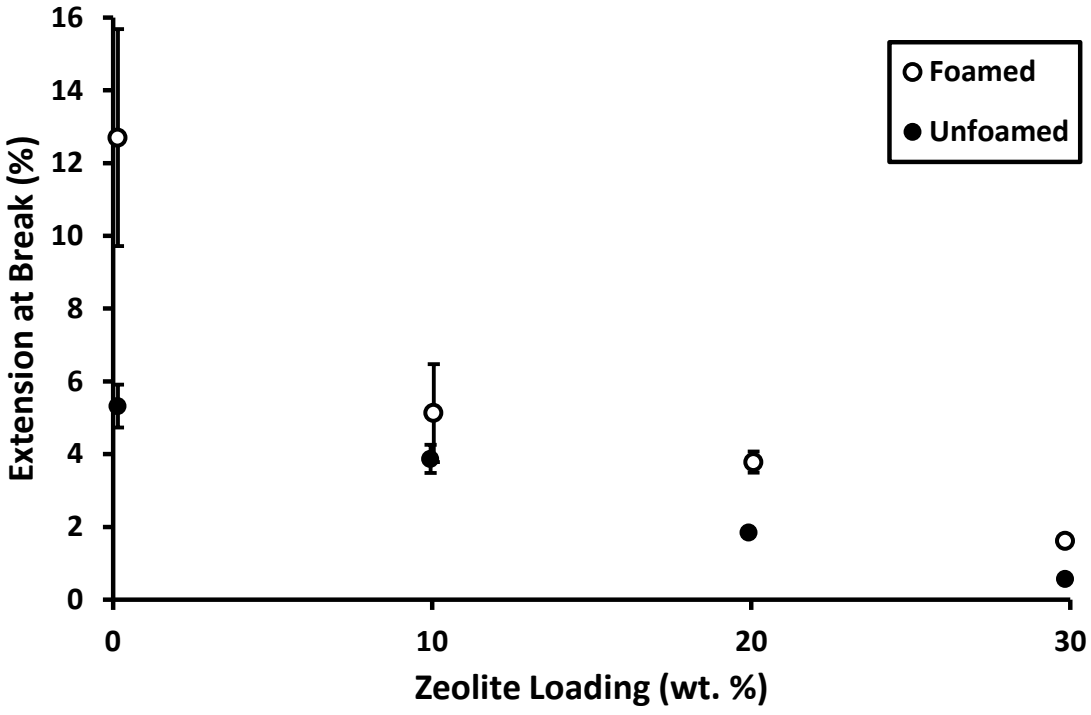

Figure 4-15. Extension at break of PES-zeolite film samples, n=5

Modulus shows a steady increase as zeolite weight loading increases, as shown in Figure 4-16. Foaming consistently decreased modulus between 42-45% for each weight loading except the first, which decreased by 79%. The consistent modulus reduction is a result of the material thickness gained from increased porosity due to foaming.

Figure 4-16. Modulus of PES-zeolite film samples, n=5

The tradeoff between modulus and extension at break is illustrated in Figure 4-17, where a representative stress-strain curve from one sample of each test condition is shown. Within foamed samples, an increase in zeolite weight loading leads to a lower extension at break and a steeper initial slope, which represents a higher modulus. The 10% and 20% foamed samples achieve higher peak stress than the 0% foamed samples due to wrinkling in the 0% foams, as discussed earlier. The unfoamed films display a much cleaner trend, with higher weight loading consistently leading to fracture at lower stress and strain values, but a higher modulus. Comparing foamed to unfoamed films shows a higher modulus across the board for unfoamed films. The increased porosity of the foamed films allows them to deform a greater distance before the polymer starts to stretch. Figure 4-15 and Figure 4-17 both show that foamed samples with a 10% higher weight loading than unfoamed samples achieve very similar extension at break, since the increased brittleness from a higher zeolite loading is offset by the foaming process.

Figure 4-18 shows a typical grouping of stress strain curves from a given test condition, specifically unfoamed 10% zeolite.

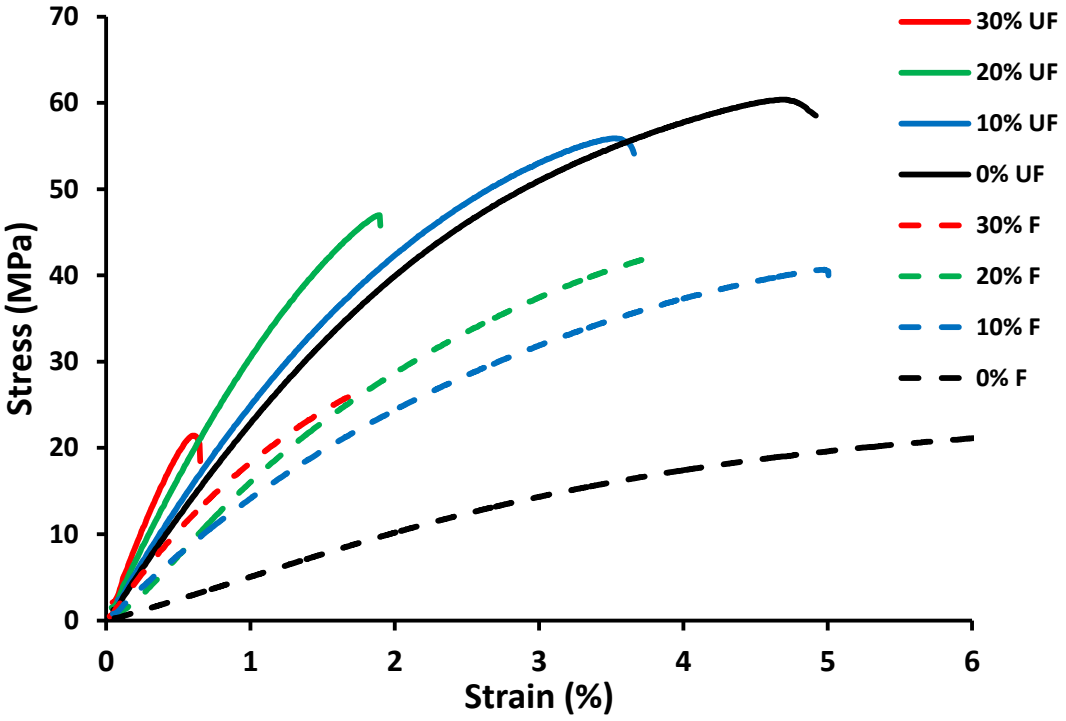

Figure 4-17. Stress-strain curves of representative PES-zeolite samples

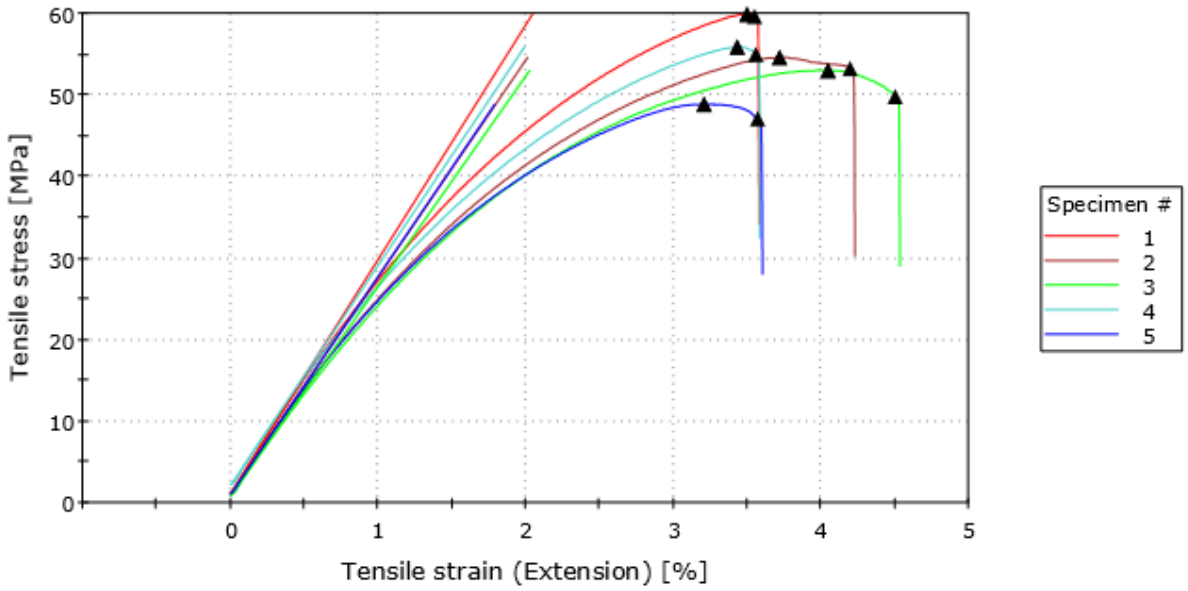

Figure 4-18. Stress-strain curves of unfoamed PES with 10% zeolite samples

4.3.3 Thermal Testing Results

Dynamic mechanical analysis was performed in order to predict performance of the membranes at high temperatures. Tan delta peak was measured for all samples to determine the glass transition temperature, T_g, where the polymer transitions into viscous, glassy behavior. All samples greatly exceeded the 105°C T_g of Nafion, with a minimum value of 240°C, as seen in Figure 4-19. This higher T_g value is required in order to surpass current fuel cell operating limits. Foamed samples had a tan delta peak 4-8°C higher than their unfoamed counterparts. Both air and zeolite have a lower thermal conductivity than PES. The unfoamed films increase in tan delta peak as zeolite loading increases. The foamed films have relatively constant tan delta peak values across all weight loadings greater than zero.

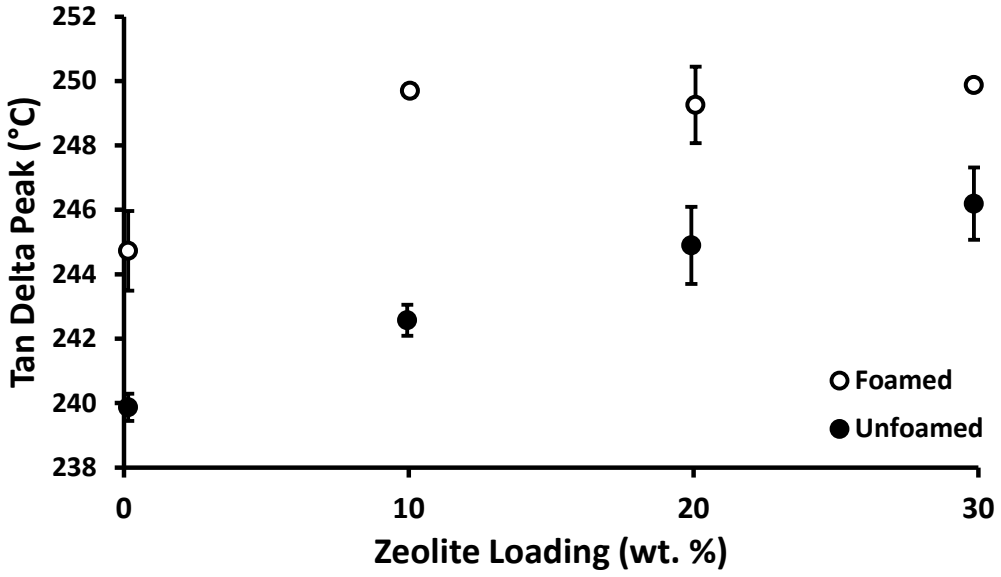

Figure 4-19. Zeolite loading versus tan delta peak for foamed and unfoamed samples, n=2

Storage modulus was plotted for all eight membrane test conditions at three temperatures of interest: 100°C, 165°C and 240°C. The low end of the temperature range was selected as a baseline performance metric, on the order of the maximum operating temperature of Nafion. The high end was selected as a value past the expected T_g, where mechanical properties begin to rapidly decline. Storage modulus is a measure of a material's elasticity or energy storage in response to repeated loading. Figure 4-20 shows unfoamed films attained a storage modulus of ~3 times that of foamed films for the same zeolite weight loading at both 100°C and 165°C. This trend is consistent with the tensile test results discussed earlier, where unfoamed films measured ~2 times higher in Young's Modulus than the foamed films (at room temperature). Interestingly, the foamed materials vary less in storage modulus across all weight loadings, and experience less of a drop in storage modulus at 240°C, where the unfoamed films drop off significantly. The plots reveal that foaming has a much larger effect on storage modulus than zeolite weight loading.

The high temperature performance of foamed films is of more interest than their unfoamed counterparts, due to their better water permeation performance. At 100°C, the worst performing foamed PES-zeolite MMM has a higher storage modulus than Nafion at 30°C [88]. Nafion storage modulus becomes negligible after 130°C, whereas the foamed PES-zeolite membranes retain an average of 91.6% of their storage modulus from 100°C to 240°C.

Loss modulus represents the energy lost due to heating, or viscous behavior. Figure 4-21 shows loss modulus for all tested materials at 100°C, 165°C and 240°C. Loss modulus was higher in all unfoamed films at the same weight loading when compared to their foamed counterparts. However, the relative magnitude of loss modulus to storage modulus was similar for foamed and unfoamed films. It is difficult to draw meaningful conclusions from the loss modulus data since the overall magnitudes are quite low and the error bars overlap on many of the data points. The clearest trend is that from 165°C to 240°C the loss modulus significantly increases for all cases as the materials transition to glassy behavior.

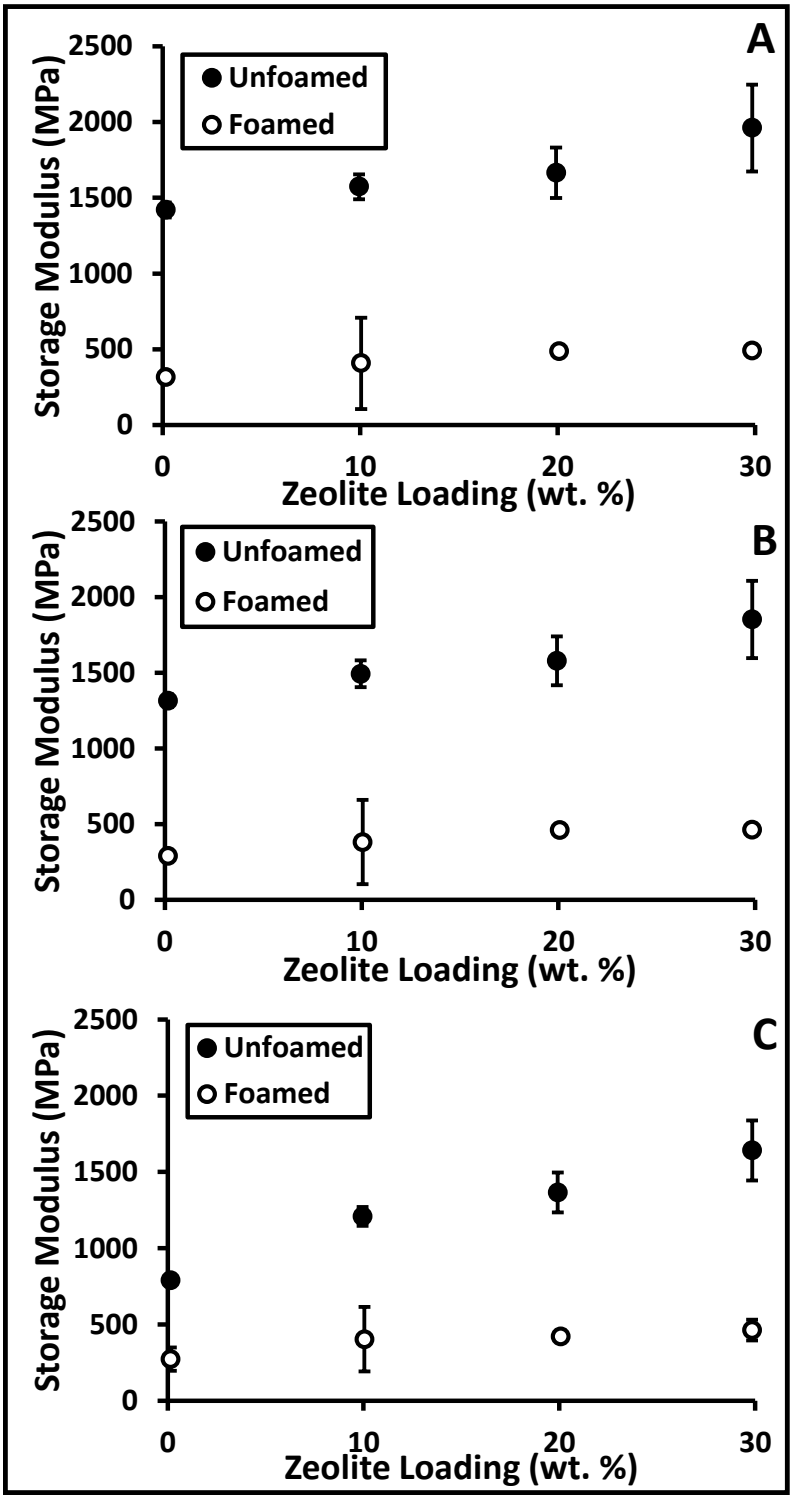

Figure 4-20. Plot of zeolite loading versus storage modulus at 100°C (A), 165°C (B) and 240°C (C), respectively

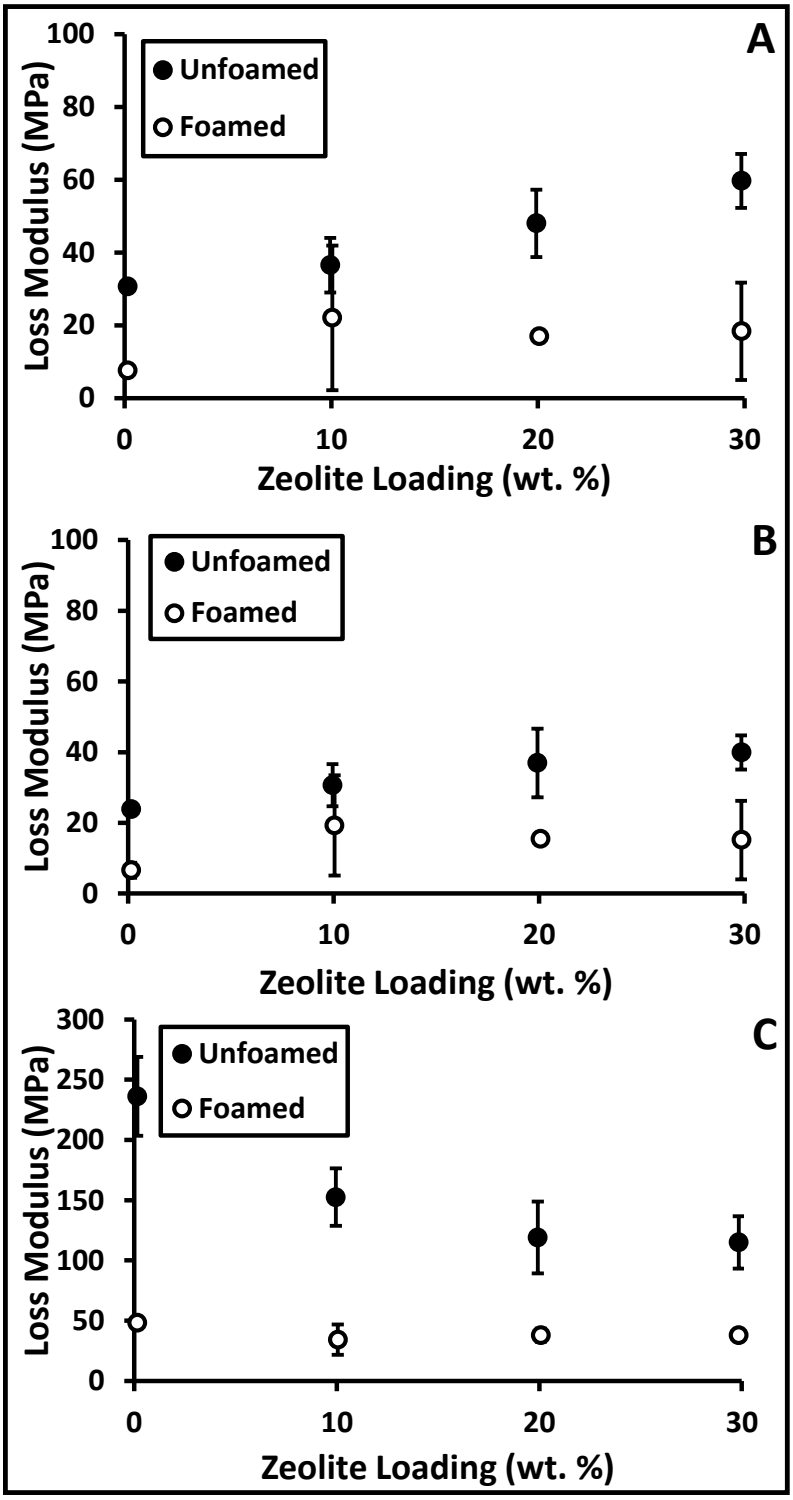

Figure 4-21. Plot of zeolite loading versus loss modulus at 100°C (A), 165°C (B) and 240°C (C), respectively

4.3.4 Water Permeation Results

Water permeation performance in terms of relative humidity increase was plotted versus time for unfoamed PES-zeolite films in Figure 4-22 and foamed films in Figure 4-23. Temperature was held constant at 30°C and the surrounding RH at 95%, thus the plot of RH% in the container represents the water vapor that has passed through the test membrane due to the RH concentration gradient. The unfoamed films exhibited low water permeability overall, with higher zeolite loadings generally increasing the final relative humidity of the system more than lower weight loadings. Aluminum foil was plotted as a baseline impermeable material. Over the course of the experiment the aluminum foil test reached a final value of 18.5% RH, which can be attributed to system leaks. The 0% and 10% zeolite unfoamed films finished slightly higher than the impermeable aluminum foil, with performance indistinguishable from one another at 29% RH. The 20% and 30% unfoamed films finished at 36.7 and 41.7% RH, respectively.

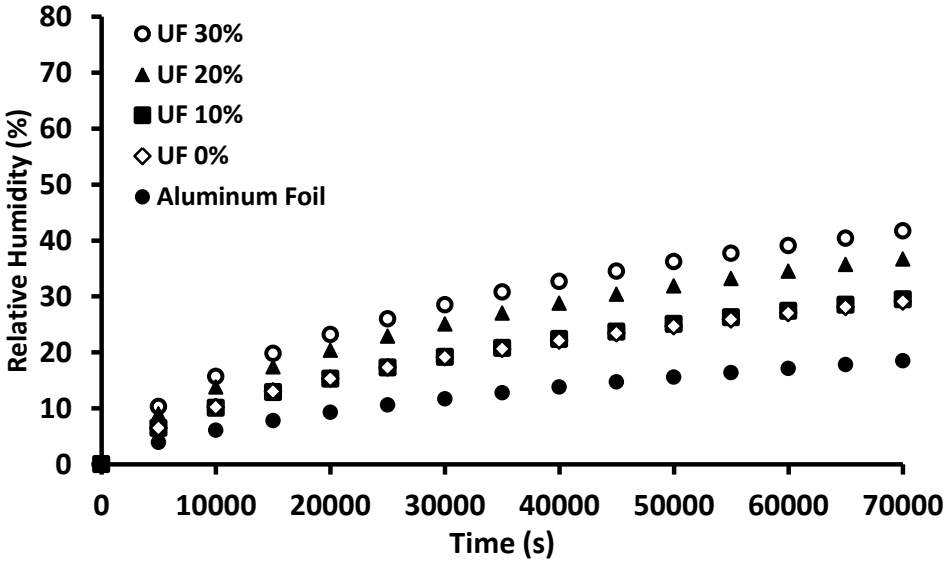

Figure 4-22. Relative humidity increase versus time for unfoamed PES-zeolite samples of various weight loadings

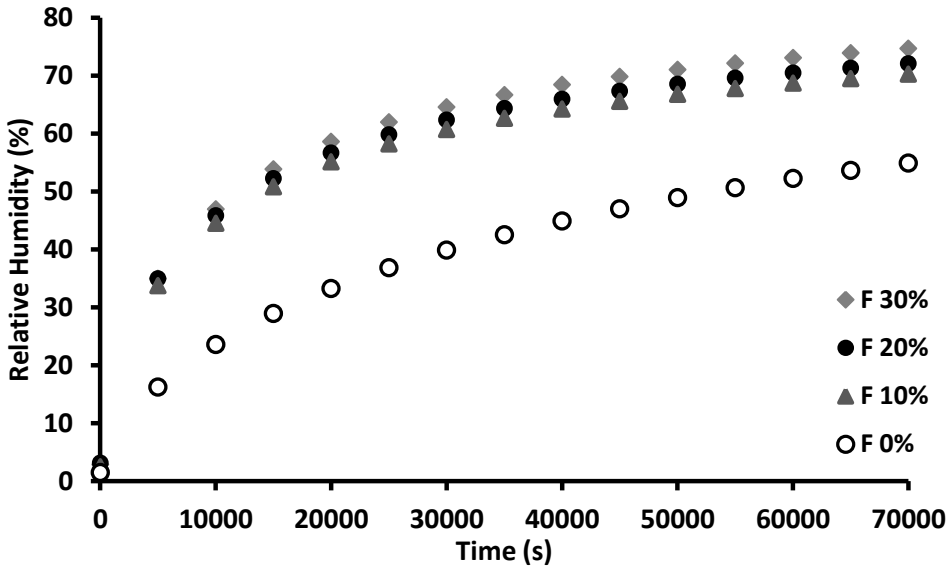

Figure 4-23. Relative humidity increase versus time for foamed PES-zeolite samples of various weight loadings

The performance curves of the foamed PES-zeolite films in Figure 4-23 are grouped much closer together than those of the unfoamed films. The 0% foamed case achieved a final RH of 54.9%, higher than all of the unfoamed films but significantly lower than any of the zeolite loaded foamed films. The rest of the foamed zeolite films finished between 70% and 75% RH, nearly overlapping for most of the figure. These results lend support to there being a combined effect between the foaming and zeolite, where the presence of both greatly outperforms either variable in isolation. Figure 4-24 shows the best performing foamed 30% film in comparison to Nafion. Nafion has a quicker initial RH rise, but the two materials eventually reach nearly the same RH value indicating very similar performance. Both foamed and unfoamed 0% were also plotted to show the baseline performance level, as well as the effect of foaming without added zeolite.

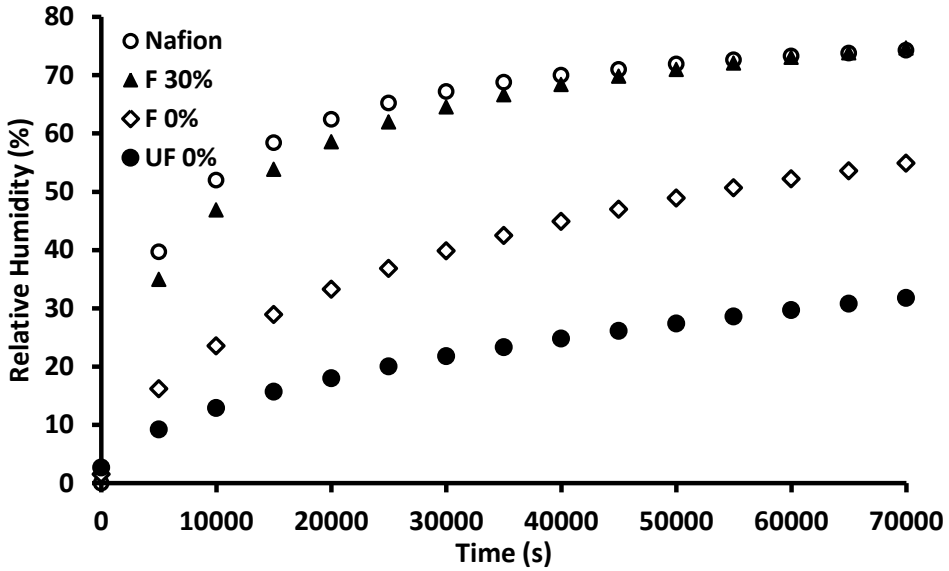

Figure 4-24. Relative humidity increase versus time for various PES-zeolite samples, foamed and unfoamed

While the permeation performance curves are excellent at illustrating relative film performance, they are largely useful for qualitative comparisons. Applying a method similar to the one detailed in ASTM E398 allows for a more direct measure of performance [72]. Figure 4-25 shows the time required for each sample to go from a measured container RH of 10% to 30%. All of the foamed samples reached 30% RH much faster than the unfoamed samples. Average time to reach 30% RH for unfoamed films ranged from seven times higher for 0% zeolite up to ~20 times higher for the rest of the weight loadings.

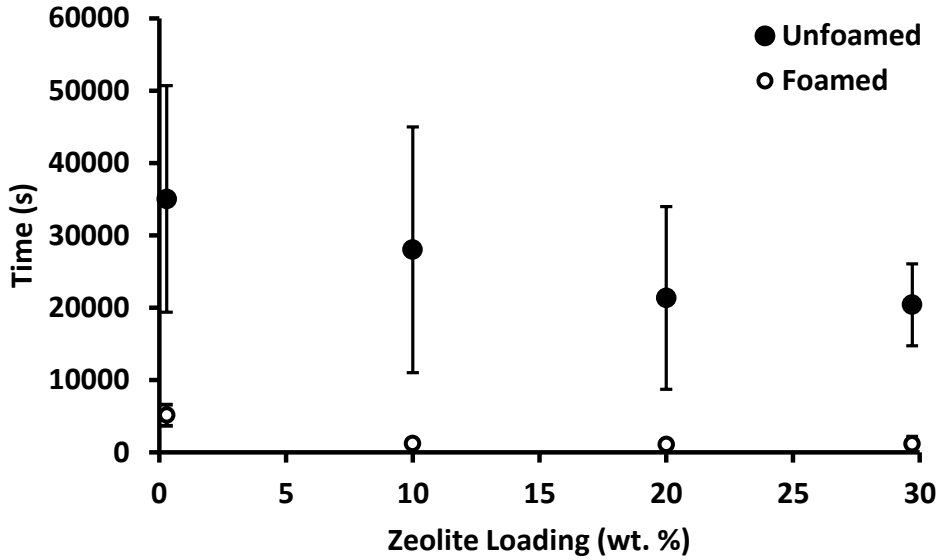

Figure 4-25. Time required for films to go from 10% to 30% RH

Standard deviation for the unfoamed films was very large, reaching ~50% of average measurement values. Although average time decreased with increased weight loading for the unfoamed films, uncertainty was high enough that no meaningful comparisons between the unfoamed loadings can be made. There are a few reasons for the large standard deviation. The first is due to the shape of the permeation curves. The curves are nonlinear and the unfoamed film curves were starting to flatten out before 30% RH. A small change in experimental conditions or membrane to membrane variance could easily lead to a huge variation in measurement time. Some of the uncertainty can also be attributed to the role leaks and film defects play when measuring films with such a small cross sectional area in the system. When the permeation rate through the film is low, a pinhole or imperfect seal will have a relatively large impact on performance. For the foamed films with higher permeability, such defects caused fewer measurement disturbances.

Only the foamed films were plotted in Figure 4-26, this time over a larger RH range of 10% to 50%. The higher permeability of these films reduced measurement uncertainty. From the plot it is evident that the foamed 10-30% samples were ~4 times quicker to hit the target RH than the 0% zeolite sample. However, a more universal measurement than time is desirable to improve the ability to compare different samples.

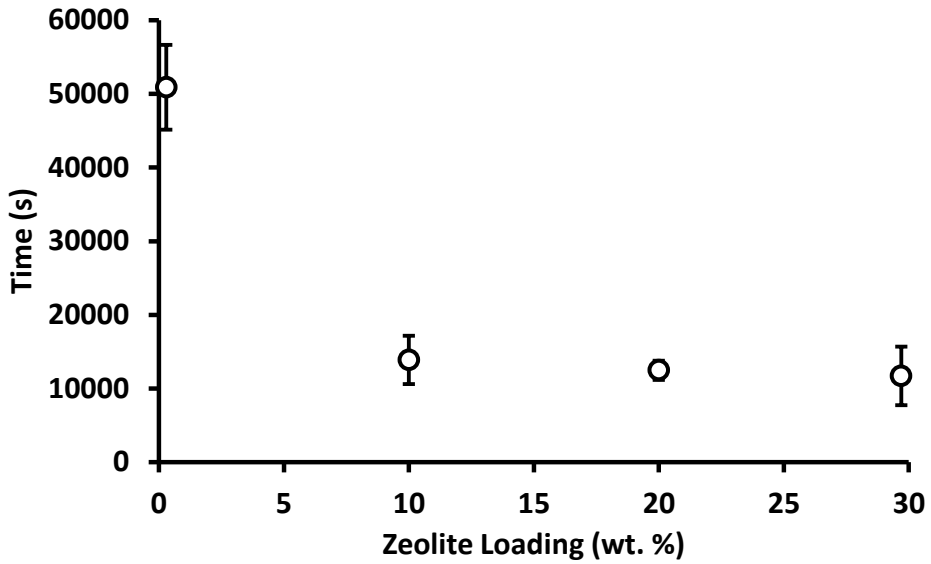

Figure 4-26. Time required for foamed films to go from 10% to 50% RH

Normalized performance of the foamed zeolite samples was calculated by dividing the time PES-zeolite films took to go from 10% RH to 50% RH by the time required for Nafion 212 to do the same, multiplied by the ratio of the film thicknesses. The 10%, 20% and 30% zeolite films performed similarly before normalization, however, normalized performance increased with increased zeolite loading. The thicker films were relatively more permeably when compared per unit of thickness. The results are shown in Figure 4-27, which clearly shows the performance of each foamed film in relation to Nafion 212. The 30% zeolite foamed film achieved three times the performance of Nafion when normalized for thickness. This comparison has limitations, however, since it

could be difficult to produce a PES-zeolite membrane as thin as the comparison Nafion 212 membrane.

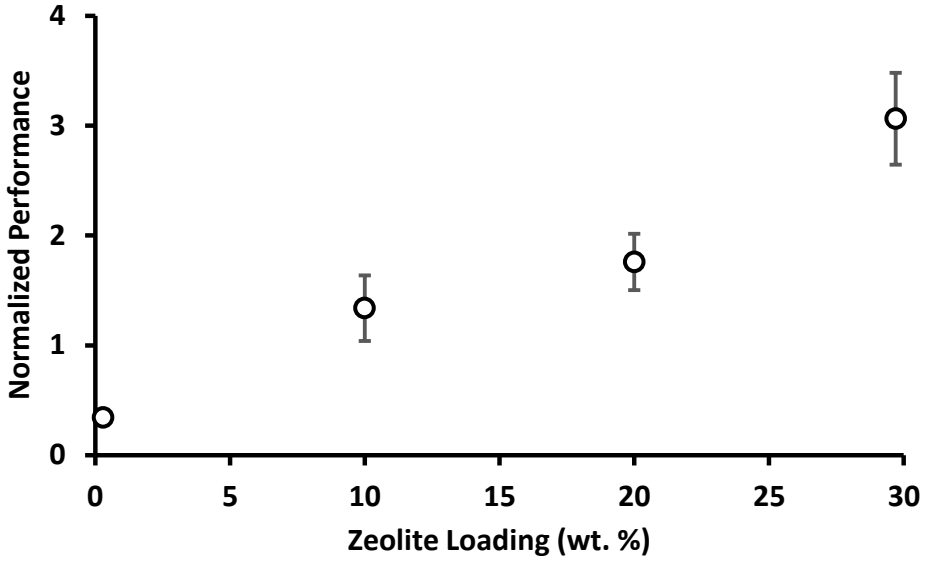

Figure 4-27. Zeolite loading versus performance normalized with respect to Nafion and film thickness

A statistical analysis of variable interactions was run in JMP to determine whether foaming and zeolite loading were significant input variables with normalized performance set as the output. A relative humidity range of 10-30% was used for both the foamed and unfoamed films, since this was the largest range the unfoamed films could achieve during testing. As before, the performance was normalized with respect to film thickness and Nafion run time from 10-30% to compare unitless performance. The interaction plots in Figure 4-28 show that zeolite loading, foaming and the zeolite loading*foaming interaction all have an effect on normalized performance. The results in Table 4-2 show the null hypothesis of variable insignificance can be rejected with a 99.98% or greater probability for all three variables.

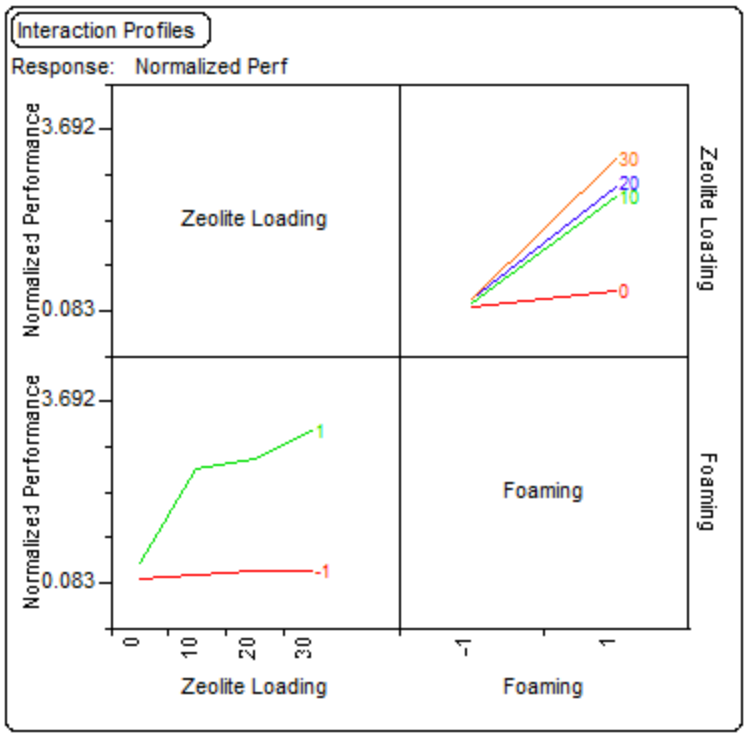

Figure 4-28. Interaction plots for zeolite loading and foaming variables for normalized performance with respect to Nafion and film thickness

Table 4-2. Effect test table, Rsquared = .9699

Source	Nparm	DF	Sum of Squares	F Ratio	Prob>F
Zeolite Loading	3	3	5.533731	24.865	<.0001
Foaming	1	1	14.89917	200.8418	<.0001
Zeolite Loading*Foaming	3	3	4.158409	18.6852	0.0002

4.4 Conclusions

PES-zeolite films were extruded, hot pressed and then solid state foamed to successfully improve zeolite dispersion over previously made solvent cast foamed films. The films exhibit greatly improved mechanical properties over their solvent cast counterparts. Tensile tests and dynamic mechanical analysis were performed to study the effects of both zeolite loading and foaming on the mechanical properties of the films. In

general, both foaming and increased zeolite loading decrease film tensile strength and extension at break. However, the films still compare favorably to Nafion from a physical property standpoint, and offer greatly improved physical properties at high temperatures. The T_g and storage modulus data indicate the foamed PES-zeolite can operate at temperatures past 200°C with similar properties to Nafion, which is limited to 100°C. Finally, the effects of zeolite loading and solid state foaming on the water permeation performance of extruded films were studied. The best performance was achieved with both foaming and 30% zeolite loading; this film essentially overlapped with Nafion performance when evaluated as a permeation performance curve. Further analysis and normalization with respect to film thickness revealed the 30% foamed film achieved better permeation performance than Nafion on a per unit basis.

Chapter 5: Modeling and Analysis of a Transient Fuel Cell Humidification Membrane Measurement System

5.1 Introduction

Polymer electrolyte membrane (PEM) fuel cells require proper humidification to function at maximum efficiency [35, 71, 75]. Insufficient humidity levels in the electrolyte membrane result in reduced stack power output. Excess humidity causes channel flooding which intermittently halts the flow of electrical current [9]. Controlling fuel cell humidity to ensure optimal operating conditions is an important step towards increasing efficiency and therefore the economic viability of fuel cells. Membrane humidifiers have been identified by the Department of Energy (DOE) as the most promising method of fuel cell humidification due to their simplicity, effectiveness and cost efficiency. Membrane humidifiers recycle heat and water vapor from the fuel cell waste stream to pre-humidify incoming dry gas to optimal levels.

Nafion is the current industry standard for humidification materials due to its excellent water transport properties [35]. However, a maximum operating temperature of ~90°C and cost of ~\$1000/m^2 limit the viability of using Nafion as the humidification membrane for the fuel cell applications [38, 39]. There is an increasing amount of research dedicated to developing alternative humidification membranes but none has succeeded in producing one that is both high temperature and low cost [8, 10-14]. Furthermore, there is a need for rapidly evaluating both existing and candidate membrane performance if a competitive membrane is to be developed.

Many water transfer measurement systems have been developed in the past. However, published values on the same material, e.g., Nafion, can differ by orders of magnitude [64]. Most of these systems measure humidification membrane properties under steady state conditions. Liquid water or humidified air flows past the feed side of

the test membrane and dry gas flows past the permeant side. Membrane vapor transfer rate is dependent on the relative humidity difference across the membrane as well as the mass flow rate of dry gas. The membrane vapor transfer rate is low compared to the mass flow rate of air downstream and a large membrane contact area is required to achieve measureable changes in downstream relative humidity. Large membranes add expense and difficulty to material development, which by nature often yields limited quantity for testing. Furthermore, a single steady state measurement can take many hours to stabilize. Fully analyzing a membrane across a range of temperature and relative humidity values is time consuming and not conducive to rapid material development.

We sought to build a humidification measurement system to directly compare candidate membranes of small size (<2 cm^2) in order to facilitate testing of newly developed experimental materials. This goal was achieved by designing a transient measurement system, where water vapor permeates through the membrane into a sealed container. By continuously monitoring relative humidity in the container over the course of the experiment, membrane vapor transfer data across a wide range of water activity values can be obtained. Such a method helps reduce the number of trials required to evaluate new materials. It is also arguably closer to the conditions fuel cells see in real-world operation, because automotive fuel cells must undergo a changing relative humidity gradient during start-up conditions. However, this approach introduces new challenges in modeling and data reduction. The lack of information on transient fuel cell RH measurements provided further motivation to for this study [9].

In this paper, we introduce the design and analysis of the transient membrane permeability measurement system. A mass transfer circuit model is developed and system characterization experiments were carried out to assist in developing a model to improve measurement accuracy. The resistance model compensates for measurement error due to

leaks as well as water vapor diffusion resistance in the container volume. Finally the experimental procedure and results are discussed and the measurement results of Nafion membranes are compared to results obtained from literature for system verification.

5.2 System Design

A diagram of the system design and relevant mass flows can be seen in Figure 5-1. Liquid water flows over the feed side of the humidification membrane during standard membrane measurement tests. The concentration difference between the feed and permeant sides of the membrane drives the water transfer, $\dot{m}_{in}$, through the membrane, where it accumulates in the container. Container relative humidity is monitored with a humidity sensor. The accumulation design allows for measurement of small membranes across the full range of permeant-side water activity values. The system is placed in an environmental control chamber to regulate ambient relative humidity and temperature. Temperature control ensures consistent measurement results while humidity control helps characterize system leaks, shown as $\dot{m}_{leak}$. The system has two quick disconnect ports that allow the container to be flushed with dry air in between runs. A diagram of the experimental setup can be seen in Figure 5-2.

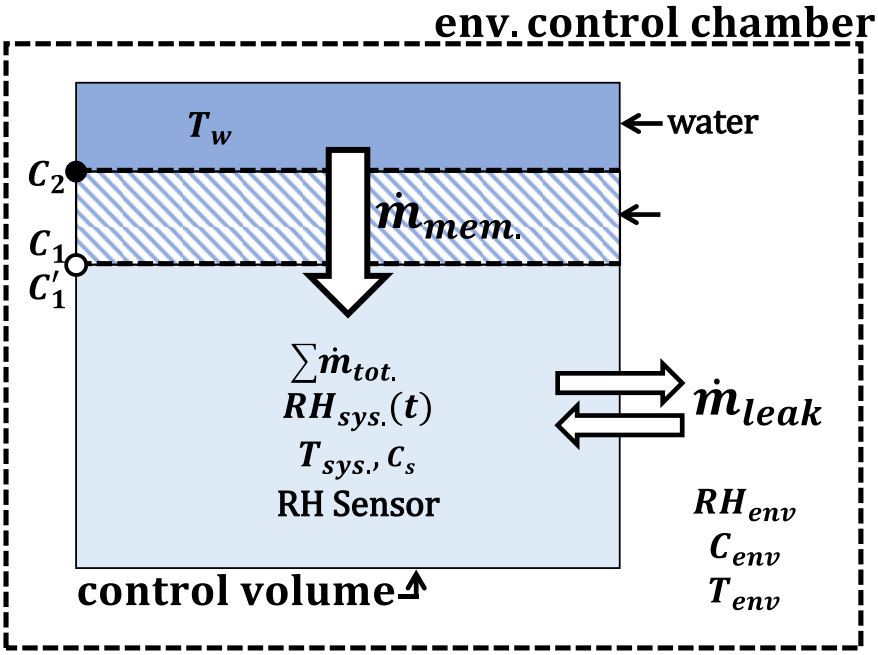

Figure 5-1. Diagram of system design and relevant mass flows

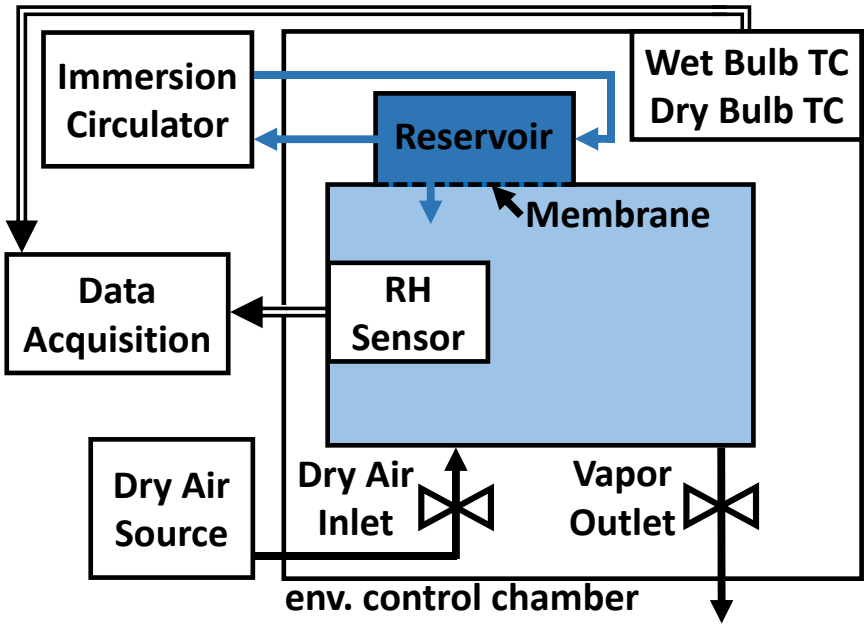

Figure 5-2. Diagram of experimental setup

5.3 System Construction

The system permeant container was constructed with solvent-welded polyvinylchloride (PVC) pipe fittings to minimize water absorption. Threaded nylon quick connect fittings were used to allow for flushing of the system with dry air between experiments. A stainless steel threaded face seal connector with a rubber O-ring secures the test membrane.

An immersion circulator (model number) was used to control the temperature of water in contact with the top side of membrane. Relative humidity within the container is recorded by an Omega RH-USB capacitive relative humidity sensor. The sensor was selected for its compact size, accuracy and ability to recover from condensation exposure. The humidification cell was set in an environmental control chamber (ESPEC SH-240). Relative humidity in the chamber is recorded via wet and dry bulb measurements from thermocouples installed in the chamber. Voltage outputs from the thermocouples are collected with an Omega OM-USB-TC-AI DAQ module and then converted into temperature using NIST standards. The wet and dry bulb temperatures are used to calculate relative humidity of the environmental control chamber.

5.4 Modeling

5.4.1 Model Assumptions

The container, chamber and water supply are in thermodynamic equilibrium [66]. This assumption is supported by the temperature data from the chamber dry bulb thermometer, RH-USB sensor in the container and the immersion circulator. Liquid water is in contact with the upper membrane surface and dominates membrane average water activity [35]. Membrane vapor transfer is driven by the water concentration gradient, not pressure [9, 35]. Water vapor in the container follows the ideal gas law [9, 66, 89]. The

container walls are rigid and container volume is constant for the duration of each experiment. The pressure in the container is ambient and constant. Membrane vapor transfer is limited by vapor side resistance [35]. The water concentration gradient is one dimensional across the membrane (top to bottom).

5.4.2 Mass Balance

The system model, seen in Figure 5-3, is an equivalent circuit with resistors to symbolize mass transfer resistance, current to represent water vapor mass flow, and water vapor concentration as the driving voltage.

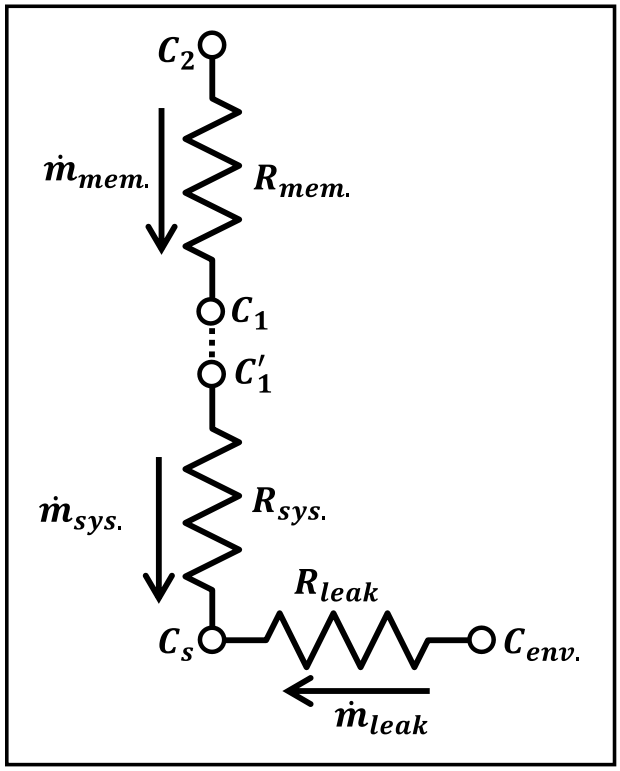

Figure 5-3. Mass transfer circuit model of system

The system mass balance at node C_s (RH sensor location within the container) is the sum of contributions from membrane mass flow and container leak rate

$$\sum \dot{m}_{tot.} = \dot{m}_{mem.} + \dot{m}_{leak} \tag{5.1}$$

The rate of mass accumulation in the container, $\dot{m}_{tot.}$, is determined by applying the Ideal Gas Law to water vapor within the container control volume:

$$P \cdot V = n \cdot R \cdot T \tag{5.2}$$

where P is water vapor partial pressure, V is container volume, n is moles of water vapor, T is temperature and R is the universal gas constant. Molar mass of vapor, G_v, is defined as

$$G_v = \frac{m}{n} \tag{5.3}$$

where m is the mass of water vapor. Relative humidity is defined as

$$RH = \frac{P_v}{P_{sat}} \tag{5.4}$$

where P_v is partial vapor pressure of water vapor in air and P_{sat} is the saturation vapor pressure required to boil a liquid at a given saturation temperature. Saturation pressure depends on temperature and was calculated from the following polynomial [90]:

$$ln(p_{sat}) = g_0 T^{-2} + g_1 T^{-1} + g_2 T^0 + g_3 T^1 + g_4 T^2 + g_5 T^3 + g_6 T^4 + g_7 ln(T) \tag{5.5}$$

$$g_0 = -2.8364744 * 10^3$$

$$g_1 = -6.028076559 * 10^3$$

$$g_2 = 1.954263612 * 10^1$$

$$g_3 = -2.737830188 * 10^{-2}$$

$$g_4 = 1.6261698 * 10^{-5}$$

$$g_5 = 7.0229056 * 10^{-10}$$

$$g_6 = -1.8680009 * 10^{-13}$$

$$g_7 = 2.7150305$$

Water vapor pressure can be determined for a given temperature and relative humidity. Substituting (3) and (4) into (2) gives the accumulated mass of water vapor in the closed container

$$m = \frac{RH \cdot V \cdot P_{sat} \cdot G_v}{R \cdot T} \tag{5.6}$$

Differentiating both sides with respect to time produces the rate of water vapor accumulation in the closed container.

$$\dot{m} = \frac{\dot{RH} \cdot V \cdot P_{sat} \cdot G_v}{R \cdot T} \tag{5.7}$$

Membrane and system resistances were determined next since they could not be directly measured during a membrane measurement.

5.4.3 Determining R_{leak}

The equivalent leak resistance was found by altering the experimental setup. A barrier membrane was used to eliminate membrane mass flow, simplifying the mass balance equation to

$$\sum \dot{m}_{tot.} = \dot{m}_{leak} \tag{5.8}$$

The rate of mass accumulation is known from equation 7 and the leak rate contribution follows Fick's First Law

$$\dot{m}_{leak} = \frac{D \cdot G_v \cdot A(C_{env.} - C_s)}{L} \tag{5.9}$$

where *D* is leak diffusion rate, A is equivalent leak cross sectional area, and C_{env} and C_s are the volumetric water concentrations over leak length L. The concentrations were calculated using the Ideal Gas Law. C_{env} was held constant by setting the environmental control chamber to 50% RH. Leak path length and cross sectional area are unknown and are combined with the diffusion coefficient into R_{leak}.

$$R_{leak} = \frac{L}{D \cdot A} = \frac{G_v(C_{env.} - C_s)}{\dot{m}_{leak}} \quad (5.10)$$

5.4.4 Determining R_{sys}

The diffusion coefficient of water vapor in air is an order of magnitude larger than the self-diffusion coefficient of water through Nafion. However, the container volume creates a long diffusion path from membrane to sensor compared to membrane thickness, making R_{sys} on the same order of magnitude as $R_{mem.}$. An experiment was designed to characterize the system resistance. The test membrane was removed from the system and the environmental control chamber set to 95% RH. With no membrane in place, the leak rate was assumed to be negligible in cross sectional area compared to the large opening created by the missing membrane. Water vapor entering the container through the opening follows the same path to the sensor as water vapor passing through a test membrane, thus the system and membrane resistances are drawn in series on the circuit diagram. System resistance was calculated via equation 11.

$$R_{sys} = \frac{G_v(C\prime_{env.} - C\prime_s)}{\dot{m}_{sys}} \quad (5.11)$$

where C'_{env} and C'_s are the volumetric water concentrations during the open container humidity test.

5.4.5 Determining R_{mem}

Once R_{sys} and R_{leak} were characterized, membrane resistance, $R_{mem.}$, was measured via

$$R_{mem.} = G_v \frac{(C_2 - C_1)}{\dot{m}_{mem.}} \quad (5.12)$$

Nafion membrane water concentration on the feed and permeant sides were calculated from [71, 91]

$$C_1 = \frac{\rho_{m,dry}}{M_{m,dry}} \lambda_1 \tag{5.13}$$

$$C_2 = \frac{\rho_{m,dry}}{M_{m,dry}} \lambda_2 \tag{5.14}$$

where $\rho_{m,dry}$ is membrane dry density, $M_{m,dry}$ is membrane dry molar mass and λ_1 and λ_2 are membrane water content. There is a discontinuity for Nafion in contact with liquid water versus saturated water vapor known as Schroeder's Paradox. On the feed side, membrane water content is fixed at a value of 22 where it makes contact with water. On the permeant side, membrane water content depends on the relative humidity of the air in contact with the membrane. This relationship has been empirically determined for Nafion as [92, 93]

$$\lambda_1 = .043 + 17.8RH_1 - 39.9RH_1^2 + 36.0RH_1^3 \tag{5.15}$$

RH in the above equation can be determined by applying the Ideal Gas Law to concentration C_1' because water vapor concentration in the system must be converted to the proper membrane concentration at the air-membrane interface. This concept is illustrated in Figure 5-3 as a discontinuity between C_1 and C_1'. Concentration C_1' was calculated from

$$\frac{\dot{RH} \cdot V \cdot P_{sat}}{R \cdot T} = \frac{(C_1' - C_s)}{R_{sys.}} + \frac{(C_{env.} - C_s)}{R_{leak}} \tag{5.16}$$

Once C_1 has been determined from C_1', $R_{mem.}$ was calculated from equation 12. The test membrane self-diffusion coefficient is then calculated via

$$D_w = \frac{t_m}{A_m \cdot R_{mem.}} \tag{5.17}$$

5.5 Experimental Procedure

To ensure consistent initial experimental conditions, dry air was circulated through the container and water supply lines for 12 hours before each experiment. The environmental control chamber held the relative humidity and temperature around the experimental setup constant. An impermeable membrane was installed in the system to run the initial leak analysis, while no membrane was used for the system resistance characterization. The quick connect air supply tubes were removed from the container and the system was allowed to run for 20 hours, tracking the humidity increase due to leaks. Next, the system was dried by reconnecting the air tubes and circulating dry air through the system for ~12 hours. The test membrane was then clamped into the system. A constant supply of water was supplied to the feed side of the membrane by a circulation pump connected to the immersion water circulator. The air tubes were again disconnected and then the container relative humidity and temperature were recorded for the duration of the experiment. A list of experimental conditions can be seen in Table 5-1.

Table 5-1. List of experiments conducted in system

Experiment	Feed side RH	Env. RH
Open System	N/A	50
Leak Test	95	95
	72	72
	50	50
Nafion 212	Liquid water	50
	95	95
	72	72
	50	50

5.6 Experimental Results & Discussion

For the first system characterization experiment, the test membrane was removed to determine open system resistance. Equation 9 was used to model the expected humidity increase over time at the sensor with diffusion length defined as the distance from the container opening to the relative humidity sensor and area set equal to the container opening cross section. The average diffusion coefficient for the experiment was $2.37 \times 10^{-5}\ m^2/s$, which is within 3% of the accepted value for water vapor in air at 30°C ($2.4 \times 10^{-5}\ m^2/s$). System resistance was fitted to a curve dependent on system relative humidity to compensate for system material and geometry effects that caused deviations from the average diffusion value.

The next characterization experiment determined the system leak rate through an equivalent leak rate resistance. The container was sealed with a barrier membrane and environmental humidity outside of the container was set to three different levels: 50, 72 and 95% RH. Container ingress versus time for the three different levels is shown in Figure 5-4.

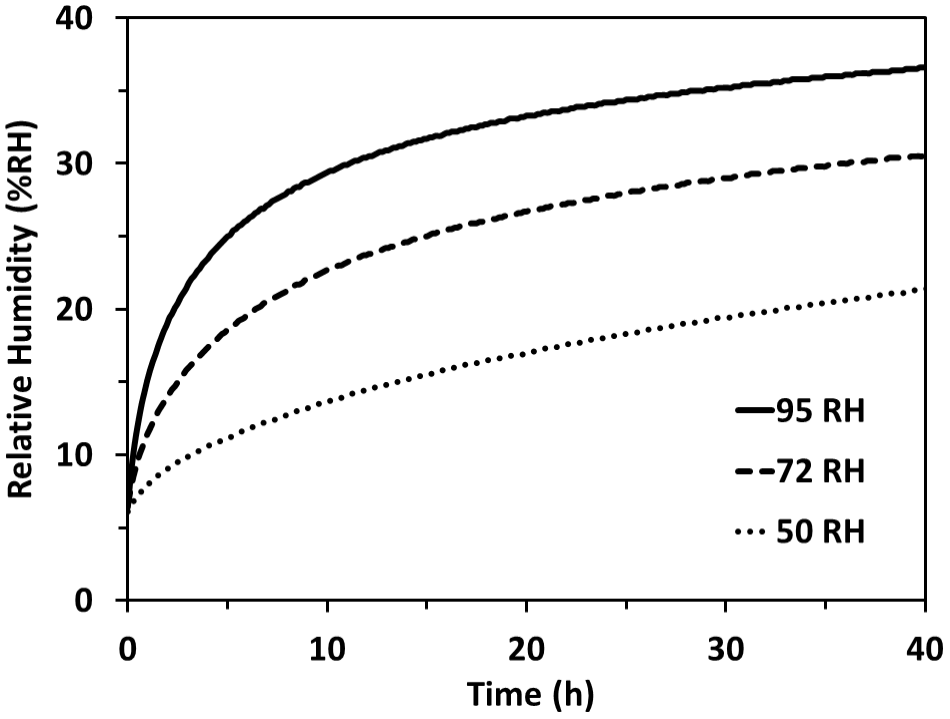

Figure 5-4. Container RH due to ingress versus time with a sample frequency of .2 Hz

Leak rate depends on environmental relative humidity as evidenced by the offset between the container ingress lines in Figure 5-4. Container relative humidity due to leak ingress approached an equilibrium value lower than the surrounding humidity for each case. Compensating for the concentration difference created by the different environmental humidity levels still produced different leak rates. Average relative humidity may play a role in addition to concentration difference. As average RH increases condensation in the leak paths is more likely which leads to reduced vapor diffusion rates. The individual leak resistances measured at each of the three relative humidity levels were selected for modeling membrane tests with matching external relative humidity.

Once container water vapor concentration exceeds environmental water vapor concentration the leak changes direction. It was assumed that leak magnitude remains

equal for ingress and egress with equal concentration gradients. Although the leak tests in Figure 5-4 approach a high equilibrium relative humidity they are actually quite small in magnitude compared to flow through the membrane. The ratio of membrane molar flow rate to leak molar flow is shown in Figure 5-5. Initially membrane flow is ~250 times larger than the leak rate and only contributes .4% of the total system mass accumulation rate. The small leak contribution further decreases as relative humidity in the container reaches equilibrium with the environmental humidity; at 50% RH the leak rate becomes zero and then changes direction, making the membrane flow to leak ratio infinite. The leak rate becomes significant at higher relative humidity values, comprising 30% of the flow contribution when system RH reaches 85% and the concentration difference across the membrane is reduced.

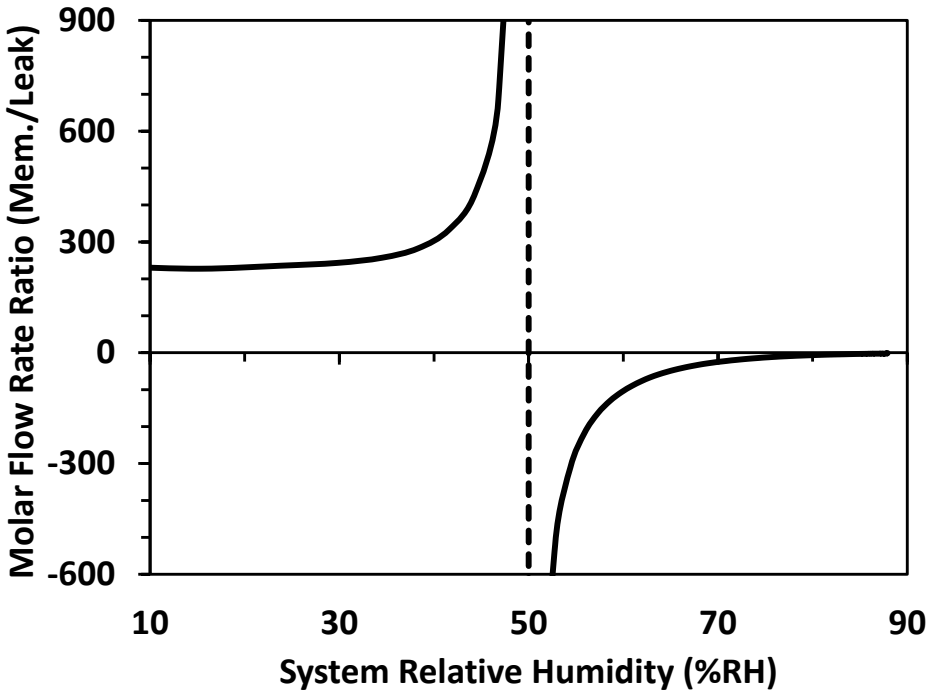

Figure 5-5. Ratio of membrane molar flow rate to leak molar flow rate versus system relative humidity for water and 50 env. RH test

Nafion 212 membranes were tested in the system at a range of relative humidity values on the feed side, the results of which can be seen in Figure 5-6. The plot of system relative humidity shows a higher feed side relative humidity results in a higher rate of system relative humidity rise, as expected.

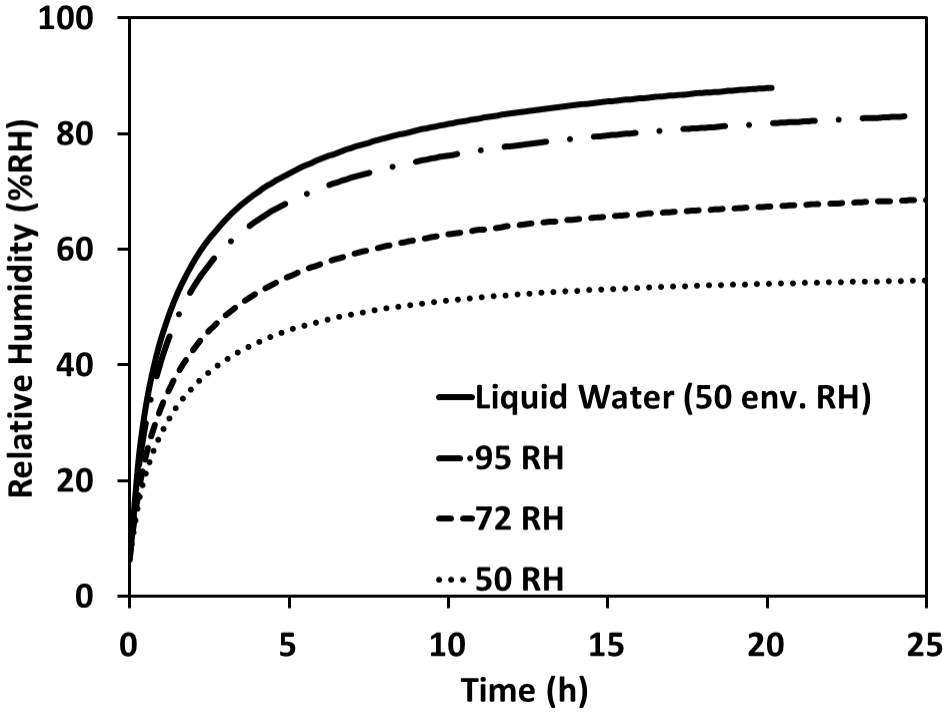

Figure 5-6. Container RH versus time with a sample frequency of .2 Hz

The measured self-diffusivity of Nafion 212 versus average membrane water content over the course of a single experiment is shown in Figure 5-7. For this experiment, the feed side of the membrane is exposed to liquid water at 30°C. The change in average membrane water content is due to the increasing water activity in the sealed container on the permeate side. Membrane D_w ranges from a maximum of $1.4 \cdot 10^{-6}\, cm^2/s$ at $\lambda_{avg} = 12.5$ to $0.2 \cdot 10^{-6}\, cm^2/s$ at $\lambda_{avg} = 14.5$. The range of

values is in agreement with those from Zawodzinski, Hensley, Ye, Gong and Roy [94]. However, at higher water content values D_w falls to a minimum value of $2 \cdot 10^{-8}\, m^2/s$ which is an order of magnitude lower than that reported by studies. Similarly, membrane D_w is actually decreasing with increasing λ_{avg} in our system which is opposite of the expected trend.

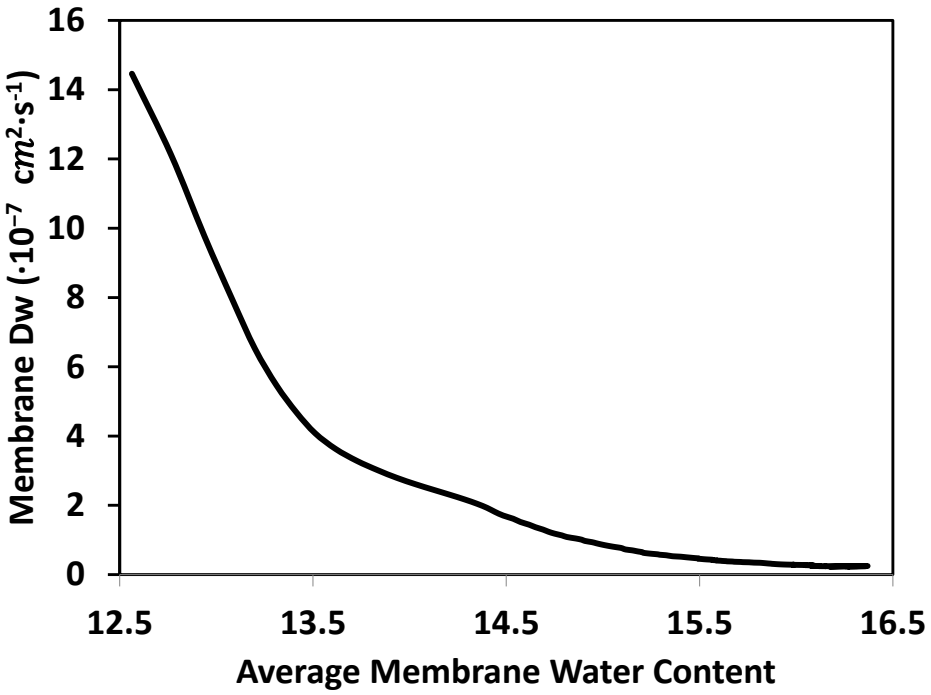

Figure 5-7. Nafion 212 diffusivity versus average membrane water content

There are a few possibilities that may explain these results. Many of the studies used x-ray scattering to measure diffusion data during sorption experiments (>100 μm) [64-66, 95]. These setups allow for more precise control of humidity conditions but do not closely replicate real-world fuel cell conditions. The dynamic nature of our system made it difficult to accurately determine local water vapor concentration; slight variations

in concentration resulted in large swings in calculated diffusivity, especially near the end of the experiment when the concentration gradient was very small.

Discrepancies between measurements obtained with this system and other permeation systems can be attributed to fundamental design differences. In steady-state systems the permeate side of the test membrane is usually exposed to dry, flowing air; an increase in average membrane water content corresponds to an increase in concentration gradient across the membrane. The opposite is true in our system. Since the feed side has a fixed water content, concentration gradient will always decrease as water vapor diffuses across the membrane and increases average membrane water content. Furthermore, the presence of stagnant air on the permeate side of the membrane could lead to boundary layer formation making accurate concentration estimation difficult at higher system relative humidity values. Steady state systems also generally use a large membrane area (>100 cm^2) for measurement. The relatively small size of membrane used for our experiments (.71 cm^2) means edge effects and air gap formation could reduce measurement values.

The lack of similar systems made measurement verification results difficult. However, taking the peak D_w value from each experiment and plotting against data from Weidner et al. resulted in close agreement in 3 out of 4 cases, shown in Figure 5-8. The outlying case at λ = 3 is ~3 times as high as that reported by Weidner which is acceptable since self-diffusion results often vary by an order of magnitude depending on experimental setup. The peak value in each case occurred at the start of an experiment when the slope of the relative humidity versus time curve was nearly linear, meaning the system was operating close to steady state conditions. It is unclear how D_w values would compare for λ < 3 as our humidity control chamber could not control at a low enough RH values to test below λ = 3.

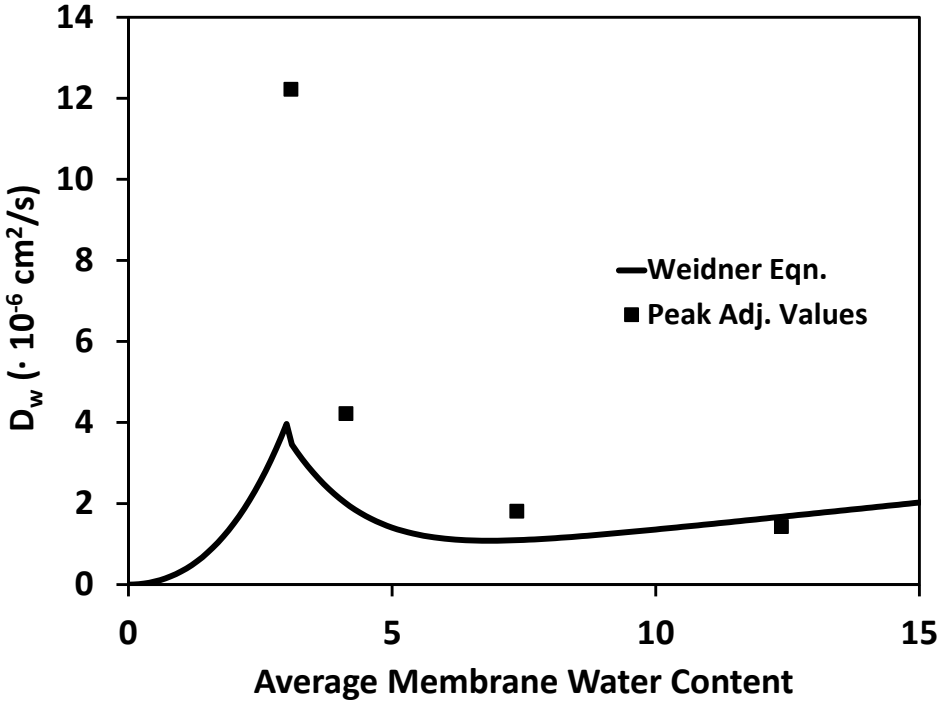

Figure 5-8. Peak Nafion 212 self-diffusion rates versus average membrane water content

An uncertainty analysis was performed to determine the sensitivity of calculated self-diffusion values to changes in R_{sys} and R_{leak}, seen in Table 5-2. The system was 6-8 times more sensitive to perturbations in perturbations in system resistance than leak resistance, which was expected due to the relatively small contributions from leaks to overall mass flow. Overall, diffusion values were robust to changes in resistance and the maximum error from a 10% change in any resistance value was only 1.27%.

Table 5-2. Sensitivity analysis of model resistance values

Parameter	Perturbation	Avg. % Error	Max. % Error
R_{sys}	+10%	0.67	1.27
	-10%	0.64	1.18
R_{leak}	+10%	0.09	0.16
	-10%	0.11	0.21

5.7 Conclusions

A fixed volume system was designed to rapidly measure the diffusivity of humidification membranes. A resistance model was developed and the system was successfully used to measure the performance of Nafion 212 membranes. Experimental results obtained for the system were in agreement with values reported in literature for sorption experiments measured by NMR and steady-state permeation systems. Reported results diverged at higher membrane water content values, possibly due to the increased relative magnitude of leak rate and condensation/boundary layer formation on the permeant side of the membrane. Peak values of D_w measurements taken from the segment of experiments most closely resembling steady-state conditions were in agreement with results from steady-state systems reported in literature.

Chapter 6: Conclusions and Future Work

6.1 Conclusions

- A novel PES-zeolite MMM with water permeability close to Nafion and mechanical stability at high temperatures was created using two different methods. The first method utilized solvent casting to combine PES pellets and zeolite particles into thin films, followed by solid state foaming to generate a porous microstructure. The second method utilized a combination of melt mixing with a twin screw compounder followed by hot pressing and solid state foaming. The second method allowed for vastly improved particle dispersion and is less expensive, more scalable for manufacturing, and more environmentally friendly than solvent casting. The extruded films were able to achieve water permeation performance more than three times that of Nafion when adjusted for thickness. They achieved higher tensile strength and storage modulus than Nafion, as well as a T_g more than 100°C higher than that of Nafion.
- Understanding of solvent cast versus extruded, hot pressed membranes was improved via examination of film cross sections as well as analysis of water vapor permeation, mechanical properties and dynamic mechanical analysis. The solvent casting process caused dense zeolite particles to settle at the bottom of the PES-DMF solution during solvent evaporation. Reducing solvent content to increase solution viscosity proved ineffective in combatting settling, as PES pellets never fully dissolved in solvent concentrations above 10% PES by weight. Melt mixing at 320°C with 100 psi barrel pressure allowed for high shear forces for proper PES-zeolite mixing while keeping viscosity high to prevent settling. The resulting films were far stronger than their solvent cast counterparts, ranging from 20-60 MPa in tensile strength at break; the solvent cast films were not able to be measured due to lack of mechanical stability. Although the extruded films were not evaluated for gas permeability, no pinholes were visible upon visual inspection against a bright light. Pinholes commonly formed in the solvent cast films, especially when they were uncovered or heating temperature exceeded 60°C.

- An interactive effect between zeolite particles and the solid state foaming process was discovered. Both the solvent cast films and extruded films showed low, but slightly improved permeability when zeolite loading and foaming were performed independently. SEM images revealed the presence of a solid skin layer for films foamed without the addition of zeolite. Ciobanu et al. found zeolite alone could only achieve significant permeability when added in greater than 30% loadings by volume. We were able to achieve permeability in loadings as low as 10% by weight with the combination of zeolite addition and solid state foaming. Inspection of the SEM images revealed zeolite acts as a nucleation agent for foaming, with many pores forming with zeolite particles at the center. Furthermore, pores are located at and near the surface of the film, effectively eliminating the skin layer commonly present during solid state foaming. Zeolite particles were also visible poking through the surface of the materials, creating an entry path for water vapor.
- A new fixed volume water vapor permeation measurement system was developed to quickly analyze the performance of small size (<2 cm^2) membranes. The system allows for quick evaluation of membrane water vapor permeability relative to other membranes to aid in new material development. Current measurement systems often take many hours to return a result and operate at steady state, only returning a data for a single set of conditions. The developed system returns data over a wide range of relative humidity gradient values in less than a day. The small membrane surface area results in high levels of uncertainty for barrier materials and is better suited to measuring materials designed for humidification where these errors are smaller in magnitude compared to the material permeation rate.
- A resistive model was developed to extract further information about membrane performance, including membrane diffusion coefficient in response to a changing concentration gradient. The model was used to measure water concentration values in Nafion 212 membranes. Results obtained from the model were in agreement with values reported in literature for sorption

experiments measured by NMR and steady-state permeation systems. Reported results diverged at higher membrane water content values, possibly due to the increased relative magnitude of leak rate and condensation/boundary layer formation on the permeant side of the membrane. Peak values of D_w measurements taken from the segment of experiments most closely resembling steady-state conditions were in agreement with results from steady-state systems reported in literature.

6.2 Future Work

- The extruded, hot-pressed PES-zeolite films still need to be characterized for gas crossover, as well as long-term reliability after RH and temperature cycling. No pinholes or defects were visible before foaming which is an improvement over the solvent cast films, but this suspected improvement needs to be quantified. The zeolite particles were embedded within the material rather than bonded to a support structure, which should help combat separation due to humidity and temperature cycling. However, the long term effects of cycling are still unknown and should be characterized.
- The 30% zeolite loaded extruded films achieved the best water vapor performance after thickness normalization. However, their actual performance does not exceed that of Nafion due to membrane thickness. The films also vary in thickness along their cross section and are limited in surface area due to the pressing method used. A new method of hot rolling should be developed to increase film surface area, reduce thickness to 50 μm, and reduce thickness variation to improve film homogeneity and performance.
- The final hurdle in material fabrication lies in the solid state foaming process. The 0% zeolite foamed films produced inconsistent results during mechanical testing due to large wrinkles formed during the solid state foaming process. The wrinkling was likely

due to film thickness, as the thicker films were much flatter. However, the wrinkling will likely become more of an issue if thickness is reduced using hot rolling. Therefore a new solid state foaming method using in vessel pressure drop foaming or a fixture to restrict the films from deforming during solid state foaming should be developed.

- Finally, the resistance model was able to measure the water diffusivity of Nafion at various water content values, but only the peak values of each experiment were in agreement with those found in literature. Most systems found in literature operate at steady state with a fixed water concentration gradient whereas our system experiences a continuously changing concentration gradient. One way to verify the results is by developing a model in COMSOL using Fick's Second Law to characterize the changing water vapor concentration with respect to time in different sections of the measurement system. This method would also account for the geometric effects of the measurement system on local concentration values.

References

[1] James, B. D., Moton, J. M., and Colella, W. G., 2014, "Fuel Cell Transportation Cost Analysis," U.S. Department of Energy Hydrogen and Fuel Cells Program 2014 Annual Merit Review and Peer Evaluation Meeting Washington, DC.

[2] United States Department of Energy, 2014, "Diagram: How a Polymer Electrolyte Membrane (PEM) fuel cell works," http://energy.gov/eere/fuelcells/types-fuel-cells.

[3] Hsieh, Y.-C., Zhang, Y., Su, D., Volkov, V., Si, R., Wu, L., Zhu, Y., An, W., Liu, P., and He, P., 2013, "Ordered bilayer ruthenium–platinum core-shell nanoparticles as carbon monoxide-tolerant fuel cell catalysts," Nature communications, 4.

[4] Cheon, J. Y., Kim, T., Choi, Y., Jeong, H. Y., Kim, M. G., Sa, Y. J., Kim, J., Lee, Z., Yang, T.-H., and Kwon, K., 2013, "Ordered mesoporous porphyrinic carbons with very high electrocatalytic activity for the oxygen reduction reaction," Scientific Reports, 3.

[5] Ahluwalia, R. K., and Wang, X., 2014, "Fuel Cells Systems Analysis," U.S. Department of Energy Hydrogen and Fuel Cells Program 2011 Annual Merit Review and Peer Evaluation Meeting Washington, D.C.

[6] Rayment, C., and Sherwin, S., 2003, "Introduction to fuel cell technology. Dept. Aerospace & Mechanical Engineering, Notre Dame."

[7] Satyapal, S., Mills, M., Byham, S., Hou, Z., and Nahm, K. S., 2008, "Fuel Cell Cost Analysis Summary," IPHE.

[8] Wagener, E. H., and Morgan, B. P., 2014, "New High Performance Water Vapor Membranes To Improve Fuel Cell Balance of Plant Efficiency and Lower Costs," U.S. Department of Energy Hydrogen and Fuel Cells Program 2014 Annual Merit Review and Peer Evaluation Meeting Washington, D.C.

[9] Chen, D., and Peng, H., 2005, "A Thermodynamic Model of Membrane Humidifiers for PEM Fuel Cell Humidification Control," Journal of Dynamic Systems, Measurement, and Control, 127, pp. 424-432.

[10] Kraton Polymers LLC, 2010, "NEXAR Polymers," from http://www.kraton.com/products/pdf/NEXAR_brochure.pdf

[11] Zhao, N., Edwards, D., Shi, Z., and Holdcroft, S., 2013, "Interfacial vs. Internal Water Transport Resistance of Sulfonated Hydrocarbon Proton-Exchange Membranes," ECS Electrochemistry Letters, 2(3), pp. F22-F24.

[12] Geise, G., Freeman, B., and Paul, D., 2010, "Characterization of a sulfonated pentablock copolymer for desalination applications," Polymer, 51(24), pp. 5815-5822.

[13] Park, C. H., Lee, C. H., Guiver, M. D., and Lee, Y. M., 2011, "Sulfonated hydrocarbon membranes for medium-temperature and low-humidity proton exchange membrane fuel cells (PEMFCs)," Progress in Polymer Science, 36(11), pp. 1443-1498.

[14] James, B. D., Moton, J. M., and Colella, W. G., 2013, "Fuel Cell Transportation Cost Analysis," U.S. Department of Energy Hydrogen and Fuel Cells Program 2013 Annual Merit Review and Peer Evaluation ReportArlington, Virginia.

[15] Johnson, W. B., "V.I.1 Materials and Modules for Low-Cost, High-Performance Fuel Cell Humidifiers," Proc. U.S. Department of Energy Hydrogen and Fuel Cells Program 2012 Annual Merit Review and Peer Evaluation Meeting, pp. V 261-265.

[16] Johnson, W. B., 2012, "Materials and Modules for Low-Cost, High-Performance Fuel Cell Humidifiers," U.S. Department of Energy Hydrogen and Fuel Cells Program 2012 Annual Merit Review and Peer Evaluation Meeting, Arlington, Virginia.

[17] James, B. D., and Spisak, A. B., 2012, "Mass Production Cost Estimation of Direct H2 PEM Fuel Cell Systems for Transportation Applications: 2012 Update."

[18] Mirza, Z., 2011, "Development of Thermal and Water Management System for PEM Fuel Cell," U.S. Department of Energy Hydrogen and Fuel Cells Program 2011 Annual Merit Review and Peer Evaluation Meeting, Washington, D.C.

[19] Energy, U. S. D. o., 2012, "Fuel Cell Technologies Office Multi-Year Research, Development, and Demonstration Plan - 3.4 Fuel Cells," United States Department of Energy.

[20] Majsztrik, P. W., 2008, Mechanical and transport properties of Nafion (RTM) for PEM fuel cells; temperature and hydration effects, Princeton University.

[21] Emprise Corporation, 2014, "Humidicore Application Manual," from http://www.humidicore.com/Humidicore_Application_Manual.pdf

[22] Sinha, J., Lasher, S., Yang, Y., and Kopf, P., 2010, "Direct hydrogen PEMFC manufacturing cost estimation for automotive applications," U.S. Department of Energy Hydrogen and Fuel Cells Program 2010 Annual Merit Review and Peer Evaluation Meeting, Washington, DC.

[23] Burioka, N., Chikumi, H., Suyama, H., Sako, T., Teramoto, H., Matsumoto, Y., and Takano, K., 1999, "Membrane Humidifier That Does Not Require Addition of Water," Yonaga Acto medica, 42, pp. 185-188.

[24] Air Products, 2014, "Cactus PC Dryers," from http://www.airproducts.com/~/media/Files/PDF/products/supply-options/prism-membrane/cactus-pc-dryers-membrane-air-dehydration.pdf

[25] Perma Pure LLC, 2014, "FC Series Manual,"from http://www.permapure.com/wp-content/uploads/2013/08/FC-Series-Manual.pdf

[26] Hamrock, S., 2011, "New Fluorinated Ionomers and Membranes for PEM Fuel Cells," Fuel Cell Seminar & Energy ExpositionOrlando, Florida.

[27] Hughes, R., 1996, Industrial membrane separation technology, Springer.

[28] Baker, R. W., 2004, Membrane Technology and Applications, John Wiley & Sons.

[29] Gongping, L., Wang, W., Wanqin, J., and Nanping, X., 2012, "Polymer/ceramic composite membranes and their application in pervaporation process," Chinese Journal of Chemical Engineering, 20(1), pp. 62-70.

[30] Basile, A., and Nunes, S., 2011, Advanced membrane science and technology for sustainable energy and environmental applications, Elsevier.

[31] Schult, K., and Paul, D., 1996, "Water sorption and transport in a series of polysulfones," Journal of Polymer Science Part B: Polymer Physics, 34(16), pp. 2805-2817.

[32] Schult, K., and Paul, D., 1997, "Water sorption and transport in blends of polyethyloxazoline and polyethersulfone," Journal of Polymer Science Part B: Polymer Physics, 35(6), pp. 993-1007.

[33] March, J., 1985, Advanced Organic Chemistry: Reactions, Mechanisms, and Structure (3rd ed.), Wiley, New York.

[34] Gates, C. M., and Newman, J., 2000, "Equilibrium and diffusion of methanol and water in a Nafion 117 membrane," AIChE Journal, 46(10), pp. 2076-2085.

[35] Duan, Q., Wang, H., and Benziger, J., 2012, "Transport of liquid water through Nafion membranes," Journal of Membrane Science, 392, pp. 88-94.

[36] Goswami, S., Klaus, S., and Benziger, J., 2008, "Wetting and absorption of water drops on Nafion films," Langmuir, 24(16), pp. 8627-8633.

[37] Benjamin, T. G., 2007, "Membrane and MEA Accelerated Stress Test Protocols," U.S. Department of Energy Hydrogen and Fuel Cells Program 2007 Annual Merit Review and Peer Evaluation Meeting, Arlington, Virginia.

[38] Sahu, A., Pitchumani, S., Sridhar, P., and Shukla, A., 2009, "Nafion and modified-Nafion membranes for polymer electrolyte fuel cells: An overview," Bulletin of Materials Science, 32(3), pp. 285-294.

[39] Yang, C., Srinivasan, S., Bocarsly, A., Tulyani, S., and Benziger, J., 2004, "A comparison of physical properties and fuel cell performance of Nafion and zirconium phosphate/Nafion composite membranes," Journal of Membrane Science, 237(1), pp. 145-161.

[40] Johnson, W. B., "V.J.1 Materials and Modules for Low-Cost, High-Performance Fuel Cell Humidifiers," Proc. U.S. Department of Energy Hydrogen and Fuel Cells Program 2011 Annual Merit Review and Peer Evaluation Meeting, pp. 879-882.

[41] TeGrotenhuis, W., Caldwell, D., Lavender, C., and Roberts, B., 2008, "Low-Cost Manufacturable Microchannel Systems for Passive PEM Water Management," U.S. Department of Energy Hydrogen and Fuel Cells Program 2008 Annual Merit Review and Peer Evaluation Meeting, Washington, D.C.

[42] de Bock, H. P. J., Varanasi, K., Chamarthy, P., Deng, T., Kulkarni, A., Rush, B. M., Russ, B. A., Weaver, S. E., and Gerner, F. M., "Experimental investigation of micro/nano heat pipe wick structures," Proc. ASME 2008 International Mechanical Engineering Congress and Exposition, American Society of Mechanical Engineers, pp. 991-996.

[43] TeGrotenhuis, W., and Lavender, C., "V.K.2 Low-Cost Manufacturable Microchannel Systems for Passive PEM Water Management," Proc. U.S. Department of Energy Hydrogen and Fuel Cells Program 2008 Annual Merit Review and Peer Evaluation Meeting, pp. 1075-1078.

[44] Norris, I. D., Morrison, M. C., and Mattes, B. R., "High Flux Polyamide Composite Hollow Fiber Membranes for Reverse Osmosis Applications," Proc. MRS Proceedings, Cambridge Univ Press, pp. 0930-JJ0901-0907.

[45] Chemical, D., 2014, "FILMTEC Membranes: A Comparison of Cellulose Acetate and FILMTEC FT30 Membranes, Tech Facts," D. Chemical, ed.Dow Website.

[46] UBE America Inc., 2014, "Dehydration Systems ", from https://www.ube.com/content.php?pageid=21.

[47] Bowen, T. C., Noble, R. D., and Falconer, J. L., 2004, "Fundamentals and applications of pervaporation through zeolite membranes," Journal of Membrane Science, 245(1), pp. 1-33.

[48] Bowen, T. C., Li, S., Noble, R. D., and Falconer, J. L., 2003, "Driving force for pervaporation through zeolite membranes," Journal of Membrane Science, 225(1), pp. 165-176.

[49] Ciobanu, G., Carja, G., and Ciobanu, O., 2007, "Preparation and characterization of polymer–zeolite nanocomposite membranes," Materials Science and Engineering: C, 27(5), pp. 1138-1140.

[50] Kim, S. G., Hyeon, D. H., Chun, J. H., Chun, B.-H., and Kim, S. H., 2013, "Nanocomposite poly (arylene ether sulfone) reverse osmosis membrane containing functional zeolite nanoparticles for seawater desalination," Journal of Membrane Science, 443, pp. 10-18.

[51] Cho, C. H., Oh, K. Y., Kim, S. K., Yeo, J. G., and Sharma, P., 2011, "Pervaporative seawater desalination using NaA zeolite membrane: Mechanisms of high water flux and high salt rejection," Journal of Membrane Science, 371(1), pp. 226-238.

[52] Li, Y., and Yang, W., 2008, "Microwave synthesis of zeolite membranes: a review," Journal of Membrane Science, 316(1), pp. 3-17.

[53] Lind, M. L., Ghosh, A. K., Jawor, A., Huang, X., Hou, W., Yang, Y., and Hoek, E. M., 2009, "Influence of zeolite crystal size on zeolite-polyamide thin film nanocomposite membranes," Langmuir, 25(17), pp. 10139-10145.

[54] Sandström, L., Palomino, M., and Hedlund, J., 2010, "High flux zeolite X membranes," Journal of Membrane Science, 354(1), pp. 171-177.

[55] Shao, J., Zhan, Z., Li, J., Wang, Z., Li, K., and Yan, Y., 2014, "Zeolite NaA membranes supported on alumina hollow fibers: Effect of support resistances on pervaporation performance," Journal of Membrane Science, 451, pp. 10-17.

[56] Shu, X., Wang, X., Kong, Q., Gu, X., and Xu, N., 2012, "High-flux MFI zeolite membrane supported on YSZ hollow fiber for separation of ethanol/water," Industrial & Engineering Chemistry Research, 51(37), pp. 12073-12080.

[57] Yang, Z., Liu, Y., Yu, C., Gu, X., and Xu, N., 2012, "Ball-milled NaA zeolite seeds with submicron size for growth of NaA zeolite membranes," Journal of Membrane Science, 392, pp. 18-28.

[58] Zhou, H., Korelskiy, D., Leppäjärvi, T., Grahn, M., Tanskanen, J., and Hedlund, J., 2012, "Ultrathin zeolite X membranes for pervaporation dehydration of ethanol," Journal of Membrane Science, 399, pp. 106-111.

[59] Tavolaro, A., and Drioli, E., 1999, "Zeolite membranes," Advanced materials, 11(12), pp. 975-996.

[60] Adachi, M., Navessin, T., Xie, Z., Frisken, B., and Holdcroft, S., 2009, "Correlation of in situ and ex situ measurements of water permeation through Nafion NRE211 proton exchange membranes," Journal of the Electrochemical Society, 156(6), pp. B782-B790.

[61] Wiederhorn, S., Fields, R., Low, S., Bahng, G.-W., Wehrstedt, A., Hahn, J., Tomota, Y., Miyata, T., Lin, H., Freeman, B. D., Aihara, S., Hagihara, S., and Tagawa, T., 2006, "Mechanical Properties," Springer Handbook of Materials Measurement Methods, H. Czichos, T. Saito, and L. Smith, eds., Springer Science+Business Media, Inc., Wurzburg, pp. 371-396.

[62] Koros, W. J., Paul, D. R., and Rocha, A., 1976, "Carbon dioxide sorption and transport in polycarbonate," Journal of Polymer Science: Polymer Physics Edition, 14(4), pp. 687-702.

[63] ASTM International, 2013, "ASTM E96/E96M-13," Standard Test Methods for Water Vapor Transmission of MaterialsWest Conshohocken, PA.

[64] Majsztrik, P. W., Satterfield, M. B., Bocarsly, A. B., and Benziger, J. B., 2007, "Water sorption, desorption and transport in Nafion membranes," Journal of Membrane Science, 301(1), pp. 93-106.

[65] Hussaini, I., and Wang, C., 2010, "Measurement of relative permeability of fuel cell diffusion media," Journal of Power Sources, 195(12), pp. 3830-3840.

[66] Motupally, S., Becker, A. J., and Weidner, J. W., 2000, "Diffusion of water in Nafion 115 membranes," Journal of the Electrochemical Society, 147(9), pp. 3171-3177.

[67] Mocon, 2014, "Permatran-W Model 3/33," from http://www.ronox-technology.pl/download/Mocon_Permatran_3.33.pdf

[68] Illinois, S., 2013, "Lyssy L80-5000," Systech Illinois Website, S. Illinois, ed.

[69] ASTM International, 2013, "ASTM F1249-13," Standard Test Method for Water Vapor Transmission Rate Through Plastic Film and Sheeting Using a Modulated Infrared Sensor, West Conshohocken, PA.

[70] ASTM International, 1998, "ASTM F1770-97e1," Standard Test Method for Evaluation of Solubility, Diffusivity, and Permeability of Flexible Barrier Materials to Water Vapor, West Conshohocken, PA.

[71] Chen, D., Li, W., and Peng, H., 2008, "An experimental study and model validation of a membrane humidifier for PEM fuel cell humidification control," Journal of Power Sources, 180(1), pp. 461-467.

[72] ASTM International, 2013, "ASTM E398-13," Standard Test Method for Water Vapor Transmission Rate of Sheet Materials Using Dynamic Relative Humidity Measurement

[73] Schult, K., and Paul, D., 1996, "Techniques for measurement of water vapor sorption and permeation in polymer films," Journal of applied polymer science, 61(11), pp. 1865-1876.

[74] Chor, M. V., and Li, W., 2007, "A permeability measurement system for tissue engineering scaffolds," Measurement Science and Technology, 18(1), p. 208.

[75] Hinatsu, J. T., Mizuhata, M., and Takenaka, H., 1994, "Water uptake of perfluorosulfonic acid membranes from liquid water and water vapor," Journal of the Electrochemical Society, 141(6), pp. 1493-1498.

[76] Mittal, V., 2013, Polymer nanocomposite foams, CRC Press.

[77] Krause, B., Mettinkhof, R., Van der Vegt, N., and Wessling, M., 2001, "Microcellular foaming of amorphous high-T g polymers using carbon dioxide," Macromolecules, 34(4), pp. 874-884.

[78] Krause, B., Boerrigter, M., Van der Vegt, N., Strathmann, H., and Wessling, M., 2001, "Novel open-cellular polysulfone morphologies produced with trace concentrations of solvents as pore opener," Journal of Membrane Science, 187(1), pp. 181-192.

[79] Gargiulo, M., Sorrentino, L., and Iannace, S., "High performance polymeric foams," Proc. IV International Conference on Times of Polymers (TOP) and Composites, AIP Publishing, pp. 109-111.

[80] Sun, H., Sur, G. S., and Mark, J. E., 2002, "Microcellular foams from polyethersulfone and polyphenylsulfone: preparation and mechanical properties," European Polymer Journal, 38(12), pp. 2373-2381.

[81] Siripurapu, S., DeSimone, J. M., Khan, S. A., and Spontak, R. J., 2005, "Controlled foaming of polymer films through restricted surface diffusion and the addition of nanosilica particles or CO2-philic surfactants," Macromolecules, 38(6), pp. 2271-2280.

[82] Tanahashi, M., 2010, "Development of fabrication methods of filler/polymer nanocomposites: With focus on simple melt-compounding-based approach without surface modification of nanofillers," Materials, 3(3), pp. 1593-1619.

[83] Liu, X., Wang, T., Chow, L. C., Yang, M., and Mitchell, J. W., 2014, "Effects of inorganic fillers on the thermal and mechanical properties of poly (lactic acid)," International journal of polymer science, 2014.

[84] Yuzay, I. E., Auras, R., and Selke, S., 2010, "Poly (lactic acid) and zeolite composites prepared by melt processing: morphological and physical–mechanical properties," Journal of applied polymer science, 115(4), pp. 2262-2270.

[85] Solvay, 2014, "Sulfone Polymers Processing Guide," from http://www.solvay.com/en/binaries/Sulfones-Processing-Guide_EN-227543.pdf

[86] ASTM International, 2008, "D638-08," Standard Test Method for Tensile Properties of Plastics.

[87] FuelCellsEtc, 2017, "Nafion Membrane Comparison Table," from https://www.fuelcellsetc.com/store/DS/nafion-comparison-chart.pdf

[88] Chien, H.-C., Tsai, L.-D., Kelarakis, A., Lai, C.-M., Lin, J.-N., Fang, J., Zhu, C.-Y., and Chang, F.-C., 2012, "Highly hydrated Nafion/activated carbon hybrids," Polymer, 53(22), pp. 4927-4930.

[89] Park, S., and Oh, I.-H., 2009, "An analytical model of Nafion™ membrane humidifier for proton exchange membrane fuel cells," Journal of Power Sources, 188(2), pp. 498-501.

[90] Hardy, B., "ITS-90 formulations for vapor pressure, frostpoint temperature, dewpoint temperature, and enhancement factors in the range–100 to+ 100 C," Proc. Proceedings of the Third International Symposium on Humidity and Moisture, Teddington, London, England.

[91] Nguyen, T. V., and White, R. E., 1993, "A water and heat management model for Proton-Exchange-Membrane fuel cells," Journal of the Electrochemical Society, 140(8), pp. 2178-2186.

[92] Springer, T. E., Zawodzinski, T., and Gottesfeld, S., 1991, "Polymer electrolyte fuel cell model," Journal of the Electrochemical Society, 138(8), pp. 2334-2342.

[93] Zawodzinski Jr, T. A., Neeman, M., Sillerud, L. O., and Gottesfeld, S., 1991, "Determination of water diffusion coefficients in perfluorosulfonate ionomeric membranes," The Journal of Physical Chemistry, 95(15), pp. 6040-6044.

[94] Zhao, Q., Majsztrik, P., and Benziger, J., 2011, "Diffusion and interfacial transport of water in Nafion," The Journal of Physical Chemistry B, 115(12), pp. 2717-2727.

[95] Borduin, R., and Li, W., "Design and Construction of a Membrane Analysis System for Fuel Cell Humidification Applications," Proc. ASME 2013 International Mechanical Engineering Congress and Exposition, American Society of Mechanical Engineers, pp. V02AT02A055 1-5.